

COLLECTIVE CHAOS

(集団的カオス)

Tatsuo Shibata

COLLECTIVE CHAOS

Tatsuo Shibata

Ph.D. Dissertation

January 1999

*Graduate School of Arts and Sciences,
The University of Tokyo*

COLLECTIVE CHAOS

PhD Dissertation. The university of Tokyo, 1999.

Tatsuo Shibata: shibata@complex.c.u-tokyo.ac.jp

© Copyright 1999 by Tatsuo Shibata. All right reserved.

PREFACE

Chaos has developed into a mature field of contemporary science. The study of chaos revealed that a deterministic system can generate in some sense unpredictable orbits. In other words, stochastic-like behavior of a system can appear not due to our lack of knowledge but as an intrinsic characteristic in the system. However, this might not be the only significance of chaos. We often find in natural systems at the same time phenomena which seems incompatible, for instance, stability and instability, order and disorder, or coherence and irregularity. The study of chaos suggests the possibility that these are compatible.

This thesis studies collective motion in a network of chaotic elements, which is a dynamical system with a huge number of degrees of freedom. Ordered motion appears as a macroscopic dynamics of the system out of disordered motion of microscopic chaos. We will study how compatible the macroscopic dynamics is with microscopic chaos from the dynamical system and thermodynamical viewpoints. We will see that both the coherence and irregularity of chaos is essential for such collective motion. We will also find in this study a suggestion about the relationship between some stable property and unstable property of chaos.

The title “*Collective Chaos*” means that a low-dimensional chaos appears in a macroscopic variable of the system with effectively high-dimensional chaotic motion. Using the method that will be presented in this work, the existence of the collective chaos was confirmed in the network of chaotic elements. This is the first case that the existence was confirmed within the present meaning of collective chaos. This dissertation does provide new insights to the study of high-dimensional chaotic systems.

Professor Kunihiko Kaneko introduced me into such a chaotic world. I like to express my special gratitude to him for invaluable advice, stimulating discussions and essential supports since the beginning of my research. Most of this thesis comes from the collaborative studies with him. Through these research, I have studied many things from his great insights entangling broad range of fields around chaos.

I am grateful to Professor Shin-ichi Sasa for a huge number of stimulating discussions about not only the topics in this thesis, but widespread topics in physics. Particularly, it was a great experience for me to collaborate with him about thermodynamics of chemical energy transduction, which is motivated by bio-molecular motors. Through these studies, I became aware the importance of thermodynamics.

A part of this thesis comes from research collaborated with Dr. Tsuyoshi Chawanya, to whom I am greatly indebted to his essential contribution to this research, and to his tolerance for exhausting discussions with me. I also thanks Dr. Satoru Morita, and Dr. Naoko Nakagawa for illuminating discussions on the collective motion of globally coupled dynamical systems.

I like to appreciate the people of and around the group of the studies on nonlinear, nonequilibrium, and complex systems at Komaba for many discussions and supports.

I like to thank Professor Takashi Ikegami, and Dr. Takashi Hashimoto for their illuminating discussions and encouragement.

I like to express my gratitude to all the people who have directly or indirectly helped me on this research endeavor. Their questions, comments and discussions associated with this research play important roles for the accomplishment of this thesis. I hope that some of their questions are settled in this thesis.

January 1999,

柴田達夫

Tatsuo Shibata

Publications

Shibata, Tatsuo, Chawanya, Tsuyoshi and Kaneko, Kunihiro (1998),
‘Noiseless collective motions out of noisy chaos’,
submitted to *Physical Review Letters*.

Shibata, Tatsuo and Kaneko, Kunihiro (1998b),
‘Tongue-like bifurcation structures of the mean-field dynamics
in a network of chaotic elements’,
Physica **124D**, 163–186.

Shibata, Tatsuo and Kaneko, Kunihiro (1998a),
‘Collective chaos’,
Physical Review Letters **81**, 4116–4120.

Shibata, Tatsuo and Kaneko, Kunihiro (1997),
‘Heterogeneity induced order in globally coupled chaotic systems’,
Europhysics Letters **38(6)**, 417–422.

Shibata, Tatsuo and Sasa, Shin-ichi (1998),
‘Equilibrium chemical engines’,
Journal of Physical Society of Japan **67(8)**, 2666–2670.

Sasa, Shin-ichi and Shibata, Tatsuo (1998),
‘Brownian motors driven by particle exchange’,
Journal of Physical Society of Japan **67(6)**, 1918–1923.

CONTENTS

<i>Preface</i>	3
<i>I. Introduction</i>	7
I.1 Deterministic Nonperiodic Flow	7
I.2 Chaotic Behavior and Information Flow	10
I.3 From Microscopic to Collective Chaos	12
I.4 Network of Chaotic Elements	13
I.5 This Thesis	14
<i>II. Collective Motion out of Desynchronized States in a Network of Chaotic Elements</i>	15
II.1 Introduction	15
II.2 A Simple Network Model of Chaotic Elements on Globally Coupled Map	16
II.3 Phenomenology of Collective Motion	18
II.4 Tongue Bifurcation Structures of Collective Motion	25
II.5 Scaling of Tongue Structures	31
II.6 Summary and Discussion	34
<i>III. Instability of Stationary State and Genesis of Collective Motion</i>	37
III.1 Introduction	37
III.2 Instability of Stationary State	38
III.3 Scaling of Fluctuation	42
III.4 Collective Behavior Through Self-Consistent Dynamics	43
III.5 Bifurcation of Tongue Structures	49
III.6 Bifurcation in a Tongue Structure	50
III.7 Summary and Discussion	52
<i>IV. Heterogeneity Induced Order</i>	57
IV.1 Introduction	57
IV.2 Effects of Heterogeneity on Collective Motion	58
IV.3 Internal Bifurcation	61
IV.4 Summary and Discussion	65
<i>V. Collective Chaos</i>	66
V.1 Introduction	66
V.2 Collective Lyapunov Exponent	67
V.3 Heterogeneity Induced Order: Revisited	69
V.4 Summary and Discussion	71

<i>VI. Noiseless Collective Motion out of Noisy Chaos</i>	74
VI.1 Introduction	74
VI.2 Effect of Noise on Collective Motion	76
VI.3 Strength of Noise and Complexity of Collective Motion	78
VI.4 Summary and Discussion	81
<i>VII. Perspectives and Concluding Remarks</i>	82
VII.1 Concluding Remarks	82
VII.2 Future Problems on Globally Coupled Map	83
VII.3 Future Problems beyond Globally Coupled Map	87
VII.4 Coherent Irregularity	88
<i>References</i>	90

CHAPTER I

INTRODUCTION

This thesis has been constructed from two viewpoints. One is the viewpoint of *collective chaos*, and the other is the viewpoint of *a network of chaotic elements*. From the former point of view, we ask how macroscopic chaotic motion is possible out of essentially very high-dimensional dynamical systems such as fluid systems. On the other hand, from the latter point of view, we ask what is universal phenomena observed in network systems consisting of a huge number of dynamical elements.

In this chapter, we will provide some of the phenomenology of chaos, and introduce some of the more basic concepts on the chaos. Reviewing the chaos, we propose a notion of collective chaos. Next we introduce a network of chaotic elements, where we are interested in the collective chaos.

I.1 Deterministic Nonperiodic Flow

Lack of periodicity is quite common in natural systems. What is responsible for the non-periodicity? In order to study nonperiodic phenomena, especially in atmospheric systems, Edward N. Lorenz studied Rayleigh-Bénard convection, in his seminal paper entitled ‘Deterministic Nonperiodic Flow’ (Lorenz 1963).

The Rayleigh-Bénard convection has been observed in fluid systems, where the bottom of a vessel containing water is maintained at a higher temperature than the temperature at the top. As a result, the water subjected to gravity expands near the bottom and buoyancy produces a tendency of this fluid to rise, whereas the water near the top has a tendency to fall. If the temperature difference between the bottom and top is beyond a certain value, aperiodic motion is observed in a macroscopic observable, as is often in nature.

By extracting the three most important Fourier modes of the fundamental equation describing the Rayleigh-Bénard convection, Lorenz obtained ordinary differential equations, given by

$$\begin{aligned}\dot{X} &= -\sigma X + \sigma Y, \\ \dot{Y} &= -XZ + rX - Y, \\ \dot{Z} &= XY - bZ,\end{aligned}\tag{I.1}$$

with dimensionless parameters σ , r and b . He solved these equations numerically and obtained the remarkable trajectory depicted in Fig.I.1. The evolution of this system was not periodic any more.

In order to elucidate the mechanism underlying this nonperiodic flow, Lorenz extracted a discrete time map from this continuous time system (Eqs.(I.1)). Fig.I.2 shows

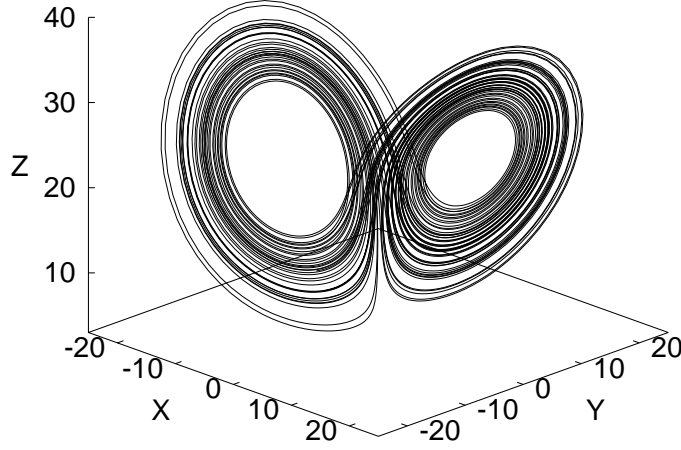


Fig. I.1: Nonperiodic flow obtained numerically from the Lorenz system (Lorenz 1963).
 $(\sigma, b, r) = (10.0, 8.0/3.0, 470.0/19.0)$.

the value of Z of the Lorenz system as a function of time. Whereas the phase of oscillation seems nearly periodic, the amplitude of oscillation shows a complicated change in time. Lorenz focused his notice on this point. He recorded successive maximal values, and then made a return map plotted the maxima as a function of the previous maxima. In this way, he obtained a one-dimensional map as is shown in Fig.I.3, which is embedded in the nonperiodic flow of the Lorenz system.

Lorenz proceeded to analyse this one-dimensional map closely. He adopted the tent map as an approximation of this one-hump map. The tent map is piecewise linear map with the slop two,

$$f(x) = \begin{cases} 2x, & 0 < x < \frac{1}{2}, \\ 2 - 2x, & \frac{1}{2} < x < 1. \end{cases} \quad (I.2)$$

He studied the trajectories of this map starting from rational numbers and irrational numbers, and showed that no repetitions occurs in the trajectory starting from a irrational number, whereas the trajectory starting from a rational number is periodic. Hence, almost all the trajectories are not periodic.

He also pointed out the orbits of the Lorenz system unstable. The map illustrated in Fig.I.3 has a slop whose magnitude is everywhere greater than unity. Consider two nearby trajectories. It is easily understood that the distance between these trajectories

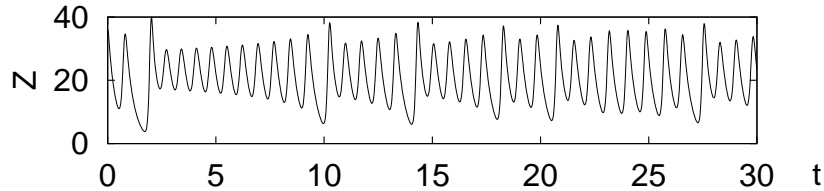


Fig. I.2: The value of Z of the Lorenz equation (I.1) is plotted as a function of time (Lorenz 1963).

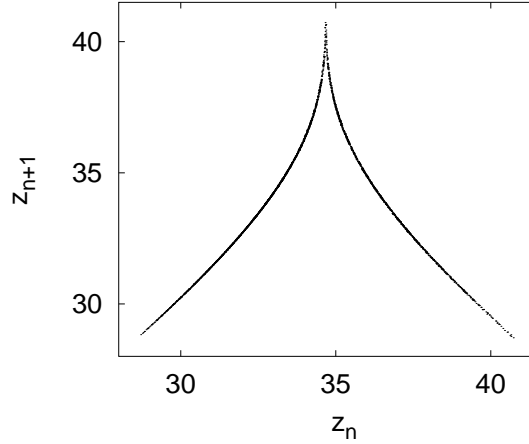


Fig. I.3: Maxima versus previous maxima of Z , illustrating the embedded one-dimensional map in the Lorenz system (Lorenz 1963).

diverges exponentially. Thus, the evolution of the system is highly sensitive to initial conditions (*sensitive dependence on initial conditions*). In this way, he has found the remarkable fact that in spite of the deterministic nature of the system, the behavior of the system is in some sense unpredictable. This deterministic nonperiodic flow is now called *chaos*.

Remembering that it is the fluid system that show just this behavior, we should notice that a very large collection of highly interacting molecules is underlying in this behavior. It has been long supposed that chaotic behavior may exist in such microscopic motions of molecules, which is responsible for macroscopic behavior of the system. This *microscopic chaos* has been called *molecular chaos*. On the other hand, since the Lorenz system describes the observable fluid flow at a macroscopic level, the nonperiodic flow of the Lorenz system should be called *macroscopic chaos*¹. And the existence of such macroscopic chaos has been confirmed experimentally in the Rayleigh-Bénard convection (Libchaber & Maurer n.d., Brandstätter et al. 1983).

Now the study of chaos has developed into a mature field of the contemporary physics (Bergé et al. 1984, Echmann & Ruelle 1985, Ott 1993). The macroscopic chaos has been observed experimentally not only in fluid systems but also in physical (Gibbs et al. 1981, Testa et al. 1982), chemical (Simoyi et al. 1982, Roux et al. 1983), and biological systems (Olsen & Degn 1977, Markus et al. 1985, Chialvo et al. 1990, Cole 1991). Before the chaos study, one might suppose that stochastic nature observed in these systems is extrinsic property generated by something at the outside of the system. The chaos has revealed, however, that a certain system itself can generate stochastic orbit as intrinsic property². In the Lorenz's work in 1963, the essence of such chaos has been already shown clearly.

¹ The word "chaos" is commonly used for this macroscopic chaos. In this thesis, "chaos" without adjectives is also used in this way.

² One may still ask the question what is the origin of randomness.

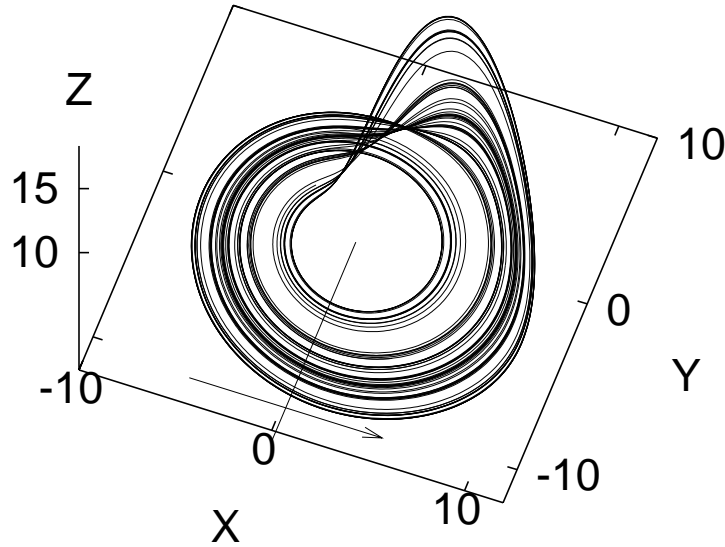


Fig. I.4: Rössler attractor. The Rössler system is given by the ordinary differential equations, $(\dot{X}, \dot{Y}, \dot{Z}) = (-Y - Z, X + \frac{1}{5}Y, \frac{1}{5} - \mu Z + XZ)$. (Rössler 1976).

I.2 Chaotic Behavior and Information Flow

Chemical reaction has also been an important field to study chaos theoretically and experimentally. Otto E. Rössler considered a simple reaction systems in 1976 (Rössler 1976). The Rössler system also consists of three nonlinear differential equations, whose evolution indicates chaotic behavior, as is illustrated in Fig.I.4.

In a dissipative system, in contrast to Hamiltonian systems, the phase space volume continues to contract onto a lower dimensional surface with increase of time. The Rössler system as well as the Lorenz system is a dissipative system, and the orbits are considered on a lower dimensional surface embedded in the three dimensional phase space. On this two dimensional surface, the orbits diverge exponentially. The exponential divergence is characterized by a positive *Lyapunov exponent*, which is the rate of growth of two nearby trajectories. How is such divergence made possible in a bounded three-dimensional phase space?

The Rössler system clearly indicates what makes it possible for nearby orbits, though bounded, to diverge exponentially. In Fig.I.4, a (quasi-) two-dimensional sheet containing many orbits goes round the origin. The sheet is expanded along its width and folded over on itself around the maximal value of Z . Since the orbits never cross in the phase space, the sheet has a certain thickness, containing infinitely many two dimensional surfaces. A particular orbit is realized on one of these surfaces.

It is so possible that orbits are bounded despite the fact that nearby orbits diverge exponentially. The sheet containing infinitely many two dimensional surfaces continues to contract along its thickness until the folding. The folded sheet contracts again. This repetition of the contraction and folding leads to construction of the structure that hold a similar pattern in each scale. This structure is called *strange attractor*, which is characterized by the concept of *fractal*.

The reduction from the three-dimensional flow of the Rössler system to a one-

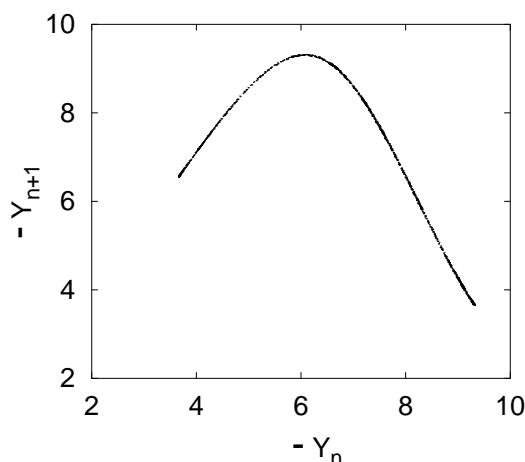


Fig. I.5: Return map, generated by intersections at the surface of section $X = 0$ within the projected Rössler attractor onto the XY -plane. The surface of section is indicated in Fig.I.4. (Shaw 1981).

dimensional map is displayed in Fig.I.5 (Shaw 1981). Since the map in Fig.I.5 has regions where the slope has a magnitude less than unity, it is not obvious whether the orbit is chaotic or not. However, the map is similar to the logistic map $f(x) = 1 - ax^2$, which shows chaotic motion via period-doubling bifurcation (Feigenbaum 1978, Collet & Eckmann 1980). Indeed, the Rössler system shows a similar route to chaos. Thus, on the one hand, the map generated from the flow is considered to approximately preserve the chaotic nature of the Rössler attractor. On the other hand, the reduction to a one-dimensional map is approximation, and should be regarded to have a finite thickness. In fact, Fig.I.5 has a finite thickness, reflecting the folding of the flow, though the contraction rate is so strong that it may be difficult to see the structure.

The exponential divergence suggests that infinitesimal structures appear in a macroscopic scale after a certain time, whereas the contraction and folding implies that a large scale structure is embedded into a microscopic scale. Robert Shaw has discussed this process as information flow between macroscopic and microscopic scales, or as a communication process from the present to the future, according to the information theory (Shaw 1981, 1984). Then, he has claimed that in a dissipative system with chaos, the separation between macroscopic and microscopic scales breaks down, and chaos transfers information from the microscopic into macroscopic scale.

Remembering that the Rössler system is a reaction system, the set of ordinary differential equations only describe the average rate of reaction. A huge number of molecules underlying the chemical reaction should also constitute a huge dimensional phase space, though one may be hardly imagine such a huge dimensional phase space whose dimensionality varies in time. Whereas the chaos appears in the macroscopic scale as in Fig.I.4, information is generated in the microscopic scale at a huge dimensional phase space. Shaw has considered chaotic dynamical systems as sources of information, which originates in the microscopic scale beyond experimental resolution (Crutchfield et al. 1982). However, if such high-dimensional information is transferred into the macroscopic scale, how is it possible to realize low-dimensional chaotic motion?

According to the metaphor from the communication theory, the chaotic dynamical system should be considered as a channel of information. Then one may argue that the dimensionality of the channel determines the dimensionality of macroscopic observables. Still, we ask how such a channel is constructed out of the motion with an effectively huge number of degrees of freedom.

1.3 From Microscopic to Collective Chaos

Studies on the relation between macroscopic and microscopic scales have a long history over a hundred years, though in these studies statistical aspects might be discussed rather than dynamical aspects which we are concerned with.

Recently, the existence of the microscopic chaos, which is responsible for the macroscopic properties, has been studied experimentally by Gaspard et al. (1998). In this case, the macroscopic motion is not chaos but a stochastic process of Brownian motion. They have recorded the position of Brownian motion with time, and have measured a sort of a mean pattern entropy per unit time of the time series generated by the collisions with molecules. Although there may be a room for discussion whether their experiment was successful to verify the existence of microscopic chaos, this is one direction to study the relevance of macroscopic properties to microscopic dynamics from the viewpoint of dynamical system (Gaspard & Wang 1993, Gaspard et al. 1998).

As for the study of construction of macroscopic chaos from a microscopic scale, we first mention the chaos in reaction systems. The chaos in chemical reaction systems has been one of the most successful examples observed experimentally. In order to study underlying dynamics in rate equations of chemical reactions, a mesoscopic description has been adopted, which is given by a set of transition probabilities among chemicals. In such a description, the underlying dynamics of macroscopic motion is stochastic processes, and the evolution of probability distribution of each chemical is investigated (Fox & Keizer 1991)³.

When the underlying dynamics of macroscopic motion is effectively high-dimensional chaos, in the sense that the Lyapunov dimension or the Kolmogorov-Sinai entropy is proportional to the system size, is it really possible to realize macroscopic low-dimensional chaotic motion? In this Thesis, let us call such macroscopic chaos out of effectively high-dimensional chaos as *collective chaos*.

So far, from such a point of view, spatially extended systems have been investigated in its fully desynchronized state. However, existence of the collective chaos in such systems has often been suspected (Bohr et al. 1987, Grinstein 1988, Bennett et al. 1990)⁴. In fact, in spatial extended systems, only quasiperiodic oscillation of a certain macroscopic variable has been observed, as a time dependent macroscopic motion (Chaté & Manneville 1992).

In this Thesis, however, we will present that the collective chaos is *possible* in certain coupled dynamical systems, where many chaotic elements organize a huge network.

³ Discussion on the macroscopic description of chaos and large-scale fluctuations in chemical reaction systems is given in Nicolis & Balakrishnan (1992) and Keizer & Fox (1992).

⁴ They have discussed a correlation length scale in spatially extended chaotic systems. The correlation length scale is finite. This is the reason why they have suspected the existence of the collective chaos.

I.4 Network of Chaotic Elements

We have acquired the viewpoint to describe natural phenomena as a collection of various elements. It may be quite difficult problem in effect to partition some system into subsystems. However, considering a certain unit in the system as an element, it would be practical to explore the consequences of interactions among these elements.

For example, in order to discuss thermodynamic properties of nonequilibrium systems, in many cases, we partition the system into subsystems, in each of which equilibrium properties are locally assumed (Glansdorff & Prigogine 1971). Then the system is described as a many-body system of these subsystems so as to study the entire nonequilibrium process. In a similar way, we can study the system far away from equilibrium, supposing a certain property of the subsystems and the interaction among them. For instance, we postulate that local subsystem in a spatially extended system has chaotic property such as the Lorenz system, and the subsystems diffusively interact each other. Then spatiotemporal phenomena has been studied by partial differential equations (Nicolis & Prigogine 1977), or coupled map lattice (Kaneko 1984, 1993).

The viewpoint of the interacting elements also provides a strong tool to understand living systems. For instance, many living systems consist of a huge number of subsystems of cells. The cell is considered as a huge network of interacting metabolic reactions. Whereas various of proteins catalyze the reactions in the metabolic network, the proteins are many-body systems of twenty types of amino acid. Let us go back to the cellular systems, which constitute various kind of organs which organize a living system (Godin & Buchman 1996, Buchman 1996). In individual organisms that live in social groups, interactions among group members often produce behavioral organization (Cole 1991, Miramontes et al. 1993).

These systems consist of many subsystems with not simple interaction, and show as a whole interesting macroscopic phenomena, whose spatiotemporal scales is over the scale of the subsystems. In such complex systems, even if we know properties of the subsystems and mechanism of its interaction, it would be worthwhile to discuss properties of the entire system (Simon 1981).

Each subsystem itself is also considered to consist of interacting subsystems. Hence, the system forms a hierarchical structure. For such a hierarchical system, we need to discuss not only the interaction among subsystems, but also *interactions between*⁵ the system and its subsystems. An comprehensive discussion on this topic is found in Simon (1981).

A common approach to such complex phenomena is to construct a model of the individual phenomena. However there are two difficulties in such an approach.

The first lies in the construction of the model. Many people have discussed what a good model is, and there are often many different models for the same phenomena. A model will depend on the choice of what is important for understanding and describing the phenomena. How do we compare different models? And what might these comparison mean?

The second difficulty lies in how to understand the behavior in a model. For this, properties found over individual systems should be discussed. With the theories for such properties, since these theories are abstract entities, one may comprehend some concepts relevant (or applicable) to various of fields over individual systems. (These two difficulties in understanding phenomena entangle with each other. The choice of what is important in individual models is relevant to what should be developed into the

⁵ Neither top down nor bottom up.

concepts.)

Throughout this thesis, we study an abstract model of networks consisting of dynamical elements. The dynamical elements often show chaotic dynamics as is seen in the previous sections. Since the model is so abstract, we have believed that the concepts developed in the model is relevant to a variety of natural systems, which consist of many dynamical elements. In particular, we are interested in the collective chaos observed in the network of chaotic elements.

I.5 This Thesis

In a network of chaotic elements when the strength of the interaction among elements is small enough, motion of elements seems to be independent each other. Accordingly, the system is in a high-dimensional chaotic state. However, a certain macroscopic quantity shows some dynamical property, rather than fluctuations. This has been called *collective motion* in a network of chaotic elements. The purpose of this Thesis is to study the nature of such collective motion, and to present a mechanism for the origin of such collective dynamics.

We will first introduce globally coupled chaotic elements, called globally coupled map in Chapter II. We will provide some of the phenomenology of the collective motion. With the change of the control parameters, the collective dynamics shows some sort of bifurcation. Such a bifurcation is called *Tongue-like bifurcation structure* of the collective motion. Some scaling properties of the collective motion against the change of parameters are also presented.

In Chapter III we shall demonstrate how such collective motion is possible. First stationary states of the macroscopic quantity is shown to be unstable. The characteristic time scale of the collective motion are much longer than the time scale of individual elements. Next we shall present a certain bifurcation structure in individual elements makes the longer time scale of the collective motion possible. Some bifurcations of the collective motion are also presented.

We will introduce globally coupled map with some heterogeneity in Chapter IV. In such a system ordered collective motion is clearly found, ranging from quasiperiodic motion to low and high dimensional chaos. The collective motion in the globally coupled map with heterogeneous chaotic elements suggests the existence of the collective chaos.

An algorithm to characterize collective motion is presented in Chapter V, with the introduction of *collective Lyapunov exponent*, as the orbital instability at a macroscopic level. By applying the algorithm to a globally coupled map with heterogeneous chaotic elements, existence of low-dimensional collective chaos is confirmed, where the scale of high-dimensional microscopic chaos is separated from the macroscopic motion, and the scale approaches zero in the thermodynamic limit.

Effect of microscopic external noise on the collective motion is studied in Chapter VI. With the increase of external noise intensity, the collective motion is successively simplified. The number of effective degrees of freedom in the collective motion is found to decrease as $-\log \sigma^2$ with the external noise variance σ^2 . It is shown how the microscopic noise can suppress the number of degrees of freedom at a macroscopic level.

CHAPTER II

COLLECTIVE MOTION OUT OF DESYNCHRONIZED STATES IN A NETWORK OF CHAOTIC ELEMENTS

Collective behavior is studied in globally coupled maps. Several coherent motions exist, even in fully desynchronized state. The macroscopic variable is found to show some kind of ordered motion distinguishable from noise, ranging from torus to high-dimensional chaos. To characterize the collective behavior, we introduce scaling transformation of parameters, and detect in parameter space a *tongue-like bifurcation structure* in which collective motions is possible.

II.1 Introduction

Whereas the research of low dimensional chaos provided us with important notion of unpredictability in deterministic systems, it was soon realized that many natural systems show much more complicated behavior than low dimensional chaos. One of the important features in natural systems is high dimensionality. Although deterministic aspects remain in the high dimensional chaos, the present nonlinear dynamics tools are not sufficient to distinguish it clearly from noise. Hence, the study of high-dimensional chaos is important both from a theoretical and from a practical point of view.

Globally coupled dynamical systems, consisting of many dynamical elements interacting all-to-all, are good examples using which we can develop notions in high dimensional systems. This class of dynamical systems is seen in physical, chemical and biological systems. In physics, coupled Josephson junction arrays (Watanabe & Strogatz 1994) are a coupled nonlinear oscillator circuit with global feedback. In nonlinear optics with multi-mode excitation (Bracikowski & Roy 1991, Arecchi 1991) many modes are often coupled globally through energy currency. In bioscience and medical science, neural (Aertsen & M. Erb 1994), cellular (Ko et al. 1994, Kaneko & Yomo 1994), and vital (Godin & Buchman 1996, Buchman 1996) organizations, that are known to exhibit complex chaotic behaviors, are described in terms of a network of active elements. Several examples in ecological and economic systems are also seen in terms of a network of active agents. Among these complex networks, a globally coupled dynamical system is the simplest case.

So far, study of globally coupled dynamical systems has revealed novel concepts such as clustering, chaotic itinerancy, and partial ordering (Kaneko 1990a). In partic-

This Chapter is partly based on Shibata & Kaneko (1998b, Section 2, 3, 4, 5, 8 and 9).

ular, the study of collective dynamics has got much attention (Kaneko 1990b, 1992, Perez & Cerdeira 1992, Chaté & Manneville 1992, Perez et al. 1993, Pikovsky & Kurths 1994b,a, Just 1995, Kaneko 1995, Ershov & Potapov 1995, Morita 1996, Chaté et al. 1996, Shibata & Kaneko 1997, Ershov & Potapov 1997, Nakagawa & Komatsu 1998, Chawanya & Morita 1998, Shibata & Kaneko 1998b,a). When the interactions between elements are small enough, each element oscillates independently, without synchronization between them. Thus the number of degrees of freedom of the system is effectively proportional to the system size. If each element has chaotic dynamics, the system is in a high dimensional chaotic state. Even in such a case, a macroscopic variable shows some kind of complicated dynamics rather than noise, ranging from low-dimensional torus to high-dimensional chaos (Shibata & Kaneko 1997, Pikovsky & Kurths 1994b,a). This may imply that any weak interaction between active elements necessarily brings about some sort of correlation¹ between the elements.

This Chapter is organized as follows. In Section II.2, the globally coupled logistic map is introduced and its characteristic behavior is presented as a brief review. In Section II.3, an overview of different kinds of collective dynamics is presented. In the macroscopic dynamics, a lower dimensional motion and a much longer time scale than those of microscopic dynamics are observed. We focus on the thermodynamic limit of such collective behavior. The time scale and the amplitude of collective motion are studied in the large system size limit. In Section II.4, a global phase diagram in the parameter space is presented. Because the phase diagram shows a complicated structure, we introduce a scaled nonlinearity parameter so that *tongue-like bifurcation structures* are clarified. Collective dynamics with a larger amplitude exists in each tongue structure that corresponds to a periodic window in the single logistic map. Since windows of the single logistic map exist in any neighborhood in the parameter space, the clarification of the collective dynamics with such bands is necessary to understand the collective dynamics in general. A scaling relation between the growth of tongue structure and the coupling strength is given in Section II.5.

II.2 A Simple Network Model of Chaotic Elements on Globally Coupled Map

Here we adopt one of the most simplest model among networks of chaotic elements. The model consists of N elements iterated by an internal dynamics with a global coupling among elements. The present globally coupled map (GCM) is given by the equation,

$$x_{n+1}(i) = (1 - \epsilon)f(x_n(i)) + \frac{\epsilon}{N} \sum_{j=1}^N f(x_n(j)), \quad (i = 1, 2, 3, \dots, N), \quad (\text{II.1})$$

where $x_n(i)$ is the variable of the i 'th element at discrete time step n , and $f(x)$ is the internal dynamics of each element. For the internal dynamics we choose the logistic map

$$f(x) = 1 - ax^2, \quad (\text{II.2})$$

where a is the nonlinear parameter. The logistic map has been studied in detail as a typical of dissipative chaos (Collet & Eckmann 1980, Ott 1993). The nonlinear param-

¹ This means that two point mutual correlation does not vanish in the limit of $N \rightarrow \infty$.

eter a , , the coupling strength ϵ , and the total number of elements N are the control parameters of the present GCM.

The GCM can be considered as a mean-field extension of the coupled map lattice (CML), in which elements are located at discrete spatial coordinates and interact with their neighbors (Kaneko 1984, 1989b, 1990c). It is given by

$$x_{n+1}(i) = (1-\epsilon)f(x_n(i)) + \frac{\epsilon}{2} \{f(x_n(i-1)) + f(x_n(i+1))\} \quad (i = 1, 2, 3, \dots, N). \quad (\text{II.3})$$

It is easy to extend the spatial dimension of CML to d -dimension. A GCM can be also considered as a CML in which the number of spatial dimensions goes to infinity.

In the GCM model, two opposite tendencies coexist: all-to-all coupling tends to synchronize elements, while chaotic instability in each element tends to desynchronize them. Depending on the balance between the two tendencies, a rich variety of phenomena has been found (Kaneko 1990a). When the coupling strength is strong enough, all elements are synchronized each other and the dynamics is nothing more than the single logistic map as is called *coherent phase*. As the coupling strength is smaller or the non-linearity larger, elements split into some groups, in each of which they are synchronized each other. This regime is called *ordered phase*, while the phenomena are called *clustering*. The clustering is common characteristics in globally coupled systems, including globally coupled oscillator systems (Okuda 1993, Nakagawa & Kuramoto 1993).

In the region, called *partially ordered phase*, where the two opposite tendencies are somewhat balanced, some part of the elements makes a few clusters, while the rest elements do not form clusters and their oscillations are desynchronized. In the phase space, there are a lot of ‘attractor ruins’ with lower dimensionality, at which the trajectory is attracted and stays over some duration, but then the trajectory goes out from them into much higher dimensional phase space, till they are again attracted to another attractor ruin. In this phenomenon, called *chaotic itinerancy*, the number of effective degrees of freedom changes with time (Kaneko 1990a, Ikeda et al. 1989, Tsuda 1992, Kaneko 1997, 1998).

If the coupling strength ϵ is small enough, none of the elements take the same values, and the correlation between elements gets smaller. This parameter regime is called *desynchronized phase*. The motion of each element seem to be independent from the others. Even in such cases, however, the motion in macroscopic variables counterintuitively does not vanish in the thermodynamic limit ($N \rightarrow \infty$). This has been studied as *collective motion* in GCM (Kaneko 1990b, 1992, 1995, Pikovsky & Kurths 1994b,a, Perez et al. 1993, Ershov & Potapov 1995, Morita 1996, Ershov & Potapov 1997, Shibata & Kaneko 1997, Chawanya & Morita 1998, Shibata & Kaneko 1998b,a, Nakagawa & Komatsu 1998, Shibata et al. 1998), which implies some sort of coherence between elements.

In the desynchronized phase, the microscopic motion shows high dimensional chaos in the sense that the Lyapunov dimension is proportional to the number of element N . In almost all the parameter values, however, the mean field motion shows some coherence ranging from quasiperiodic-like motions to higher dimensional motions distinguishable from random motions (Shibata & Kaneko 1998b), whereas the macroscopic motions are believed to be infinite dimensional motions even when the torus like structure is observed (Ershov & Potapov 1997, Chawanya & Morita 1998, Shibata & Kaneko 1998b,a, Shibata et al. 1998).

In the next section, we will show some phenomena of macroscopic dynamics in the desynchronized state.

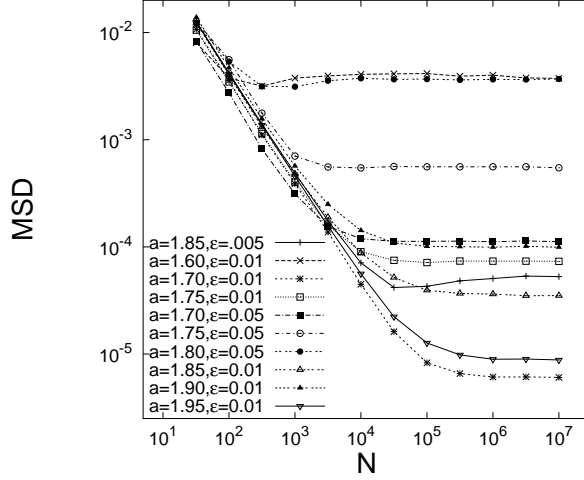


Fig. II.1: Mean square deviation (MSD) of the mean field distribution $\langle(\delta h)^2\rangle = \langle h^2\rangle - \langle h\rangle^2$ are plotted as a function of the system size N .

II.3 Phenomenology of Collective Motion

The system in the desynchronized state is high-dimensional in the sense that the Lyapunov dimension is proportional to the system size N . Thus, we may expect the existence of a certain macroscopic variable in the thermodynamic limit ($N \rightarrow \infty$), which involves almost all the variables of $x_n(i)$. Here, we adopt the mean-field

$$h_n = \frac{1}{N} \sum_{i=1}^N f(x_n(i)) = \frac{1}{N} \sum_{i=1}^N x_{n+1}(i), \quad (\text{II.4})$$

as a macroscopic observable. Since there seems to be no mutual synchronization among elements, one might imagine that the mean-field would be effectively the same as noise and, therefore the mean-field would go to a constant with the increase of N . One might expect that such a high dimensional dynamics is not distinguishable from noise. Such a case could be expected as an application of the law of large numbers.

In fact this is *not* the case. First we measure the mean square deviations (MSD) of the distribution of the mean field values. The MSD is given by

$$\langle(\delta h)^2\rangle = \langle h^2\rangle - \langle h\rangle^2, \quad (\text{II.5})$$

where the bracket $\langle \cdot \rangle$ denotes the temporal average. Then we can check whether the fluctuation of the mean field obeys the central limit theorem of the standard probability theory. Fig.II.1 shows the MSD of the mean field values as a function of the system size N for several parameters. The values seem to converge to some limit for $N \rightarrow \infty$. These show the distinction of the mean-field dynamics from pure noise and suggest the existence of some coherence among elements. This phenomena have been called ‘collective motion’ in GCM.

Fig.II.2(a) shows an example of the time series of the mean field values as a function of time step n at every two steps, and the corresponding return map of the mean field for $N = 10^5$. The coupling strength is too small to synchronize any two elements.

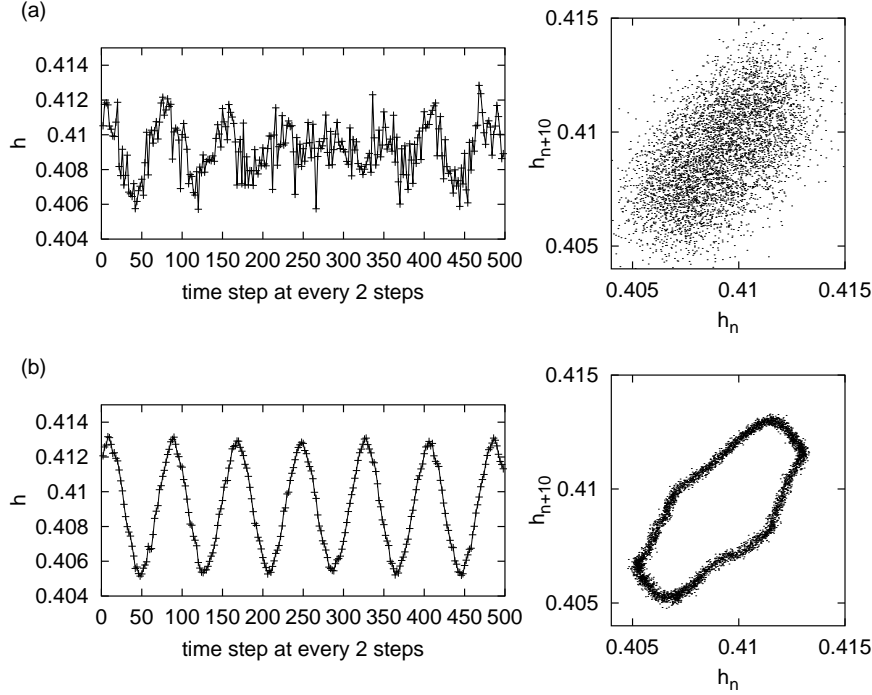


Fig. II.2: Time series and return map. Time series are plotted at every 2 steps after transients are discarded. $a = 1.5449205$, $\epsilon = 0.0005$. (a) $N = 10^5$, (b) $N = 10^7$. Corresponding return maps (h_n, h_{n+10}) are plotted over 50000 steps after transients are discarded.

The trajectory of the mean-field has some fluctuation due to the finite system size. With the increase of the system size to $N = 10^7$, however, the trajectory shows some coherent motion as is shown in Fig.II.2(b). The trajectory is rather close to quasiperiodic motion, although the points are scattered around the torus-like motion.

In Fig.II.3, power spectra for the time series of a single element and for the mean-field are shown. The time scale of the mean-field dynamics is much longer than the time scale of the single element dynamics.

Note that the width around the closed curve remains finite even if N is further increased. The collective dynamics is not really on a two-dimensional torus, and it indeed is not represented by low-dimensional dynamics as will be demonstrated in the next section. On the other hand, since the mean-field dynamics does not approach a point with the increase of N , it is also different from noise. Hence the collective motion has some structure, although it is high-dimensional. (We will see this in Section II.5).

Another set of examples is given in Figs.II.4 and II.5, which are the time series plotted at every seven steps and the first return maps². In Fig.II.4(a), quasi-periodic-like motion is not detected in the mean field dynamics, but some structure exists in the return map, whereas in the time series, a characteristic time scale seems to exist. With a slight increase of a , the dynamics of the mean field is changed as in Fig.II.4(b). In this case, the return map does not show a clear structure, and the variation of the mean field remains at the same magnitude with the further increase of N . With a much slighter

² The choice of plotting only every second or seventh step in the above figures (Figs.II.2, II.4, and II.5) is not arbitrary but there is a reason for it, which will be clarified in the following chapters.

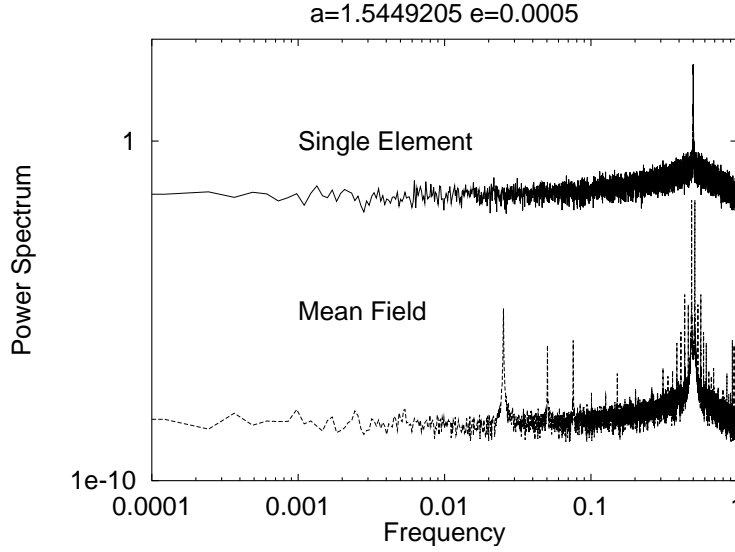


Fig. II.3: Power spectrum of time series of a single element $x_n(i)$ (upper) and the mean field h_n (lower), $a = 1.5449205$, $\epsilon = 0.0005$, $N = 10^7$. While the spectrum for a single element has a peak at the frequency 0.5, continuous component is much larger than that of the mean field dynamics. Hence, the mean field dynamics is more regular than the dynamics of each element. The slow dynamics of the mean field is shown by the peak at the frequency 0.025269.

increase of a , the mean field comes to oscillate more regularly, whereas the motion is scattered around torus motion. In Fig. II.5, the mean field values are plotted with the change of ϵ for the same value of a . The amplitude of the motion gets smaller and smaller with the decrease of ϵ .

Figs. II.2, II.4, and II.5 indicate that the mean field dynamics plotted in the return maps shows some structures, ranging from lower-dimensional structures, such as a torus, to higher-dimensional stochastic structures. In order to characterize the mean field dynamics, the MSD of the distribution of the mean field values is useful as a measure of the amplitude of the mean field dynamics³.

As we have shown in Fig. II.1, the MSD of the mean field converges to a certain value in the thermodynamic limit. Accordingly, the amplitude of the mean field dynamics has a converged value.

The collective motion, detected in the return map (Figs. II.2, II.4 and II.5), has some low-dimensional-like structure but the width of scattered points around the ‘torus’ remains finite in the thermodynamic limit. This may suggest high dimensionality of the collective motion. In order to measure the number of degrees of freedom of the mean field dynamics, we have measured the correlation dimension (Grassberger & Procaccia 1983a,b) of the mean-field time series.

In Fig. II.6, the change of slope in the correlation integral $\frac{d \log C(r)}{d \log r}$ is plotted as

³ When the mean-field does not have clear structures as in the case of Fig. II.4(b), the MSD is useful to measure the variation around a fixed point. On the other hand, when the mean field dynamics shows quasiperiodic motion as shown in the previous section, it would be reasonable to define the amplitude distinguished from “noisy component”. As we will see in the next subsection, however, such separation is impossible, because the “noisy component” does not get smaller with the increase of system size N . Even in this case, the MSD can roughly measure the size of the collective motion.

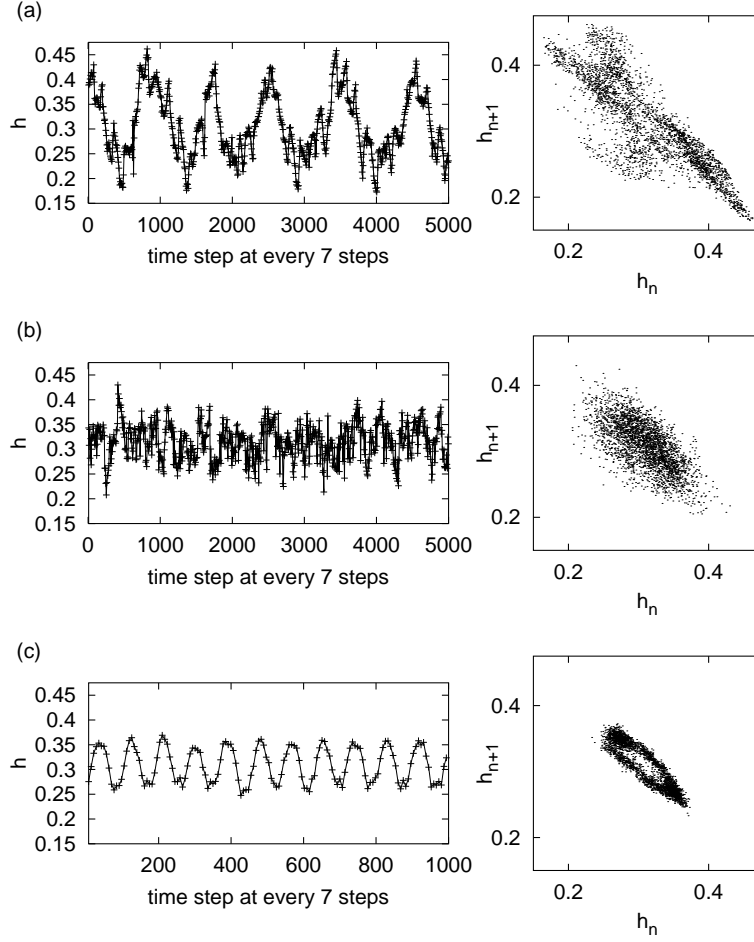


Fig. II.4: Time series and return map. Time series are plotted at every seven steps. The parameters (a, ϵ) are (a) $(1.69620, 0.008)$, (b) $(1.69755, 0.008)$, (c) $(1.69844, 0.008)$.

a function of the scale size with increasing the system size N . For a smaller system size, the correlation dimension increases monotonically for decreasing the scale as for random variables. For a larger system size, curves have a plateau at a value less than the correlation dimension two, which seems to correspond to the collective motion. In a smaller scale, however, the correlation dimension becomes large. At this smaller scale, the motion is hard to be distinguishable from noise. If the scale of this regime would get smaller with the size N , one could conclude that the collective dynamics is low-dimensional in the thermodynamic limit. As shown in Fig.II.6, this is not the case. The slope function converges to a certain curve with the increase of N where the plateau region does not get wider. Thus, the mean field dynamics does not converge to lower dimensional dynamics in the thermodynamic limit.

The characteristic time scale of the collective motion is much slower than the time scale of a single element. In order to show how the time scale of the mean field dynamics depends on the system size N , we measure the rotation number of the mean field

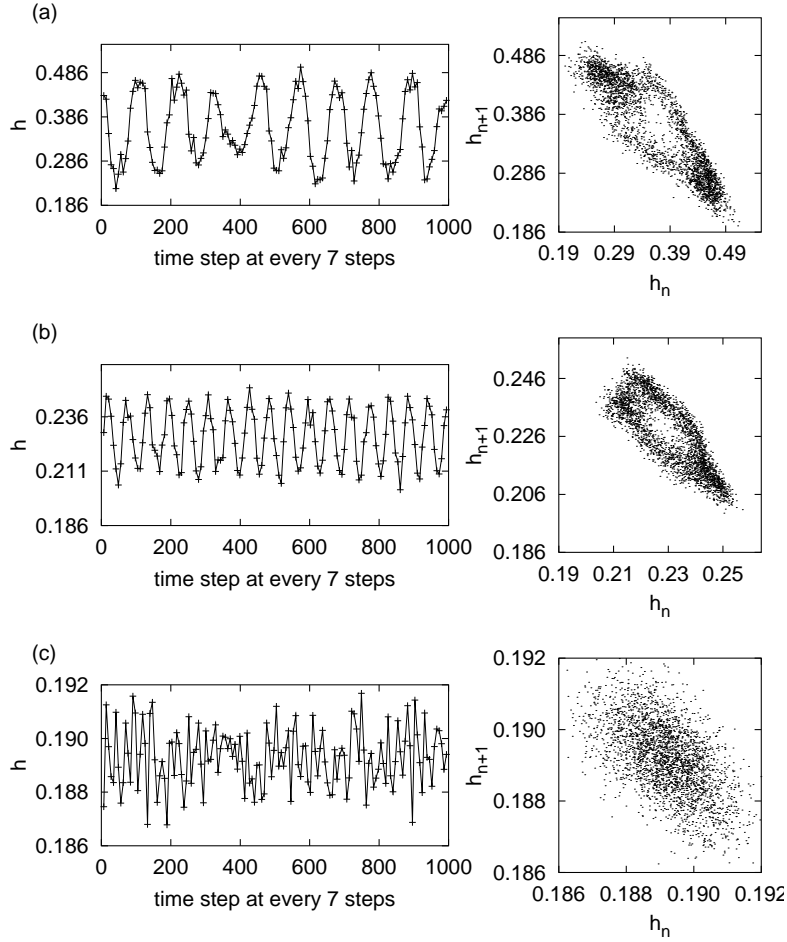


Fig. II.5: Time series and return map. Time series are plotted at every 7 steps. The parameters (a, ϵ) are (a) $(1.86, 0.1)$, (b) $(1.86, 0.01)$, (c) $(1.86, 0.001)$.

dynamics as a function of the system size N . Here, the rotation number R is defined as

$$R = \lim_{t \rightarrow \infty} \frac{1}{t} \sum_{n=1}^t \frac{\Delta \theta_n}{2\pi}, \quad (\text{II.6})$$

where $\Delta \theta_n$ is the angle variable formed by the two vector $(h_n - \langle h \rangle, h_{n+1} - \langle h \rangle)$, and $(h_{n+1} - \langle h \rangle, h_{n+2} - \langle h \rangle)$ defined around the average mean field $\langle h \rangle$ over time.

In Fig.II.7, the rotation number is plotted as a function of N . In most cases, the rotation number seems to converge to a certain value. It is suggested that the mean field dynamics approaches certain dynamics, independently of the system size for large enough N . In Fig.II.8, the power spectra of the mean field dynamics have some peaks. The low frequency components correspond to the collective dynamics, while the high frequency component represents the element dynamics. The power spectra seem to converge to a certain function, and the peaks do not sharpen any more even with the increase of N . This may corresponds to the previous observation that the correlation dimension of the mean field dynamics as a function of observed scale seems to con-

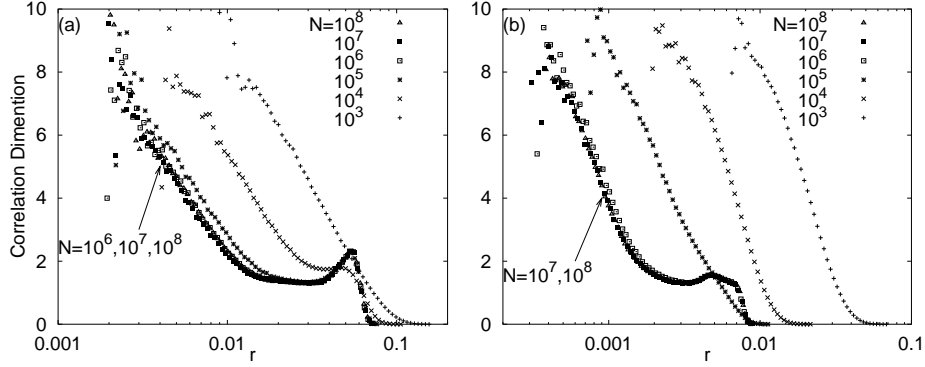


Fig. II.6: Correlation dimensions are plotted as a function of scale size r for different system size, which are indicated at the right of each figure. The mean field time series is embedded into 10 dimension. The parameters are (a) $a = 1.699$, $\epsilon = 0.008$, and (b) $a = 1.5449205$, $\epsilon = 0.00050$.

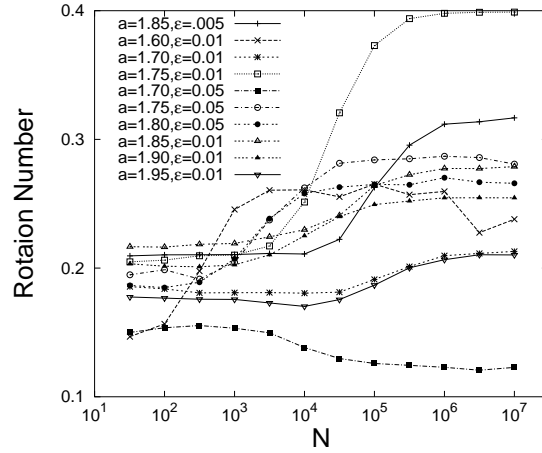
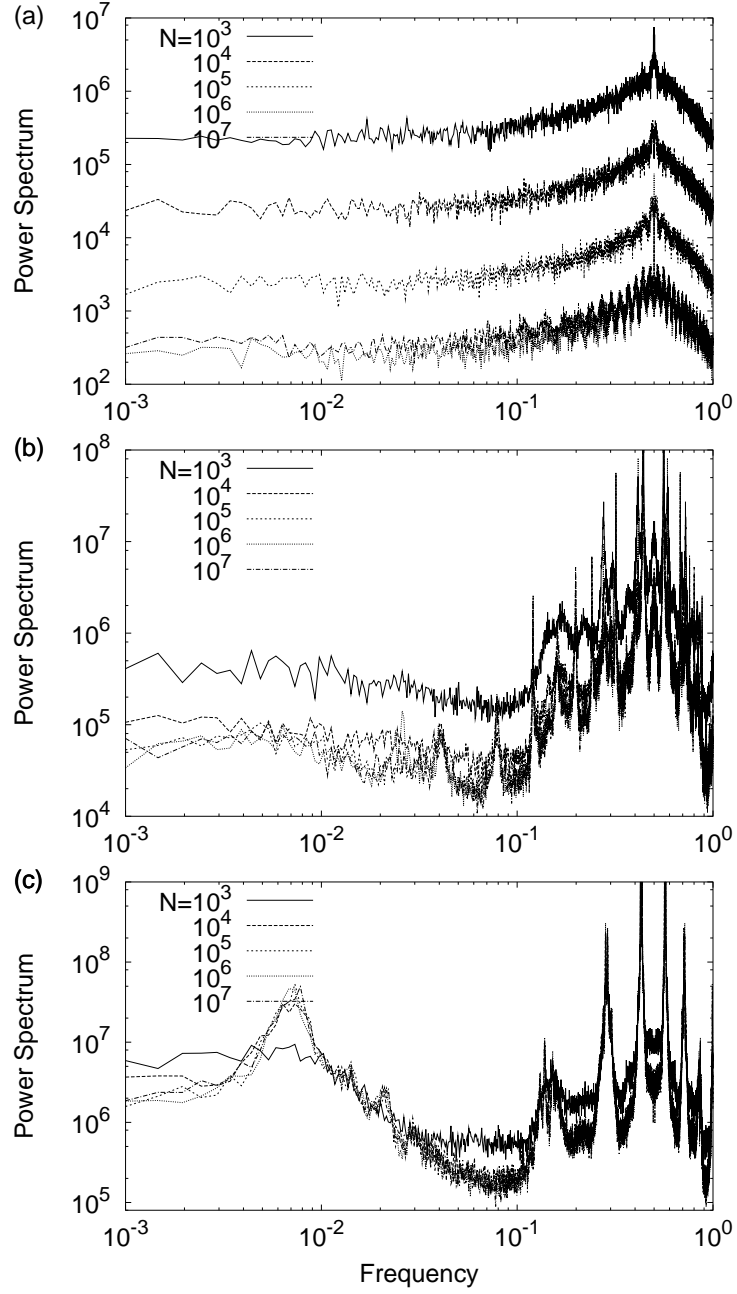


Fig. II.7: Rotation number R of the mean field dynamics, plotted as a function of system size N .

verge to a certain function, as is shown in Fig. II.6.

In Summary, the correlation dimension shows a plateau within the middle scale in Fig. II.6. This plateau corresponds to the lower dimensional dynamics, that is shown in the return maps (Figs. II.2, II.4 and II.5). For larger values of N , the amplitude and the characteristic time scale seemingly converge to certain values, which are characterizations of the collective motions.

Fig. II.8 (following page): Power spectrum for the mean field dynamics with the increase of the system size N . The paramters a , and ϵ are (a) (1.5439343, 0.0001), (b) (1.698440, 0.008) and (c) (1.6962, 0.008).



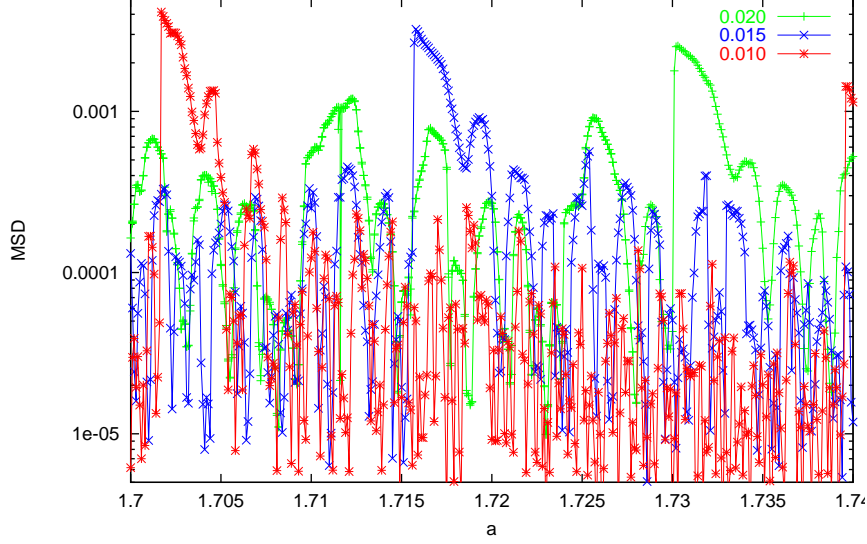


Fig. II.9: Mean square deviation (MSD) of the mean field dynamics is plotted as a function of a . $\epsilon = 0.02, 0.15, 0.01$. $N = 2^{16}$.

II.4 Tongue Bifurcation Structures of Collective Motion

We have seen that the collective motion seems to strongly depend on the parameters. In this section, we will study the dependence of the amplitude of the collective motion on the parameters a and ϵ . Accordingly the global phase diagram of the collective motion will be shown.

In Fig. II.9, the MSD are plotted as a function of the parameter a for several coupling strength ϵ . Here the system size is chosen to be large enough, to see the behavior of the MSD converged in the thermodynamic limit. Two points should be noted here. First, the change of the MSD is not monotonic with a , but is rather complicated. Second, although the change of the MSD is complicated with fine structures, these structures still keep some similarity against the changes of the coupling strength ϵ . For example, a similar but slightly different structure is visible for $a \approx 1.7025$ for $\epsilon = 0.01$, $a \approx 1.715$ for $\epsilon = 0.015$, and $a \approx 1.73$ for $\epsilon = 0.02$.

In Fig. II.10 the parameter dependence of the MSD is plotted on the 2-dimensional (a, ϵ) plane. First, regimes with larger amplitude form tongue-like structures, each of which starts at some point or intervals of parameter a at $\epsilon = 0$, and grows with ϵ . Second, the growth of the edge in a tongue-like structure has a nonlinear dependence on the parameters a and ϵ . Third, for almost all parameter values, the MSD of the mean-field remains finite in the thermodynamic limit.

To see the structure in the parameter space closely, we introduce rescaling of the parameters. For it, we note that each element obeys the following dynamics,

$$x_{n+1} = (1 - \epsilon)(1 - ax_n^2) + \epsilon h_n \quad (\text{II.7})$$

where h_n is the mean-field value at time step n , which can modify the nonlinearity of each element effectively.

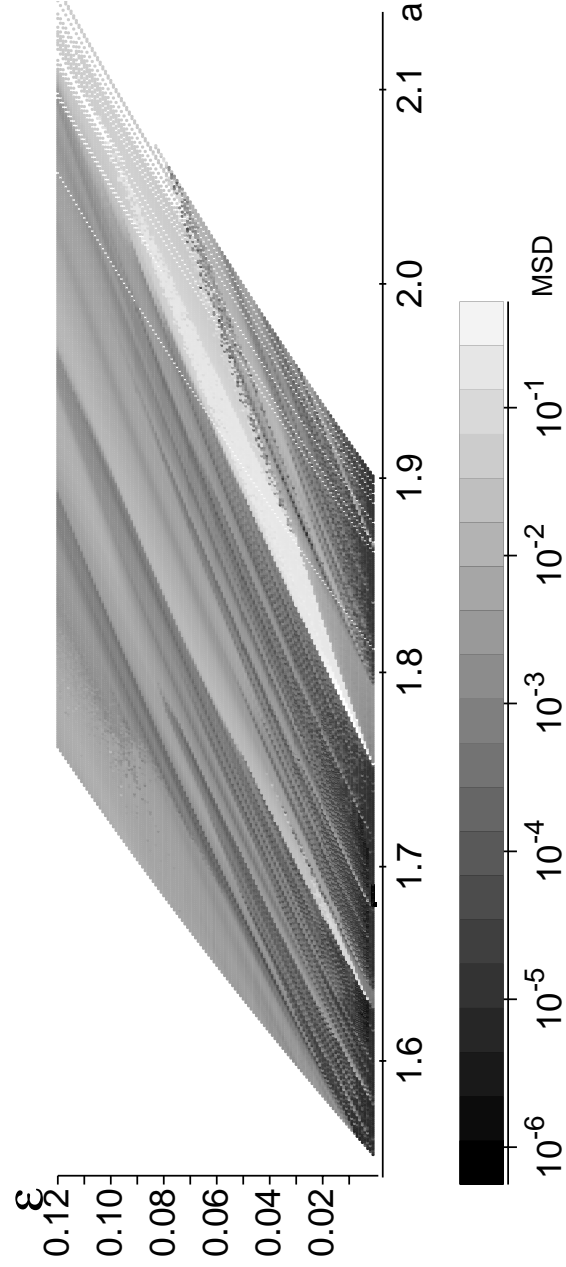


Fig. II.10: Mean square deviation (MSD) of the mean field dynamics is plotted in (a, ϵ) plane with gray scale. The scale shows the value of MSD, where the darkest one corresponds to $\text{MSD} \approx 10^{-6}$, and the brightest one to $\text{MSD} \approx 10^{-1}$.

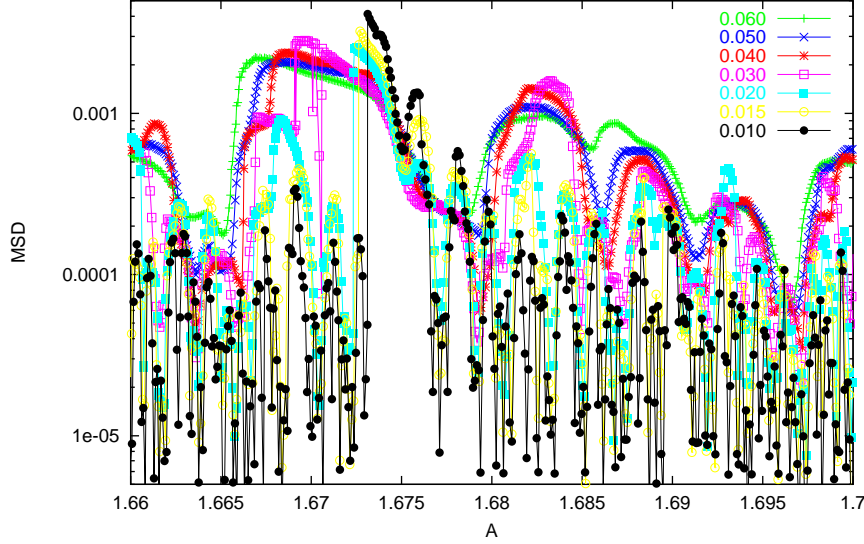


Fig. II.11: Mean square deviation (MSD) of the mean field dynamics h_n are plotted as functions of the effective nonlinearity parameter A .

Usually, the deviation of the mean field around the mean-field average $\langle h \rangle = \lim_{t \rightarrow \infty} \frac{1}{t} \sum_{n=0}^t h_n$ is small. Hence it seems reasonable to normalize the variable x_n so as to separate $\langle h \rangle$ from h_n . Introducing scaled variable,

$$X_n = \frac{x_n}{1 - \epsilon + \epsilon \langle h \rangle}, \quad (\text{II.8})$$

the dynamics of each element is given by,

$$X_{n+1} = 1 - AX_n^2 + \kappa \cdot \delta h_n \quad (\text{II.9})$$

where $\delta h_n = h_n - \langle h \rangle$, and A and κ are called *effective nonlinear parameter* and *effective coupling strength* respectively, given by

$$A = \frac{(1 - \epsilon)(1 - \epsilon + \epsilon \langle h \rangle)a}{\epsilon}, \quad (\text{II.10})$$

$$\kappa = \frac{\epsilon}{1 - \epsilon + \epsilon \langle h \rangle}. \quad (\text{II.11})$$

In Fig.II.11 we have plotted the MSD by adopting the effective nonlinearity parameter A instead of a . Note that similar structures with a different value of a in Fig.II.9 are overlapped around a certain value of A in Fig.II.11. For smaller ϵ , finer structures can be seen in a broader structure for larger ϵ . In Fig.II.12(a) the parameter dependence of the MSD is plotted on the 2-dimensional (A, κ) -plane. Regimes with the collective motion with a larger amplitude (i.e. larger variance) form tongue-like structures (called “tongue bifurcation structure”), each of which starts at some point or interval of parameter A at $\kappa = 0$, and grows with κ .

When the effective coupling strength κ approaches 0, each tongue structure corresponds to a window of the single logistic map (Fig.II.12(b)). For instance, between

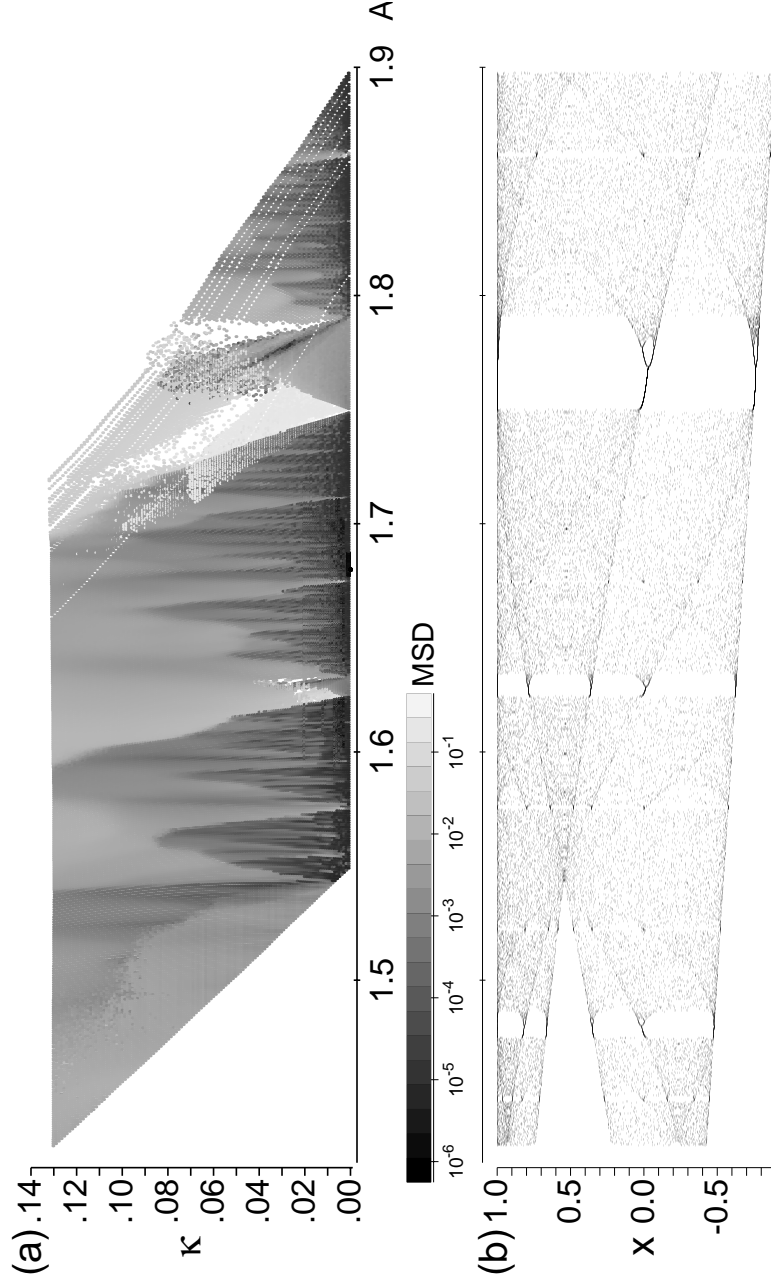


Fig. II.12: (a) The Mean Square Deviation (MSD) of the mean field dynamics is plotted as a function of the effective nonlinearity parameter A and κ . The scale shows the value of the MSD, where the darkest one corresponds to $\text{MSD} \approx 10^{-6}$, and the brightest one to $\text{MSD} \approx 10^{-1}$. (b) Logistic map bifurcation diagram with the increase of the nonlinearity parameter. Horizontal axes are common among two figures.

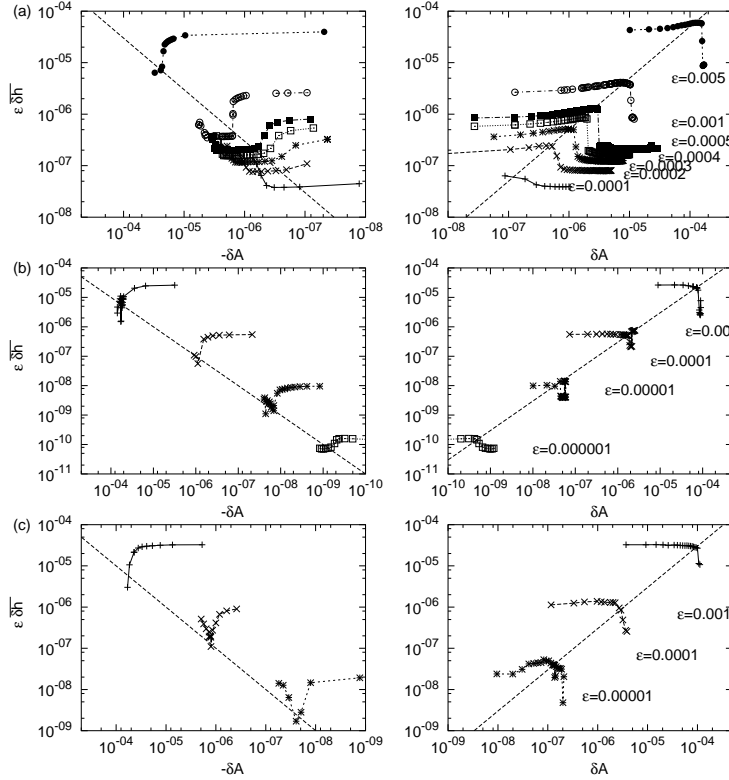


Fig. II.13: Scaling relation of tongue structure for period-2 (a), period-3(b), and period-5(c). $\epsilon\delta h$ are plotted as functions of δA , where $\delta h = \sqrt{\text{MSD}}$ and δA indicate the deviation from (a) the band merging point ($A = 1.5436890126$), (b) the crisis bifurcation point of period-3 window ($A = 1.7903274919$), and (c) the crisis bifurcation point of period-5 window ($A = 1.6333587036$) of the logistic map, respectively. Line in each figure is proportional to δA . Hence, the edge of A in a tongue structure varies linearly with $\epsilon\delta h$. The width of a tongue structure increases proportional to $\epsilon\delta h$.

$A \approx 1.75$ and $A \approx 1.79$ a tongue structure can be clearly seen in Fig.II.12(a), corresponding to the period-3 window of the single logistic map. Although there is a countably infinite number of windows in the parameter space of the logistic map, it is difficult to detect the windows for a longer period numerically. However, it is remarkable that a lot of tongue structures are visible in our model, corresponding to the windows with a longer period⁴.

Fig.II.13 shows the scaling structure of the width of each tongue. In Fig.II.13, the tongue bifurcation structures correspond to the crisis bifurcation point A_0 in the limit $\epsilon \rightarrow 0$ of the period-2 window (band merging point), period-3 window, and period-5 window of the logistic map. The amplitude $\delta h = \sqrt{\text{MSD}}$ is plotted as a function of $\delta A = |A - A_0|$. In Fig.II.13 the lines constitute a region⁵,

$$A_0 - A_1\epsilon \cdot \bar{\delta h}_{A_{\text{small}}} < A < A_0 + A_1\epsilon \cdot \bar{\delta h}_{A_{\text{large}}}, \quad (\text{II.12})$$

⁴ Similar structure has been also observed in a globally coupled tent map (Nakagawa & Komatsu 1998)

⁵ See also Fig.III.12 in Chapter III.

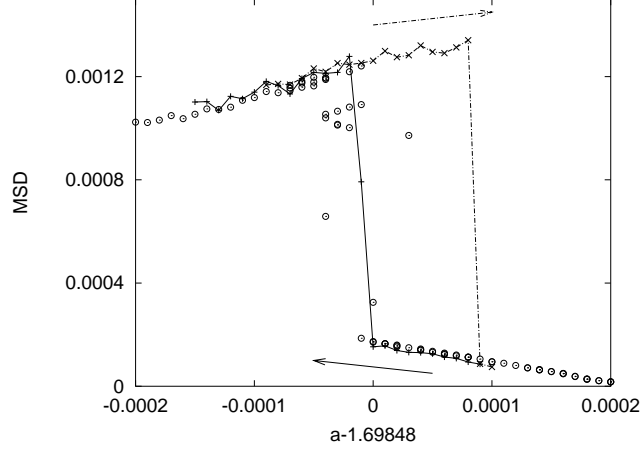


Fig. II.14: Hysteresis curve observed by increasing or decreasing progressively the control parameter a while keeping the final state of a simulation at given a as the initial condition for the neighboring value $a - \delta a(\times)$ and $a + \delta a(+)$. $\epsilon = 0.008$. The MSD calculated starting from a random initial condition is also plotted (\circ).

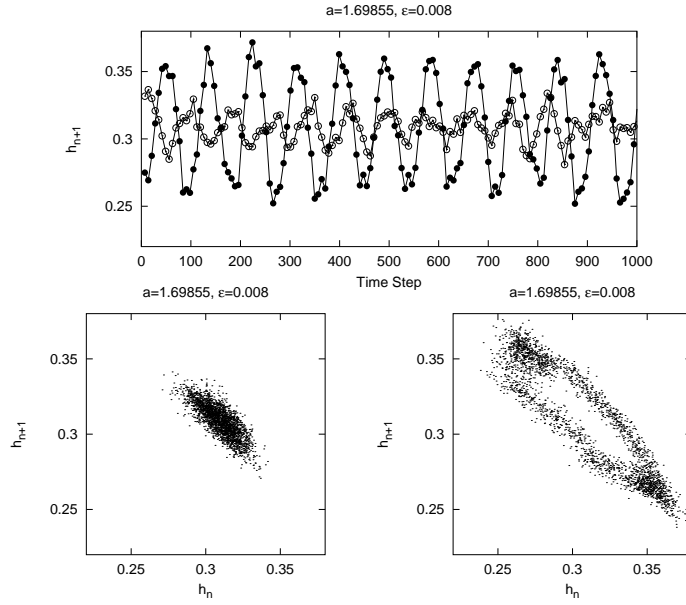


Fig. II.15: Time series and return map for two attractors in Fig.II.14. The parameters are $a = 1.69855$, $\epsilon = 0.008$.

Scaling of Tongue Structures

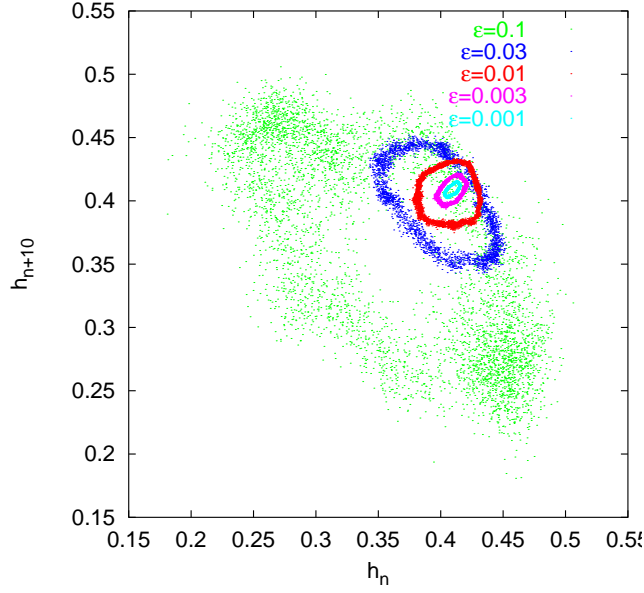


Fig. II.16: Return maps of the mean field values of the same tongue structure (period-2 tongue structure) with a different coupling strength ϵ . In this figure, the collective motions belong to the period-2 tongue structure.

where A_{small} and A_{large} increase linearly with $\epsilon \overline{\delta h}$. As a result, the width of the tongue structure grows linearly with $\epsilon \overline{\delta h}$.⁶

In each tongue structure, further internal structures exist. For instance, the tongue corresponding to period-3 window of the logistic map between $A \approx 1.75$ and $A \approx 1.79$, has three internal structures, roughly speaking. In order to understand the inner structure in each tongue, in Chapter III we shall study the dynamics of each element and its distribution.

Multiple attractors of the collective motion are found in hysteresis phenomena, that can be observed in the parameter space at the edge of the tongue bifurcation structures. In Fig.II.14, the hysteresis curve of the MSD is obtained by increasing or decreasing the control parameter a . For calculation, the final state of a simulation at the previous value of a is used for the next initial condition. Thus in $a - 1.69848 \in [0, 0.0001]$, two different collective motions exist depending on the initial condition. Hence, at least two different attractors coexist depending on the initial condition. In Fig.II.15, the time series and the return map for each attractor are shown⁷.

II.5 Scaling of Tongue Structures

In this section, we study the growth of the amplitude and the width of scattered points with $\epsilon \rightarrow 0$. In addition to these points, we study how the characteristic time scale of the mean field motion changes with ϵ .

⁶ We should note the coupling strength ϵ is so small that $\kappa \sim \epsilon$ and the dependence on κ can be replaced by the dependence on ϵ .

⁷ The topic on the multiple attractor of the collective motion shall be revisited in Chapter VII.

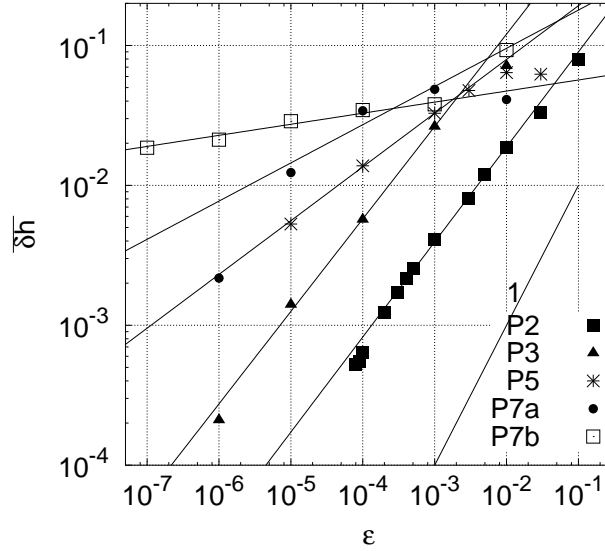


Fig. II.17: From the data shown in Fig.II.13, the maximum values of $\overline{\delta h} = \sqrt{\text{MSD}}$ are plotted. They are obtained by sampling the data of the MSD by changing A in each tongue for a given ϵ .

In Fig.II.16, the return maps of the mean field time series of the period-2 tongue structure are plotted for several values of the coupling strength ϵ . The scaled parameter A for each is almost same and the difference is not significance. In these parameters, the mean-field dynamics shows clear quasiperiodic-like motions.

With the increase of the coupling strength ϵ , the amplitude of the motion becomes large. Although the width around the quasiperiodic-like motions remains finite as is mentioned in Section II.3, the width decreases with the decrease of the coupling strength ϵ .

In Fig.II.17, $\overline{\delta h} = \sqrt{\text{MSD}}$ in a tongue structure is plotted as a function of ϵ for several tongue structures. The growth of $\overline{\delta h}$ obeys a power law relation,

$$\overline{\delta h} = \epsilon^\alpha, \quad (\text{II.13})$$

with the scaling exponent $\alpha < 1$, which depends on each tongue structure⁸.

As to the growth of the amplitude of the mean field, it has been pointed out the linear scaling of $\overline{\delta h}$ with ϵ for the globally coupled logistic map, i.e., $\overline{\delta h} \sim \epsilon$ (Kaneko 1992, Ershov & Potapov 1997), while the present result indicates the deviation from the linear scaling with ϵ . This deviation is considered to be due to the following distinction. Whereas we have paid attention mainly to tongue structures corresponding to windows of the logistic map, such window structures in the logistic map are out of consideration in Ershov & Potapov (1997)⁹. Possible differences between the collective motions originating will be discussed at the end of this Chapter again.

⁸ We should note that it is possible to take a proper limit of $\epsilon \rightarrow 0$ in a tongue structure, sustaining the high-dimensional chaotic motion. For example, take the limit as the scaled parameter A keeps the value at the crisis bifurcation point of the logistic map. In this way, the above scaling behavior is checked keeping the high-dimensional chaotic motion.

⁹ Our analysis is based on the rescaled parameter A . Although in the previous studies (Kaneko 1992, Ershov & Potapov 1997) a was used, the difference will not be essential for small ϵ .

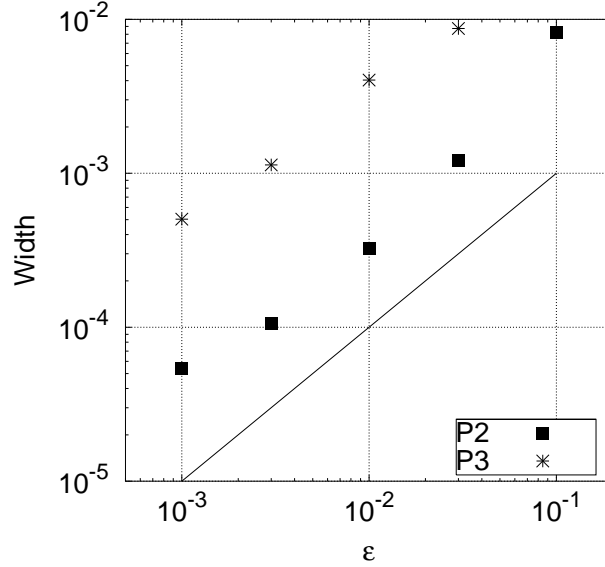


Fig. II.18: Width around the torus-like motion of the collective motion is plotted as a function of ϵ . The width increases in proportion to ϵ^1 .

Next we consider the width around torus-like motion. In Fig.II.18, the width around the quasiperiodic-like motions is plotted as a function of ϵ for several tongue structures. First we should note that not only quasiperiodic-like motions but also a variety of the mean field motion exist as is shown in Section II.3. However, here we focus only on the quasiperiodic-like mean field motions, where the width around the quasiperiodic-like motion can be relatively easily measured¹⁰. As is shown in Fig.II.18, the width decreases with the decrease of ϵ . And the growth is scaled in proportion to ϵ^1 . Remembering that the amplitude of the collective motion is growth as Eq.(II.13) with the scaling exponent $\alpha < 1$, in the small coupling regime, the torus-like motion becomes finer with the decrease of ϵ .

The much longer time scale of the mean field dynamics than the dynamics of an element is an important characteristic of the collective motion, as is shown in Fig.II.3. Asymptotic behavior of these time scales with $\epsilon \rightarrow 0$ is also an interesting problem. In Fig.II.19, the frequency of the slow component is computed from the peak of the power spectrum, and is plotted as a function of ϵ for each tongue structure¹¹. The shorter time scales are independent of ϵ , and are not shown in the figure. The longer time scales get even longer with $\epsilon \rightarrow 0$, as $\sim \epsilon^{-\beta}$, where the exponent $\beta > 0$ depends on each tongue structure. Hence, it is implied that the characteristic time scale becomes arbitrary long with the coupling strength ϵ goes to zero.

Is there any relation between the scaling relation of the amplitude and of the characteristic time scale? The exponents of α for the amplitude and β for the characteristic time scale are plotted in Fig.II.20. The exponents seems to indicate a certain relation as $\beta = -0.5\alpha + 0.5$. However, further studies will be needed to clarify this relation.

¹⁰ The method to measure the width around the torus-like motion will be described in Chapter V.

¹¹ Here the value A for each tongue structure is chosen so that $\delta\hbar$ is maximized for a given ϵ , although dependence of the frequency on A is not significant.

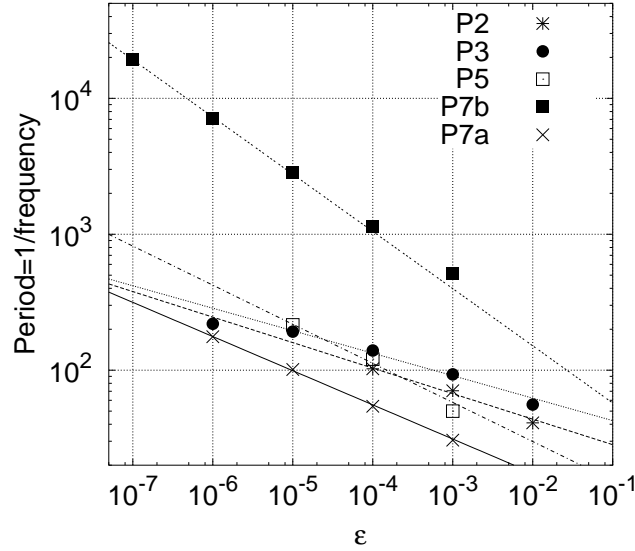


Fig. II.19: The longer time scales of the mean field dynamics are plotted as a function of ϵ . They are obtained from the power spectrum for the parameter with maximum MSD value in the period-2, 3 and 5 tongue structure for a given ϵ .

II.6 Summary and Discussion

In this Chapter, we have studied collective motion in the desynchronized state of the globally coupled logistic map. It is shown that collective motion with a much longer time scale and lower dimension can emerge at a macroscopic level. The dependence of the amplitude of the collective motion on a and ϵ is studied. After some change of variables and parameters, tongue structures are clearly seen in (A, κ) -plane. Each tongue structure corresponds to a periodic window of the logistic map.

With the increase of the coupling strength ϵ , each tongue structure grows in proportion to $\epsilon \cdot \bar{\delta h}$, where $\bar{\delta h}$ is the amplitude of the mean field variation. Hence the width of each tongue would increase with ϵ^2 , if $\bar{\delta h} \propto \epsilon$ would hold. In contrast with earlier studies (Kaneko 1992, Ershov & Potapov 1997) supporting this linear scaling, our calculation suggests that the scaling may obey a different power law. (See also the arguments below)

The tongue structure is based on the underlying windows of the single logistic map. Windows exist in any neighborhood of the parameter space of the single logistic map. The tongue bifurcation structures expands with the increase of ϵ from each window of the single logistic map at $\epsilon = 0$. So, the tongue structure is expected to occupy a relatively large region in the parameter space. This is one of the reasons why we have focused our attention on the collective behavior in the tongue structures. Still, we have to note that there is a positive measure in the parameter space of the logistic map, corresponding to chaos. Hence, at least for small coupling in the GCM, there are parameters with a positive measure which do not belong to any tongue structure. Indeed, we have observed that the amplitude of the mean-field variation drops less than to 0.1 (see Fig.II.11), at the parameter where the tongue structure disappears. Although no clear structure in the return map is detected there, this motion still indicates some

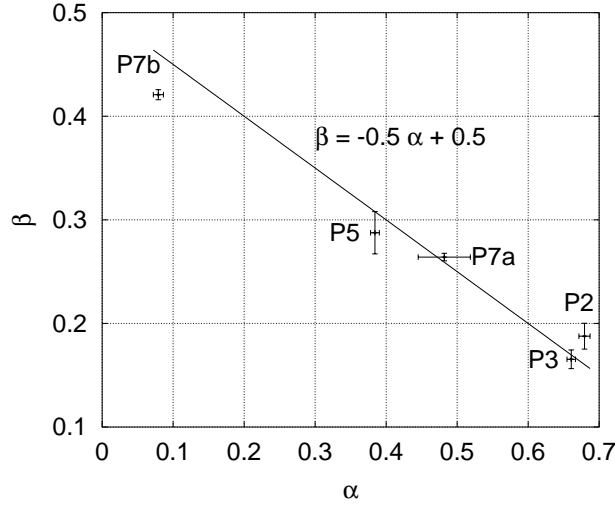


Fig. II.20: The exponents α and β are plotted. The line illustrated in the figure is roughly estimated from the data.

coherence among elements and is distinguishable from noise¹².

Analytical estimation of the mean field dynamics obtained by S. V. Ershov, et al. (Ershov & Potapov 1997) is based on singularities of distributions. Only the fluctuation due to singularities of the probability distribution function is taken into account by neglecting regular parts of the probability distribution function. Our result may imply that the regular parts, which are relevant to the windows of local mapping, should be taken into account for the collective motion. Careful analysis of both the regular and singular parts may be required. This might be the reason why the scaling of δh is different from Ershov's estimation. We will see in the next chapter the relation between the mean field fluctuation and the singularity in the distribution function.

However, as we have noted above Ershov's analysis is applied to the collective dynamics originated in the chaotic regime of the single logistic map. In Fig.II.21, the square root of MSD of the collective motion originated in the chaotic regime is plotted as a function of the coupling strength ϵ . The nonlinear parameter a is chosen such that the scaled nonlinear parameter A gives agreement with the nonlinear parameter of the logistic map, which corresponds to chaotic points¹³. The plot suggests the linear scaling of the amplitude with the coupling strength ϵ , that agrees with the Ershov's estimate.

Accordingly, we may outline a scenario as follows. On one hand, the finite interval in the parameter a for a given ϵ corresponds to the tongue structures. In this parameter region, the scaling relations depends on each of the tongue structure. On the other hand, there are points in the parameter a which do not belong to any tongue structure. In this regime, the scaling relation of the amplitude obeys the linear scaling of the coupling strength ϵ . Since such parameters do occupy not a finite domain but points in the parameter a , such regime may constitute boundaries of the tongue structures.

Even if the elements are completely desynchronized from each other, for some

¹² Kaneko called this coherence 'hidden coherence' (Kaneko 1990b, 1992).

¹³ Indeed, the parameter in the logistic map generating a chaotic orbit does not have width, while such parameters have a positive measure (Collet & Eckmann 1980).

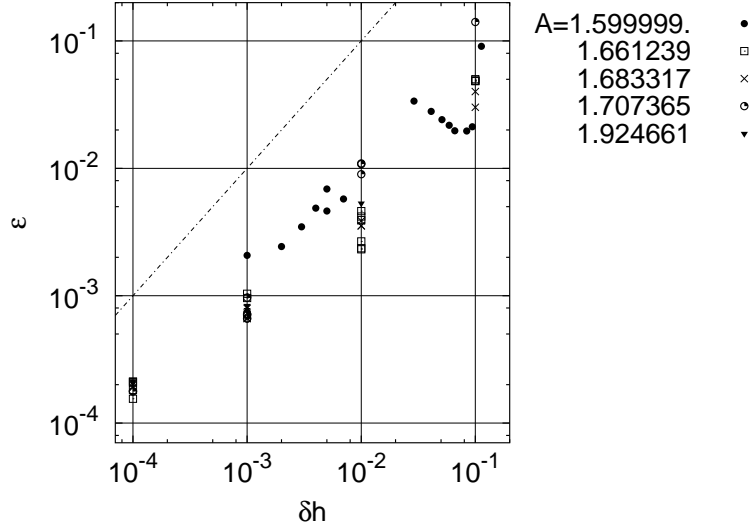


Fig. II.21: The MSD of the mean field distribution is plotted as a function of ϵ . The nonlinear parameter a is chosen such that the scaled parameter A comes to be near the chaos parameter of the logistic map. The scaled parameter A is indicated at the right of the figure.

case, some kind of predictability may emerge in the macroscopic variables, although all the Lyapunov exponents are positive. It might be also important to study how the predictability of the collective motion reflect on N -dimensional phase space structure or on microscopic quantities, such as the Lyapunov spectrum. With such study, the mechanism for the collective motion must be clearly distinguishable from the self-organization mechanism (Nicolis & Prigogine 1977) or the slaving principle (Haken 1978). Although we have presented a heuristic way to extract such dynamics in the present paper, it is hoped that a systematic method to characterize collective motion shall be developed. So far, we have no conventional tool for detecting the lower dimensional collective signals out of high dimensional signals. In Chapter V, we will develop a tool to distinguish and characterize several collective dynamics in GCM.

CHAPTER III

INSTABILITY OF STATIONARY STATE AND GENESIS OF COLLECTIVE MOTION

Stability of the stationary state of the globally coupled map in the fully desynchronized state is studied. It will be shown that the fixed point solution of the mean field dynamics is unstable. Based on this analysis, the scaling relation of the amplitude will be studied. Next, we shall demonstrate the origin of the slow motion of the collective motion. The mechanism of the bifurcation of the collective motion will be also investigated.

III.1 Introduction

As we have seen in the preceding Chapter, the mean field dynamics of globally coupled map (GCM) given by Eq.(II.1) oscillates, instead of converging to a fixed point. This implies that the distribution function of the elements does not also remain stationary but depends on time. The probability distribution function in the thermodynamic limit ($N \rightarrow \infty$) is defined as

$$\rho_n(x) = \lim_{N \rightarrow \infty} \frac{1}{N} \sum_i \delta(x - x_n(i)). \quad (\text{III.1})$$

In Fig.III.1, the evolution of the probability distribution function is shown, using numerical calculation. Indeed, the figure indicates that the distribution function is not stationary but oscillates in time. Thus, the collective motion indicated by the mean field dynamics means that the stationary state of the distribution function is *unstable*. As is shown in the preceding Chapter, the collective motion is quite common in GCM. Hence, the instability of the stationary distribution function may be a general characteristic of GCM.

In the next Section, we shall study the linear stability of stationary states in GCM. In general, it is quite difficult to discuss the stability of the distribution function. However, focusing our attention only on a characteristic structure of the distribution function, which is a common structure of the present GCM, we will study the stability of the mean field dynamics around a stationary fixed point.

The parameters for Fig.III.1 belong to the tongue structure in the period 3 window. Since the mean field dynamics has a component of period 3, the density in the figure is

This chapter is partly based on Shibata & Kaneko (1998b, Section 6 and 7).

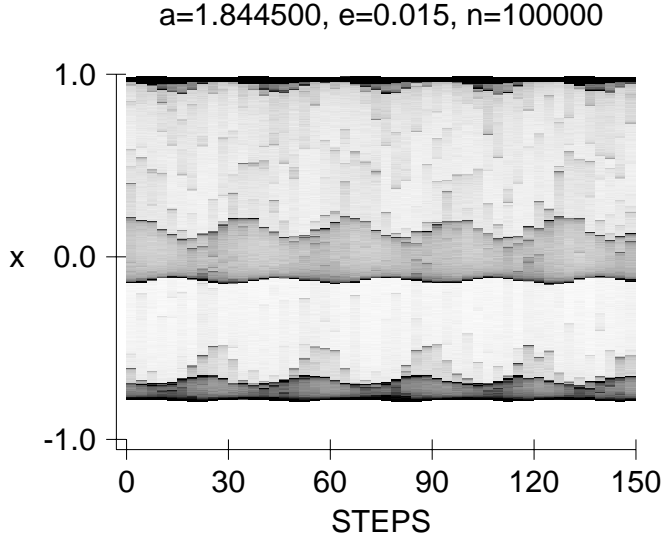


Fig. III.1: The distribution dynamics is plotted as a function of time. The density is shown with the use of a gray scale. The darker region indicates the higher density. The parameters are $a = 1.8445, \epsilon = 0.015, N = 10^5$.

plotted every third step in order to see the slow modulation of $\rho_n(x)$. Due to the chaotic oscillation of each element (the mixing property of the mapping), the distribution function spreads over $x \in [-0.8, 1.0]$. However, the distribution is not monotonous, and has some structure. The density is relatively large in the three regions around $x \approx 1.0$, $x \approx 0.0$ and $x \approx -0.8$. This number *three* is the period of the window in the logistic map for the corresponding tongue structure. The number of elements in each of the three regions oscillates in time, and the phase of each oscillation is mutually different. In Section III.4 we will briefly describe how the collective motion is formed, focusing on the tongue structure.

III.2 Instability of Stationary State

First we study the linear stability of stationary states of GCM (II.1).

In the present GCM (II.1), since the coupling among the elements is given by the mean field,

$$h_n = \int f(x) \rho_n(x) dx, \quad (\text{III.2})$$

the evolution of the distribution function $\rho_n(x)$ is written as

$$\rho_{n+1}(x) = \int dy \delta(F_n(y) - x) \rho_n(y), \quad (\text{III.3})$$

with $F_n(x) = (1 - \epsilon)f(x) + \epsilon h_n$. Eq.(III.3) is called (Self-Consistent) Perron-Frobenius equation¹ (Kaneko 1992, Pikovsky & Kurths 1994b).

For the GCM of the logistic map, the stability of the stationary solution of this equation has been discussed by Kaneko (1995), and Ershov & Potapov (1997). (Perez

¹ Sometimes, it is called Frobenius-Perron equation.

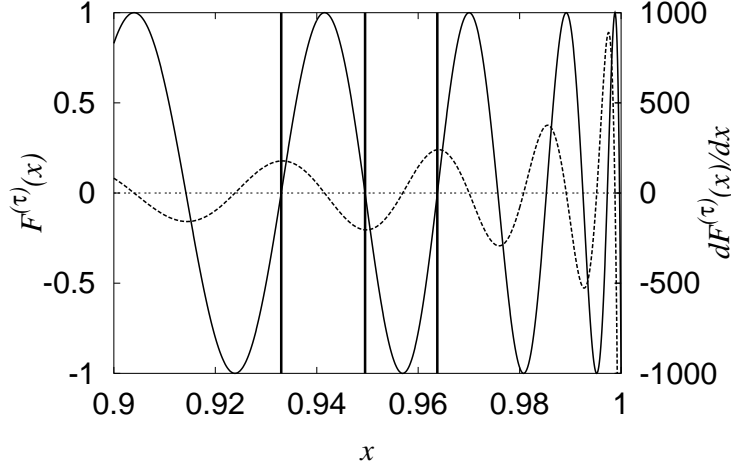


Fig. III.2: $F^{(\tau)}(x)$ (line) and $dF^{(\tau)}(x)/dx$ (dotted line) are plotted as a function of x . (In this figure, $\tau = 6$). The red lines indicates the points such that $F^{(\tau)}(x) = 0$, where the region is partitioned.

& Cerdeira (1992) also discussed the instability of the stationary state, though their analysis was not based on the Perron-Frobenius equation). For the globally coupled tent map case, where the local mapping is given by $f(x) = 1 - a|x|$, the stability of the stationary state has also been discussed more theoretically by Just (1995), Ershov & Potapov (1995), Morita (1996), and Chawanya & Morita (1998).

Here, we will study the linear stability of the mean field values of the GCM of logistic map, according to Chawanya & Morita (1998) (which is studied for the tent map case, though). Although shape of the distribution function depends strongly on the parameters, we focus only on a characteristic structure of the distribution function of the present GCM. The characteristic structure of the present GCM is the inverse square-root singularity. This means that we discuss the asymptotic behavior of a small displacement of the mean field value around a fixed point with increasing time.

The fixed point of the mean field value is given by $h_0 = \int f(x)\rho_0(x)dx$, where $\rho_0(x)$ is a fixed point solution of Eq.(III.3), i.e., $\rho_0(x) = \int dy\delta(F(y) - x)\rho_0(y)$ with $F_0(x) = (1 - \epsilon)f(x) + \epsilon h_0$. If we consider small deviation η_n of h_n from h_0 , i.e., $\eta_n = h_n - h_0$, the evolution of η_n is given by

$$\eta_n = \sum_{\tau=1}^{\infty} L_{\tau}\eta_{n-\tau} + O(\eta^2), \quad (\text{III.4})$$

where L_{τ} is a linear coefficient to give the linear response of the mean field value at n step to the displacement at $n - \tau$ step.

Let us first estimate the coefficient L_{τ} . From Eqs.(III.2) and (III.3), L_{τ} is given by

$$L_{\tau} = \epsilon \int dx \frac{dF^{(\tau)}(x)}{dx} \rho_0(x), \quad (\text{III.5})$$

where $F^{(\tau)}(x) \equiv \underbrace{F \circ \dots \circ F}_{\tau}(x)$ with

$$F(x) = (1 - \epsilon)f(x) + \epsilon h_0. \quad (\text{III.6})$$

Instability of Stationary State

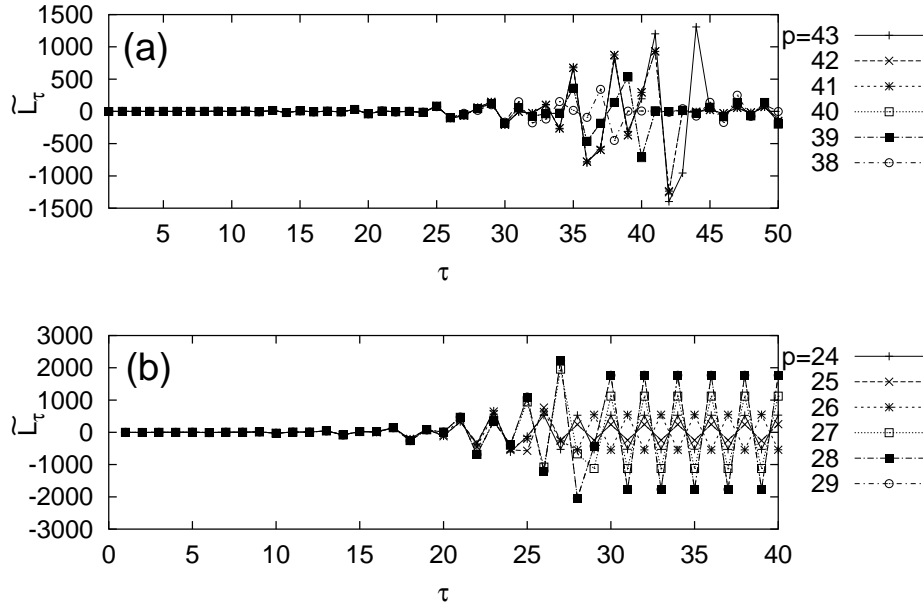


Fig. III.3: The linear coefficient \tilde{L}_τ is plotted as a function of τ . The parameter is (a) $a = 1.5443690$ or (b) $a = 1.839286755$. For the numerical calculation, first we constructed the partition with the partition points given by $\{0, f^{-1}(0), \dots, f^{-p}(0)\}$. Then, the transition matrix among the partitions is obtained from $f(x)$. In this way, the markov partition is approximately constructed. Using this markov partition, $df^{(\tau)}(x)/dx$ and $\rho_0(x)$ is obtained numerically. p is indicated at the right hand side of the figures.

When τ is small, L_τ may strongly depends on the parameters. On the other hand, for sufficiently large τ , as will show in the following, it is expected that the value of L_τ shows similar behavior asymptotically.

For $\tau \gg 1$, the value of $F^{(\tau)}(x)$ oscillates along the x -axis quite frequently. Consider the partition of x at the points such that $F^{(\tau)}(x) = 0$ (see Fig.III.2). Denoting the typical value of $|\frac{dF^{(\tau)}(x)}{dx}|$ by $d(\tau)$, the interval of partitions is estimated at $1/d(\tau)$. With the increase of τ , the number of points such that $F^{(\tau)}(x) = 0$ grows quite rapidly, and $1/d(\tau)$ decreases exponentially. If $\rho_0(x)$ is constant in a partition, the integration of Eq.(III.5) in this partition is zero (see Fig.III.2). Hence, the partitions where $\rho_0(x)$ changes drastically contribute to the estimation of L_τ much more than the partitions where $\rho_0(x)$ does not change so much.

In the present case, the most drastic change of $\rho_0(x)$ comes from the inverse square-root singularity, which is the characteristic structure of distribution function for the logistic map. The integration in the partitions containing the characteristic structure is estimated at

$$\int_c^{c+1/d(\tau)} \frac{dF^{(\tau)}(x)}{dx} \rho_0(x) dx \approx \int_c^{c+1/d(\tau)} d(\tau) |x - c|^{-\frac{1}{2}} dx \sim \sqrt{d(\tau)}, \quad (\text{III.7})$$

where c is a certain point of x . On the other hand, since $d(\tau)$ is considered as the

Instability of Stationary State

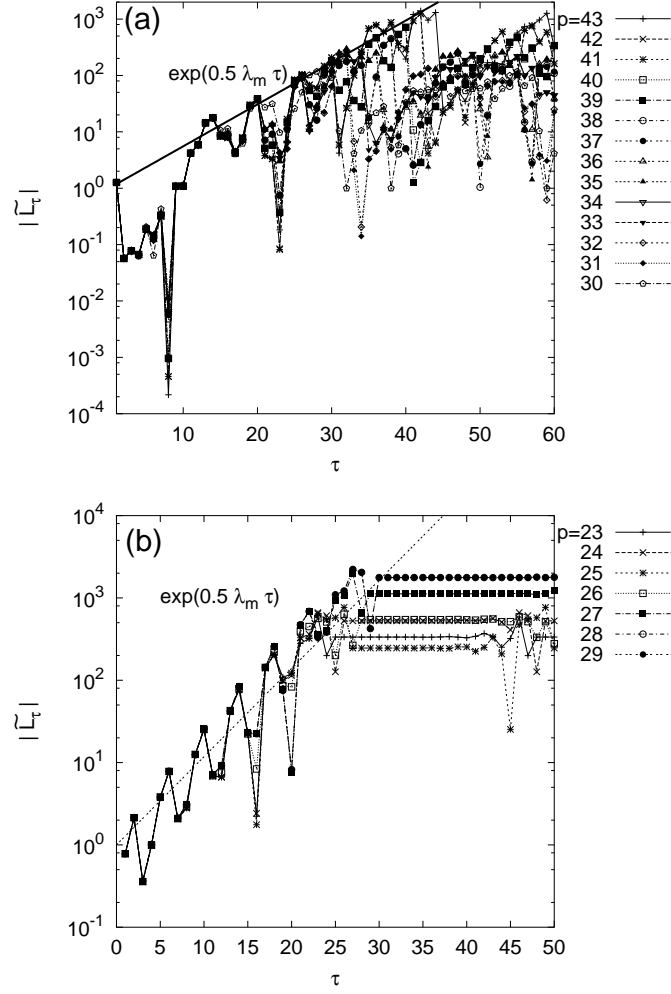


Fig. III.4: The linear coefficient $|\tilde{L}_\tau|$ is plotted as a function of τ . The parameter is (a) $a = 1.5443690$ or (b) $a = 1.83928675$. The Lyapunov exponent of $f(x)$ is obtained numerically. p is indicated at the right hand side of the figures. For $\tau < p$, \tilde{L}_τ seems to grow exponentially, while for $\tau > p$, \tilde{L}_τ does not grow exponentially. However, \tilde{L}_τ for several p constitutes an envelop, whose slope indicates $\frac{1}{2}\lambda_m$ in the semi-log plots.

average of expansion rate, $d(\tau)$ is roughly estimated at²

$$d(\tau) \sim e^{\lambda_m \tau}, \quad (\text{III.8})$$

where λ_m is the Lyapunov exponent of the mapping $F(x)$. Consequently, the coefficient of response L_τ to the perturbation grows exponentially with the rate $\frac{1}{2}\lambda_m$ as³

$$L_\tau \sim O(\epsilon e^{\frac{1}{2}\lambda_m \tau}). \quad (\text{III.9})$$

In Fig.III.3, instead of L_τ , the coefficient $\tilde{L}_\tau = \int dx \frac{df^{(\tau)}(x)}{dx} \rho_0(x)$ obtained numerically is plotted as a function of τ . (See also the caption of Fig.III.3 for the method of numerical calculation in detail). Although the \tilde{L}_τ is obtained from $f(x)$ instead of $F(x)$, notice that L_τ is essentially given by $L_\tau = \frac{\epsilon}{1-\epsilon} \tilde{L}_\tau$ when ϵ is small⁴. In Fig.III.4, $|\tilde{L}_\tau|$ is plotted. $|\tilde{L}_\tau|$ grows exponentially with the rate $\frac{1}{2}\lambda_m$ asymptotically, though some deviation from Eq.(III.9) is observed for small τ . Thus, the above estimation (III.9) is here numerically confirmed.

Let us back to Eq.(III.4). In order to study the linear stability of the stationary state, we need to analyse the eigenvalues of the coefficients $\{L_\tau\}$. If there exists the eigenvalue larger than unity, the stationary state is then linearly unstable. From the above estimation, the value of $\sum^\infty |L_\tau|$ diverges exponentially. Consequently, it is expected that the eigenvalue larger than unity exists, and the stationary state is linearly unstable even if the coupling strength ϵ is arbitrary small.

III.3 Scaling of Fluctuation

In the preceding Section, we estimate the growth rate of an infinitesimal perturbation around a stationary state. In the estimation, we take the contribution into account only from the singular part of the distribution function. Based on the above discussion, we can consider a rough estimation of the asymptotic amplitude of the mean field motion.

Due to a perturbation applied to the mean field, the displacement in the distribution function is expanded exponentially. The growth rate of this expansion is considered as the Lyapunov exponent of the local mapping. After the magnitude of the displacement in the distribution function reaches the order of unity, however, the displacement starts to decay and the information of the perturbation disappears. When the magnitude of the perturbation is $\epsilon\eta$, such a time scale τ_c is estimated at $\tau_c = -\log(\epsilon\eta)/\lambda_m$. Thus, the exponential growth of the perturbation given by Eq.(III.9) may be valid within the order of $O(\tau)$ time steps.

Then, from Eq.(III.4), the displacement η_n is estimated at $\eta_n \sim O(\sqrt{\epsilon\eta_{n-\tau_c}})$. Considering to average over the possible displacements, the asymptotic amplitude $\langle\eta\rangle$ of the mean field motion is given by $\langle\eta\rangle \sim O(\epsilon)$.

This rough estimation gives agreement with the result given by Ershov & Potapov (1997). Moreover, in the preceding Chapter, we have presented the scaling relation of the amplitude, obtained numerically, whose scaled nonlinear parameter corresponds to

² Here we neglect the fluctuation of the expansion rate.

³ This relation (III.9) can be generalized for the globally coupled logistic type maps with $f(x) = 1 - a|x|^\alpha$ ($\alpha \geq 1$), as $L_\tau \sim O(\epsilon e^{(1-\frac{1}{\alpha})\lambda_m \tau})$. (T. Chawanya 1998, private communication)

⁴ We can also consider that $f(x)$ in \tilde{L}_τ is given by $1 - Ax^2$ with the effective nonlinear parameter $A = (1-\epsilon)(1-\epsilon+\epsilon h_0)a$.

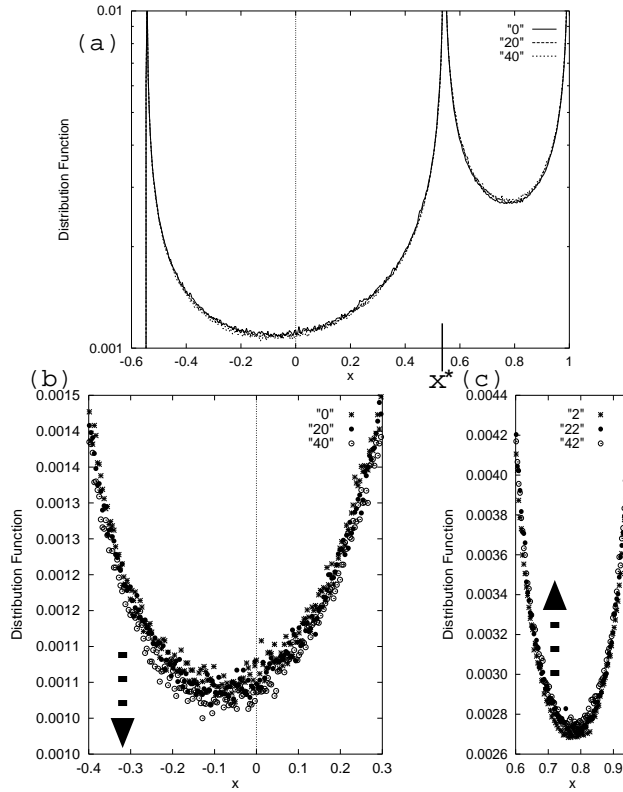


Fig. III.5: The distribution functions at time $n = 0(*)$, $20(\bullet)$, $40(o)$ are shown.

the chaotic regime of the logistic map (Fig.II.21). This numerical result suggested the linear scaling with ϵ . The present estimation also agrees with this numerical result.

Notice again that in this estimation we consider the contribution only from the singular part of the distribution function. Remember that the deviation from this linear scaling has been observed within the tongue structure, in which the coherent motion with lower-dimension-like structure such as torus is often found. The deviation implies that it is not enough to evaluate only the singular part for considering such low-dimensional slow motions.

III.4 Collective Behavior Through Self-Consistent Dynamics

It is interesting to study the collective dynamics as an interference between mean field dynamics and individual elements. Before we present a scenario for slow collective motion, we show the formation of self-consistent dynamics between the mean field dynamics and individual elements.

For simplicity, we adopt the case, in which the effective nonlinear parameter A is near the period-two band merging point. The time series and the return map are given in Fig.II.2. The distribution function is given in Fig.III.5 every twentieth step. In this case, distribution of elements can be divided into two regions around $x^* \approx$

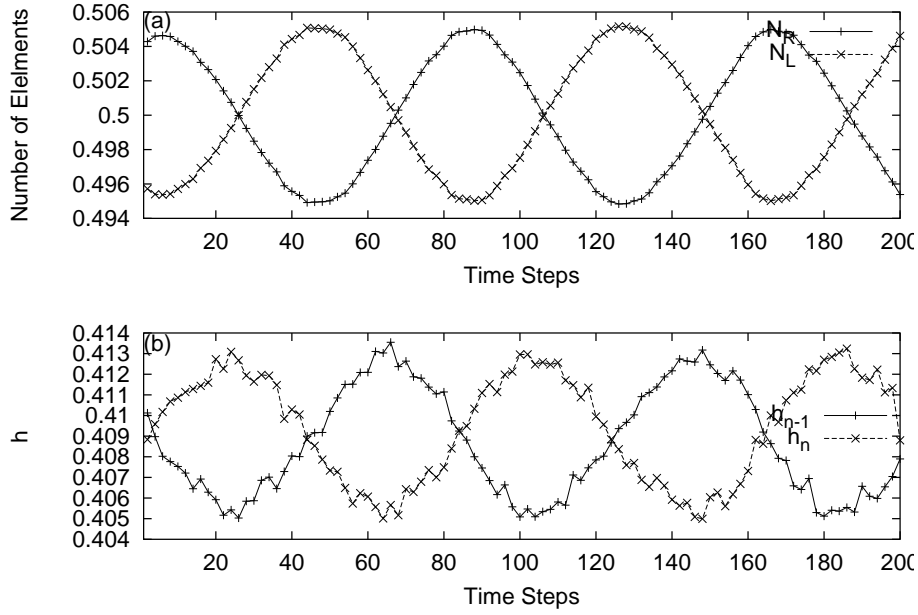


Fig. III.6: (a) Time series of the number of elements in the 2 regions, (b) time series of the mean field. $a = 1.5449205$, $\epsilon = 0.0005$, $N = 10^6$.

0.54. During these forty time steps the density at the left region ($x < x^*$), given in Fig. III.5(b), decreases with time, whereas the density in the other region plotted in Fig. III.5(c) increases with time. Although the change of the distribution is quite small, there is a systematic oscillation (cf. Fig. III.10).

Consider the density dynamics in each of the two regions. In Fig. III.6(a), the density in each region, N_L and N_R are plotted as a function of time. N_L denotes the probability in the region smaller than x^* in Fig. III.5, and $N_R (= 1 - N_L)$, i.e., $N_L = \int_{x < x^*} \rho_n(x) dx$, and $N_R = \int_{x > x^*} \rho_n(x) dx = 1 - N_L$. (The definition for each region is given below in detail). The distribution in each region oscillates in time. In Fig. III.6(b), the mean field time series h_{n-1} and h_n are plotted at every two steps, since the mean field has a period-two component. The mean field also oscillates in time with the same period as N_R , and N_L , but the phase of the mean field oscillation is different from that of the population dynamics in Fig. III.6(a).

To see how the mean field dynamics and the distribution dynamics interfere with each other, we have constructed a return map of the above two quantities. Fig. III.7 gives a return map of the distribution dynamics and the mean field dynamics. This figure implies that a self-consistent dynamics is formed as follows,

$$\begin{cases} \tilde{h}_n &= \tilde{h}(\tilde{h}_{n-1}, \tilde{N}_{n-1}), \\ \tilde{N}_n &= \tilde{N}(\tilde{h}_{n-1}, \tilde{N}_{n-1}), \end{cases} \quad (\text{III.10})$$

where each \tilde{h} and \tilde{N} is a function of $\tilde{h}_n = h_{n-1} - h_n$ and $\tilde{N}_n = N_L - N_R$. If the mean field would be an external force for each element, the population would respond to the mean field value. Since the distribution organizes the mean field dynamics, the collective motion can be described as a self-consistent relation between the distribution dynamics and the mean field dynamics.

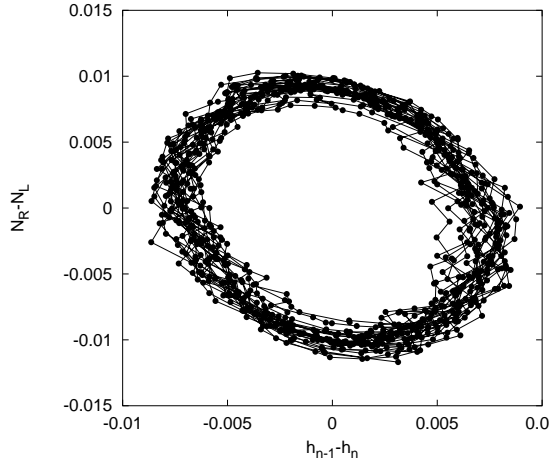


Fig. III.7: Return map of the time series of number of elements in the 2 regions and time series of the mean field, plotted per two steps for even n and odd n . $a = 1.5449205$, $\epsilon = 0.0005$, $N = 10^6$.

From the above viewpoint, we demonstrate now how the distribution is modified as the mean field varies slowly.

If the mean field would be an external force for each element, we could study the dynamics of each element as the logistic map with an external force. This is valid if the mean field varies slowly. In this case, the equation of motion for each element is given by,

$$x_{n+1} = F_n(x_n), \quad (\text{III.11})$$

with

$$F_n(x) = (1 - \epsilon)(1 - ax^2) + \epsilon\langle h \rangle + \epsilon\delta h_n. \quad (\text{III.12})$$

If we would not take δh_n into account, the dynamics of each element would be the same as the dynamics of the logistic map. Since each tongue structure has good correspondence with a window of the logistic map as shown in Section II.4, we focus on the window structure of the logistic map. In the single logistic map, the period p window starts at the tangent bifurcation point of the p 'th iterate of the map, and then the period doubling bifurcation proceeds with the increase of a , until the window ends up by crisis (see Fig.III.8). In this case, the probability distribution is stationary, and hence, the probability that an element takes a value out of p distinct regions is $\frac{1}{p}$.

Now, take δh_n in Eq.(III.12) into account as an external force. The bifurcation of the perturbed logistic map (III.12) has a crucial difference from usual bifurcation of the logistic map. In Fig.III.9, examples of the third iterates of the map with external force are shown. In Fig.III.9(a) the region around $x \approx 0$ can attract the elements, while the two regions around $x \approx 0.95$ and $x \approx -0.75$ cannot. In Fig.III.9(b)(c), while three regions cross the line $y = x$, one or two of the regions collapses due to crisis. At the tangent bifurcation, the map $y = F_n^{(3)}(x)$ is tangential to $y = x$ at only one point. This is in strong contrast with the logistic map without external force, where tangent bifurcation or crisis occurs at 3 points of x at the same value of a and ϵ for the period 3 window.

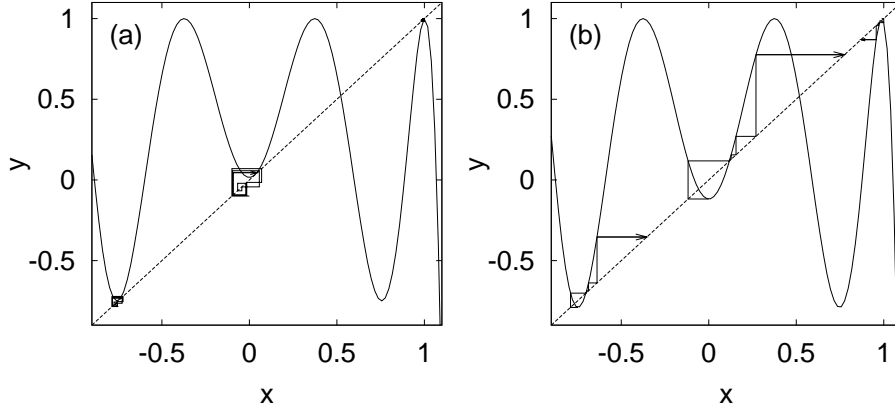


Fig. III.8: Behavior of the third iterate of a logistic map. (a) After tangent bifurcation at three points, and (b) after crisis. Solid lines with arrow indicate iterated trajectories starting from three points.

In general, consider a period p window. In the presence of the external force, for each of the p points in the p 'th iterate of the map (III.12), the tangent bifurcation, or crisis occurs at different value of a and ϵ . Hence, the number of distinct attractors can be less than p , and depending on a and ϵ . Even if the elements are attracted into p distinct regions, the probability for each of p distinct regions is not equal to $\frac{1}{p}$.

As we have seen in the previous section, slow modulation of the mean field leads to the dynamics of the distribution. With the slow modulation of δh_n in time, the behavior of each element changes as well. In other words, with the change of δh_n , bifurcation can occur in the effective map for each element,

$$F_n^{(p)} = F_n \circ F_{n-1} \circ \cdots \circ F_{n-p+1}, \quad (\text{III.13})$$

which is the p 'th iterate of the map Eq.(III.12). Since δh_n changes over time, such bifurcation occurs in time. To distinguish this bifurcation from the notion of bifurcation in parameter space, this type of bifurcation is called *internal bifurcation*⁵.

To characterize the effective map at every p time steps, we introduce the invariant measure $P_n^{(p)}(x)$ at time n determined by the solution of the Perron-Frobenius equation,

$$P_n^{(p)}(x) = \int_{-1}^1 P_n^{(p)}(y) \delta(x - F_n^{(p)}(y)) dy. \quad (\text{III.14})$$

If $P_n^{(p)}(x)$ changes slowly, the difference $\rho_n(x) - P_n^{(p)}(x)$ decreases with time.

On the other hand, a change in the distribution function $\rho_n(x)$ can lead the mean field $h_n = \int f(x) \rho_n(x) dx$ to a certain critical value, at which the internal bifurcation occurs in the effective map Eq.(III.13). For instance, a small difference of the mean field induces the effective map to be tangential to the line $y = x$ at one point, or it induces one region of the effective map to be collapsed by crisis. As a result, the

⁵ In the next Chapter, we shall study a GCM in which the nonlinearity parameter a is distributed over elements. In that case, some sort of differentiation of dynamics over elements enabled the collective motion. To characterize the differentiation, the notion of *internal bifurcation* will be introduced as a snapshot representation of one system.

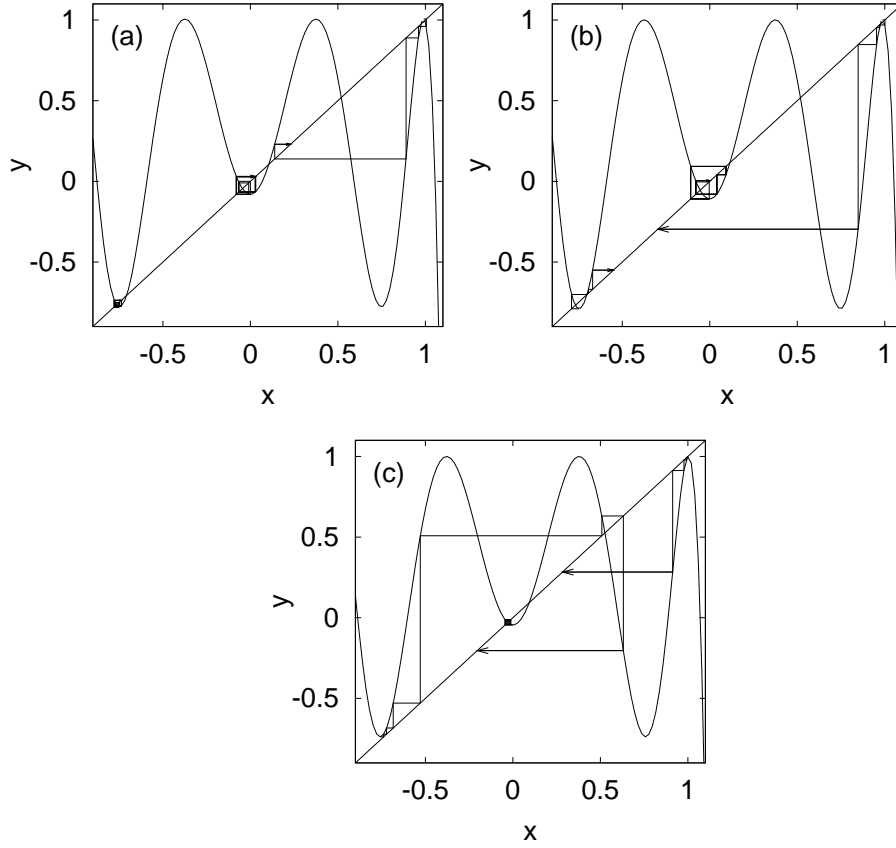


Fig. III.9: Behavior of the third iterate of a logistic map with period 3 external force. In contrast with the case of Fig.III.8, only one or two regions can attract trajectories. (a)The region around $x = 0$ attracts orbits as a region after tangent bifurcation, while the other regions, which are before the tangent bifurcation, cannot attract orbits. (b)Two regions around $x = 0$, and $x = -0.8$ attract orbits, while the region around $x = 1.0$ cannot attract orbits due to the crisis. (c)The region around $x = 0$ attracts orbits, while the other regions cannot attract orbits due to the crisis.

nature of the invariant measure $P_n^{(p)}(x)$ of the effective map changes qualitatively. This drastic change in $P_n^{(p)}(x)$ occurs, before $\rho_n(x)$ approaches $P_n^{(p)}(x)$. So, $\rho_n(x)$ cannot be close to $P_n^{(p)}(x)$.

With this internal bifurcation, the distribution $\rho_n(x)$ does not actually approach $P_n^{(p)}(x)$, because 1) the velocity of change $\rho_n(x)$ is finite, and 2) the change of $\rho_n(x)$ results in the qualitative change of $P_n^{(p)}(x)$. Consequently $\rho_n(x)$ oscillates in time. This qualitatively explains why the mean field does not approach a fixed point at the thermodynamic limit.

Let us look again at the example in Section III.4 and try to describe the dynamics under the above scenario. Since the effective nonlinearity parameter A is near the band merging point of the single logistic map, it is useful to define the two regions shown in Fig III.6, that correspond to the two bands of the logistic map near the band merging point. The effective dynamics is given by the second iterate of map,

$$F_n^{(2)}(x) = (1 - \epsilon) \left(1 - a \left\{ (1 - \epsilon)(1 - ax^2) + \epsilon h_{n-1} \right\}^2 \right) + \epsilon h_n. \quad (\text{III.15})$$

The lines $y = F_n^{(2)}(x)$ and $y = x$ cross at three points within $x \in [-1, 1]$ when $a < 2$ and $\epsilon > 0$. The middle of these points is denoted by x_n^* . R and L denote the regions where $x > x_n^*$ and $x < x_n^*$ respectively.⁶

Consider the case where A is near the band merging point of the single logistic map. If the mean field would be on an unstable fixed point, these two regions would collapse due to crisis. As we have discussed above, however, the dynamics of the mean field modulates the effective map Eq.(III.15). As a result, for this parameter regime, there are two cases: 1) the modulation of the map is large enough, so that the R region is an “unstable region”, while the L region is a “stable region” (and vice versa), and 2) the modulation of the map is small, so that both the L and the R regions are “unstable regions”. Here, we use the term “stable” and “unstable” as follows. Consider a trajectory starting from a region obtained by the iteration of the map $y = F_n^{(2)}(x)$ at a certain time step n . If the trajectory stays within the region, we call the region “stable region”. If the trajectory leave the region, we call the region “unstable region”. By analyzing the map $y = F_n^{(2)}(x)$, we can always determine the “stability of regions” at each time step.

In Fig.III.10, the oscillation of population in these two regions is shown as $\tilde{N}_n = N_L - N_R$ (see also Fig.III.6 and Fig.III.7). In Fig.III.10, the deviation of invariant measure $P_n^{(2)}(x)$ in two regions, i.e. $\tilde{I}_n = I_L - I_R$, where $I_L = \int_{x \in L} P_n^{(2)}(x) dx$ and $I_R = 1 - I_L$, is also plotted as a characterization of effective map (16). During the time steps $n \in [6, 46]$, $\rho_n(x)$ approaches $P_n^{(2)}(x)$, until the change of $\rho_n(x)$ induces $P_n^{(2)}(x)$ to change qualitatively at time step $n = 46$. This qualitative change in $P_n^{(2)}(x)$, and consequently the qualitative change in the effective map is due to crisis in the L region. In this way, the stability of the regions changes and some elements in the L region move to the R region. As a result, the distribution $\rho_n(x)$ approaches $P_n^{(2)}(x)$ again, until the next crisis enables a flow from the R region to the L region.

To sum up, the distribution function $\rho_n(x)$ changes slowly, in this way approaching $P_n(x)$ until the modulation of the mean field changes the internal bifurcation structure qualitatively. In this example, the qualitative change in the internal bifurcation structure is due to local crisis. As a result of the change of the internal bifurcation structure in

⁶ Note that if we would not δh_n into account, i.e. $h_n = \langle h \rangle$, x^* would be independent of time and x^* would denote the period-1 unstable fixed point of the single logistic map.

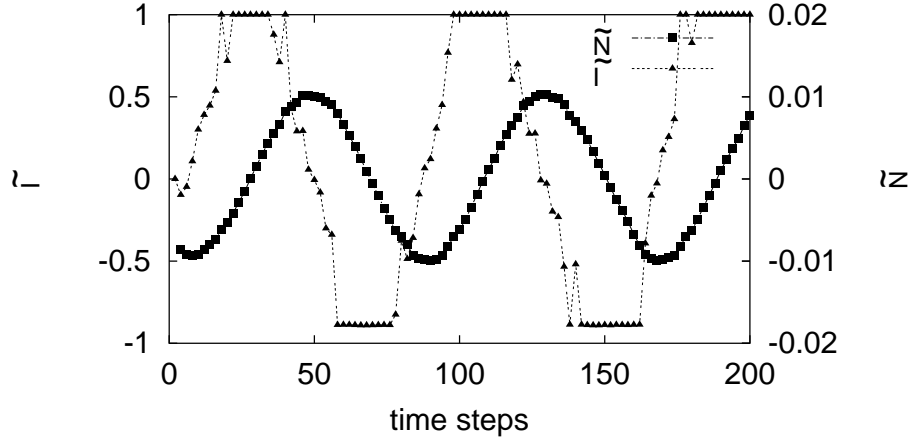


Fig. III.10: Temporal change of $\tilde{N}_n = N_L - N_R$ and $\tilde{I}_n = I_L - I_R$, where $N_L = \int_{x \in L} \rho_n(x) dx$, $N_R = 1 - N_L$, $I_L = \int_{x \in L} P_n^{(2)}(x) dx$ and $I_R = 1 - I_L$, are plotted as a function of time step. See text for the region L and R . $a = 1.5449205$, $\epsilon = 0.0005$, $N = 10^6$.

the two regions, the elements are attracted to a different region. With the repetition of this stability change of the regions, the mean field oscillates quasi-periodically. This mechanism of change in each band holds for any period- p band(window) regime where elements are attracted to and repelled from each band region successively with the internal bifurcation.

III.5 Bifurcation of Tongue Structures

As we have seen in Fig. III.10 in the previous Section, one of the two regions in the second iterate of the effective map Eq. (III.15) collapses due to crisis and the stability of the regions changes in time. In this Section, we will show that with the increase of A , the time interval during which the regions are unstable becomes longer.

There are three kinds of time intervals. In one case, both of the two regions R and L , define in the previous Section, are stable. $P_n^{(2)}(x)$ is positive for the two regions but there is no connection between the two positive regions. In the second case, only one of the two regions is unstable, and $P_n^{(2)}(x)$ is positive for one region and zero for the other. In the third case, both of the two regions are unstable. $P_n^{(2)}(x)$ is positive for the two regions and there is continuous connection between them. The ratios of these time intervals are plotted in Fig. III.11 as a function of $A - A_0$, where A_0 is the parameter for the band merging point of the logistic map. For $A - A_0 \leq -0.6 \times 10^{-6}$ crisis never occurs in both the two regions L and R , whereas for $A - A_0 > -0.6 \times 10^{-6}$, the time interval during which the regions are unstable gets longer. For the parameter beyond $A - A_0 = 3.6 \times 10^{-6}$, the two regions are unstable due to crisis bifurcation for every time step. Hence, the period-2 tongue structure starts at the parameter $A - A_0 \cong -0.6 \times 10^{-6}$, where one of the two regions of the effective map Eq. (III.15) becomes unstable for some time steps. It ends at the parameter $A - A_0 \cong 3.6 \times 10^{-6}$, where both the two regions become unstable all the time due to the crisis.

Bifurcation in a Tongue Structure

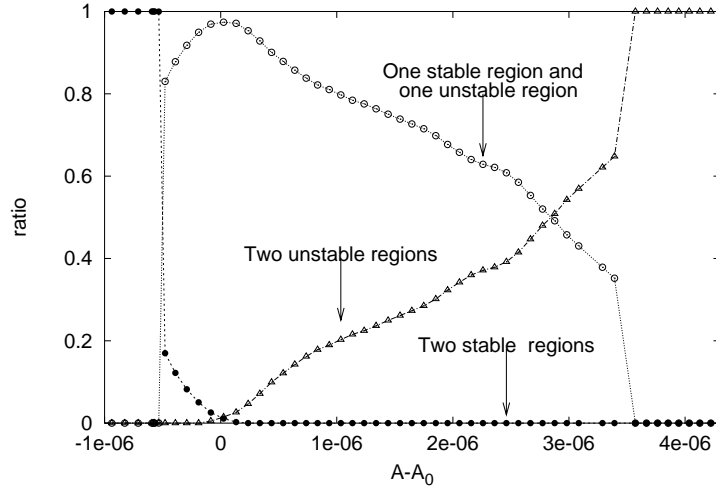


Fig. III.11: Ratio of the time steps, in which both the two regions collapse (\triangle), one of the two regions collapses (\circ), and none of the two regions collapses (\bullet). $A_0 = 1.5436890$ (band merging point), $\epsilon = 0.0005$, $N = 10^7$. The collapse is due to the crisis bifurcation in internal bifurcation.

Consider an internal bifurcation condition of Eq.(III.13) (for instance, crisis or tangent bifurcation in each element.). For $\epsilon = 0$ the bifurcation condition holds at a single parameter value. For $\epsilon > 0$, due to the oscillation of the mean field, within the parameter interval $A_{small}(\epsilon) < A(\epsilon) < A_{large}(\epsilon)$ in the (A, ϵ) -parameter space, the internal bifurcation condition is satisfied for some steps. Hence, the edge of a tongue structure starts at $\epsilon = 0$ from tangent bifurcation point and crisis bifurcation point. It is extended into the parameter space for $\epsilon > 0$, where each bifurcation condition is satisfied during some time steps (see Fig.III.12 for period-2 tongue structure). The scaling of the width of the tongue structure will be discussed in Section II.5.

III.6 Bifurcation in a Tongue Structure

Even within one tongue structure, we can observe different types of collective motion. With the change of the parameter A and κ , in the collective dynamics a kind of bifurcation occurs. Since the collective dynamics remains high-dimensional, it is not described as a standard bifurcation in low-dimensional dynamical systems. Here we study a mechanism of such change in the collective dynamics.

In Section II.3, it is shown that a slight increase in a induces a qualitative change of the collective dynamics (Fig.II.4). To see this quantitatively, it may be convenient to measure the rotation number of the collective dynamics. In Fig.III.13, the rotation number is plotted as a function of A . In the regime plotted in the figure, a period-seven tongue structure is observed between $A - A_0 \in [-0.744 \times 10^{-3}, 1.499 \times 10^{-3}]$, where A_0 denotes the tangent bifurcation point of the period-7 window of the logistic map. Typical examples of the collective dynamics are shown in Fig.II.4.

As we have already introduced in Section III.4, the invariant measure $P_n^{(7)}(x)$ of the effective map,

$$F_n^{(7)} = F_n \circ F_{n-1} \circ \cdots \circ F_{n-6}, \quad (\text{III.16})$$

Bifurcation in a Tongue Structure

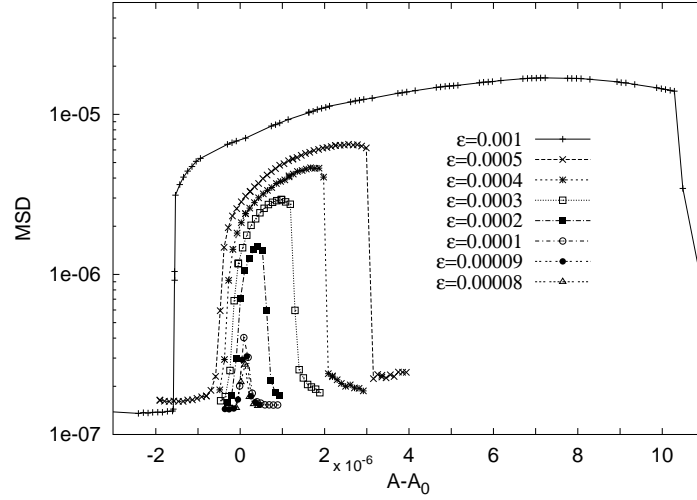


Fig. III.12: Mean square deviation (MSD) of the mean field distribution with the increase of ϵ plotted as a function of the effective nonlinearity parameter A . The region corresponds to the period-2 tongue structure. A_0 denotes the band merging point (crisis bifurcation point of 2-band) of the logistic map ($A_0 = 1.5436890126$).

may be useful to see the change of the dynamics with the increase of A . In Fig. III.14, three examples of $P_n^{(7)}(x)$ are plotted as a function of time. For the parameter of Fig. III.14(a), the parameter A is close to, but smaller than, the tangent bifurcation point of the period-7 window A_0 . Therefore, if the fluctuations of the mean field would be ignored, none of the seven regions could attract the elements because the seventh iterate of the logistic map Eq. (III.16) would not cross the line $y = x$. With the influence of the mean field dynamics, on the other hand, the effective map Eq. (III.16) is modified to cross the line $y = x$ at a few regions where $P_n^{(7)}(x) > 0$ (for instance between $n = 2000$ and 2100 in Fig. III.14(a)). These two or three regions can attract the elements until these regions come to be destabilized by crisis (for instance at $n \approx 2100$). After the crisis $P_n^{(7)}(x)$ spreads over the whole region because none of the seven regions of the map Eq. (III.16) cross the line $y = x$. Then the regions attracting the elements switch to different positions. This process continues successively.

With the increase of A , the number of regions attracting the elements due to the tangent bifurcation of the map Eq. (III.16) increases (Fig. III.14(b)). In Fig. III.14(b), 5, 6, or 7 regions are stabilized successively.

With the further increase of A , all the seven regions of the map Eq. (III.16) always cross the line $y = x$, while some of these seven regions are destabilized by crisis (Fig. III.14(c)). With the increase of A , for each of the seven regions, the time interval during which the region is unstable increases. The tongue structure ends at the parameter $A - A_0 = 1.499 \times 10^{-3}$, where all the seven regions are destabilized by crisis during every time step. Thus, the collective dynamics of the period-seven tongue structure ends. As a result, the amplitude of the mean-field dynamics reduces to about 0.1 (see Fig. III.13).

Although we have explained the bifurcation in the internal tongue structure for the period-7 case, this kind of bifurcation structure is common to a band region in any period. For instance, in Fig. II.12(a) with the period-3 tongue structure (starting from

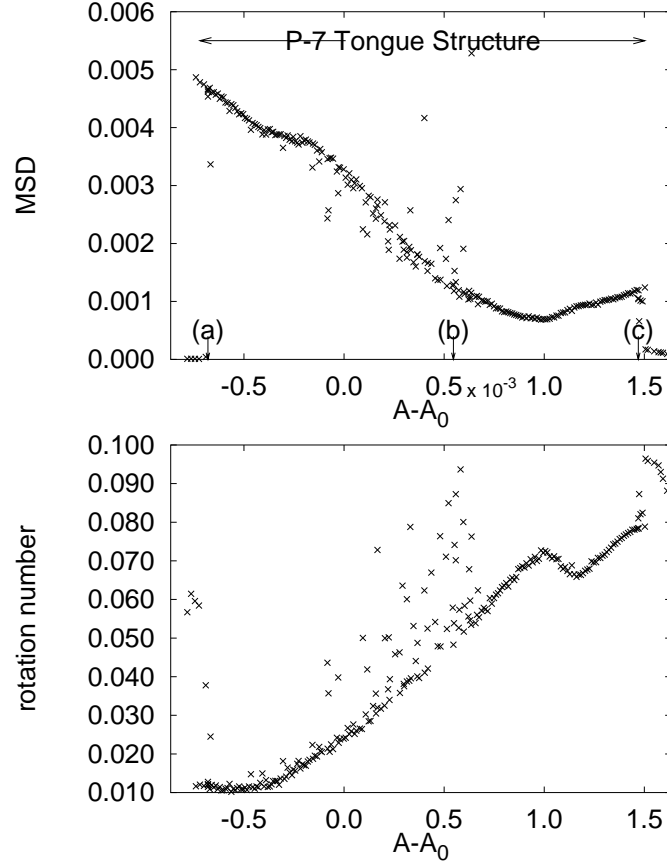


Fig. III.13: Mean square deviation and rotation number of the mean field dynamics are plotted as a function of $A - A_0$, where $A_0 = 1.67407$ denotes the tangent bifurcation point of period-seven window. In the figure (a), the parameters $a = 1.6962, 1.69755$, and 1.69844 are indicated as (a), (b) and (c), corresponding to the parameters in Fig.II.4 and Fig.III.14.

$A \in [1.75, 1.79032]$ at $\epsilon = 0$) and in the period-5 tongue structure (starting from $A \in [1.6244, 1.6333]$ at $\epsilon = 0$), similar bifurcation structure is observed, where the change in the number of coexisting stable regions corresponds to such bifurcation structure.

III.7 Summary and Discussion

In the present Chapter, we have first studied the linear stability of the stationary state of the mean field motion. The estimation considering the contribution from the singularity of the distribution function suggests that the perturbation grows exponentially and the stationary state is unstable. Based on the estimation, we have next studied the scaling relation of the amplitude of collective motion. It indicates the linear scaling with the coupling strength ϵ . Although this agrees with the scaling in the chaotic parameter regime, the deviation exists within the tongue structures.

Then, focusing on tongue structures, we have demonstrated how such a collec-

Summary and Discussion

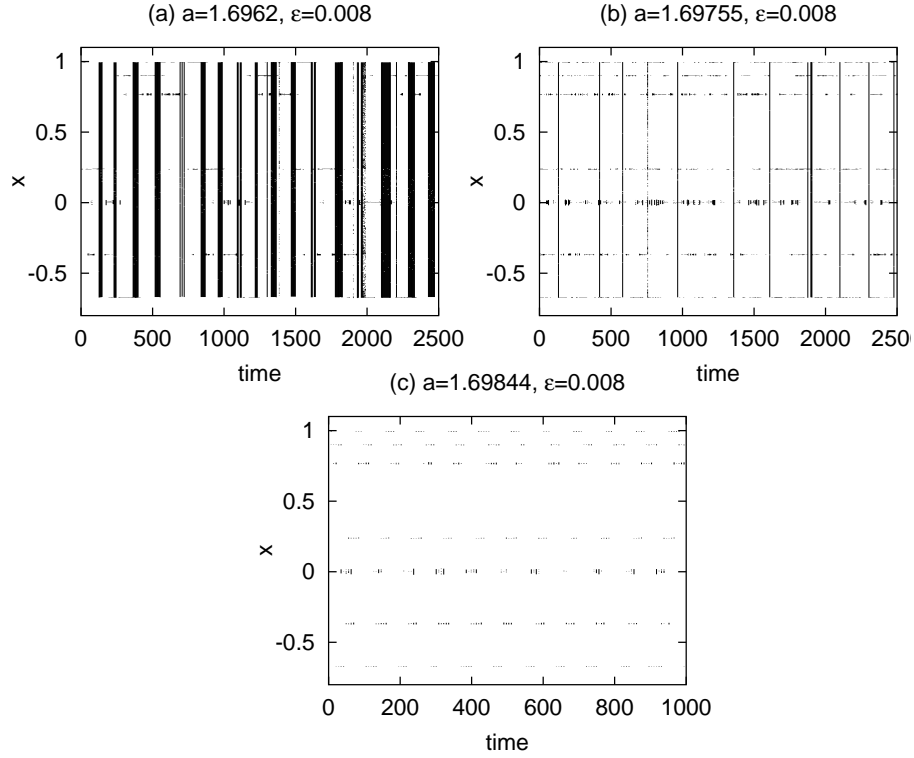


Fig. III.14: Invariant measure of the effective map Eq.(III.16) $P_n^{(7)}(x)$ is plotted as a function of time. The horizontal axis is time and the vertical axis is x . In this figure, the region with $P_n^{(7)}(x) > 0$ is plotted by a solid line. When the whole region is filled by a line, none of the seven regions of the map Eq.(III.16) cross the line $y = x$, and all the regions are connected as a single attracting set. In (a) and (b) some of the seven regions of the map Eq.(III.16) cross the line $y = x$, while the other regions do not. In (c), on the other hand, all seven regions of the map Eq.(III.16) cross the line $y = x$, while some of the seven regions are destabilized by crisis. The parameters correspond to those of Fig.II.4.

tive motion emerges. The dynamics of the mean field and each element form some self-consistent relationship, so that collective motion is possible. This self-consistent dynamics is formed by the following repetition: accumulation of elements into some regions leading to change in the mean field dynamics, which introduces a stability change of the regions, and accumulation of elements into a different region occurs, which, again..... This gives internal bifurcation in elements and in time.

The bifurcation is also seen in the parameter space. Since the nature of the internal bifurcation varies with the nonlinearity parameter a in a tongue structure, the number of coexisting regions in x changes, which makes the collective motion qualitatively different. Hence, in a tongue structure, different kinds of collective motions have been observed. A schematic figure of tongue structure is presented in Fig.III.15.

Here, we should note a future problem. In order to connect the statistical approach in Section III.2, and the studies after Section III.4, we need a further study about the eigenvalues of Eq.(III.4).

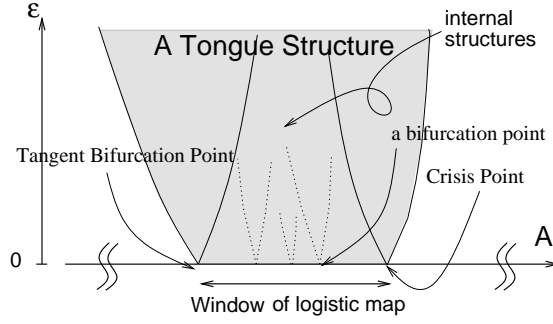


Fig. III.15: Schematic diagram of a tongue bifurcation structure. Regions that grow from a bifurcation point of the logistic map constitute a tongue structure. See Sections III.5 and III.6.

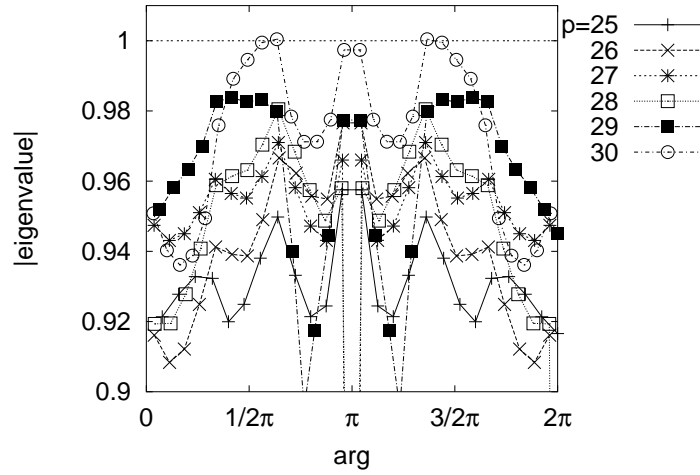


Fig. III.16: Absolute value of the eigenvalue of Eq.(III.4) is plotted as a function of the argument of the eigenvalue. $a = 1.5443690$, $\epsilon = 0.002$. The summation in Eq.(III.4) is taken within the range from $\tau = 1$ to p indicated at the right hand side of this figure.

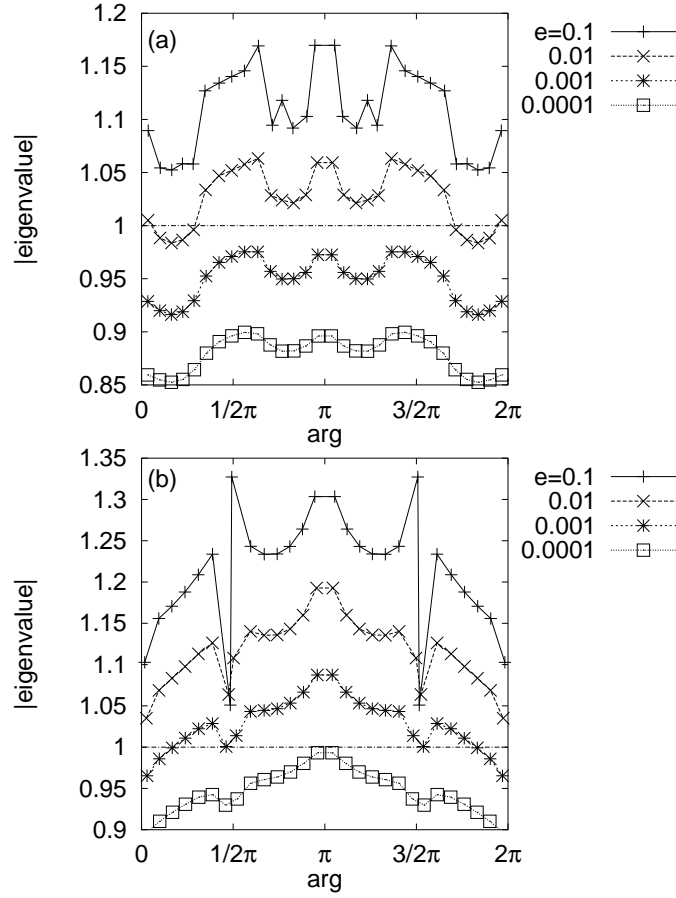


Fig. III.17: Absolute value of the eigenvalue of Eq.(III.4) for several coupling strength ϵ is plotted as a function of the argument of the eigenvalue. The values of ϵ are indicated outside the figure. (a) $a = 1.5443690$ and (b) $a = 1.83928675$. The summation in Eq.(III.4) is taken within the range from $\tau = 1$ to 30(a) or 28(b).

Fig.III.16 indicates the absolute value of eigenvalues of Eq.(III.4), which are obtained numerically. For numerical calculation, it is hardly to take the summation in Eq.(III.4) through sufficiently large τ to obtain the converged eigenvalues. Then, we consider a finite number of terms included in the summation in Eq.(III.4). Within our numerical result, Fig.III.16 may suggests that with the increase of the number of terms included in Eq.(III.4), the absolute value of eigenvalues increases, and the relative relation among the values does not change so much.

Expecting these properties, next we study the behavior of the eigenvalues for two cases, which we have seen in Fig.III.4. In Fig.III.4(a) some large deviation from the scaling relation of Eq.(III.9)(b) exists in the small τ regime, while in Fig.III.4(b) such a large deviation seems much smaller. This is the difference of these cases, though we expect that the coefficients of both cases grow similarly as Eq.(III.9) in the large τ regime. The corresponding plot of eigenvalues of each case is depicted in Fig.III.17, where the absolute values of eigenvalues for several coupling strength ϵ are plotted.

In Fig.III.17(a), the behavior of the eigenvalues suggests Hopf-like bifurca-

tion⁷. The eigenvalue with the largest absolute value might correspond to the lower-dimensional-like collective motion. On the other hand, in the case of Fig.III.17(b), the eigenvalue with the largest absolute value is around the argument of π for small ϵ . Such a case might correspond to the collective motion without low-dimensional like motion. Indeed, the mean field behavior of the parameters of Fig.III.17(b) does not show low-dimensional structure.

This implies that low-dimensional structure of the collective motion might be relevant to the behavior of L_τ of small τ regime. Remember that the behavior of L_τ within the small τ regime reflects the nature of larger scale structure of the distribution function, which strongly depends on the parameters. Therefore, on the one hand, the dependence of the eigenvalues on L_τ of the small τ regime should be studied. On the other hand, it should be investigated how L_τ depends on the large scale structure of the distribution function. As a result, it will be clarified which characteristic of GCM is relevance to the low-dimensional-like slow collective motion.

⁷ In Fig.III.17(a), the absolute values of all eigenvalues for small coupling strength are smaller than unity. However, we expect that the value increase beyond unity if we include sufficiently many terms in the summation of Eq.(III.4).

CHAPTER IV

HETEROGENEITY INDUCED ORDER

Collective behavior is studied in globally coupled maps with distributed nonlinearity. It is shown that the heterogeneity enhances regularity in the collective dynamics. Low-dimensional quasiperiodic motion is often found for the mean-field, even if each element shows chaotic dynamics. The mechanism of this order is due to the formation of an internal bifurcation structure, and the self-consistent dynamics between the structures and the mean-field.

IV.1 Introduction

Up to the present Chapter, the system consists of homogeneous elements. In other words, identical elements are coupled with each other. However, in many systems elements are heterogeneous. In Josephson junction array, each unit is not identical. In an optical system, the gain of each mode depends on its wavenumber. In a biological system, each unit such as a neuron or a cell is heterogeneous. So far the study of a coupled system with distributed parameters is restricted to synchronization of oscillators (Kuramoto 1975). Thus it is important to check how the notions constructed in globally coupled dynamical systems can be applicable to a heterogeneous case. In the present Chapter we demonstrate that the collective motion emerges in a heterogeneous system through self-consistent dynamics between the mean-field and internal differentiation of dynamics.

Here we adopt a globally coupled map with a distributed parameter,

$$x_{n+1}(i) = (1 - \epsilon)f_i(x_n(i)) + \frac{\epsilon}{N} \sum_{j=1}^N f_j(x_n(j)), \quad (i = 1, 2, 3, \dots, N), \quad (\text{IV.1})$$

where $x_n(i)$ is the variable of the i 'th element at discrete time n , and $f_i(x(i))$ is the internal dynamics of each element. For the dynamics we choose the logistic map $f_i(x) = 1 - a(i)x^2$, where the parameter $a(i)$ for the nonlinearity is distributed between $[a_0 - a_w, a_0 + a_w]$ as $a(i) = a_0 + \frac{a_w(2i-N)}{N}$. (In the following, the parameters are indicated by $a = a_0 \pm a_w$). We note that the essentially same behavior is found when $a(i)$ is randomly distributed in an interval or the coupling $\epsilon(i)$ is distributed instead of a . In this case, the mean field is given by,

$$h_n = \frac{1}{N} \sum_{j=1}^N f_j(x_n(j)). \quad (\text{IV.2})$$

This chapter is based on Shibata (1996) and Shibata & Kaneko (1997).

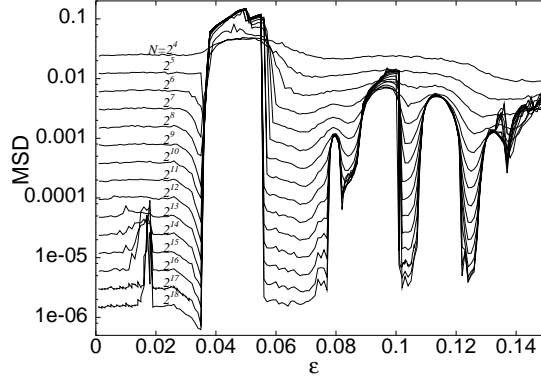


Fig. IV.1: Mean square deviation of the mean field is plotted versus coupling strength ϵ . $a_0 = 1.9$, $a_w = 0.025$. The number of elements is varied from $N = 2^4$ to 2^{18} . Collective motions are clearly seen in some parameter regimes such as $\epsilon \approx .018$, $.038 < \epsilon < .058$, $.083 < \epsilon < .1$, $.105 < \epsilon < .12$, and $.13 < \epsilon < .15$.

When elements are identical with $a_w = 0$, the present model reduces to a globally coupled map (GCM) studied in the previous Chapters.

When elements are not identical, one might expect that collective dynamics would be destroyed and the mean-field become stationary. On the contrary, the collective motion is found ranging from low-dimensional torus, and low-dimensional chaos to high-dimensional chaos, as will see in the next Section. In the homogeneous case, even if we observe a quasiperiodic-like mean field motion, the motion is still high-dimensional, as is indicated by the finite width around the torus-like structure (Section II.3). On the other hand, in the heterogeneous case, the width of scattered motion around a certain motion seems to decrease with the system size N . Thus, in the latter case, the collective motion shows complete low-dimensional coherence. This is an important distinction between the homogeneous systems and the heterogeneous systems.

In the next Section, we shall provide some of the phenomenology of the heterogeneous GCM. The existence of the complete low-dimensional collective motion is suggested. In Section IV.3, we show that the formation of a self-consistent dynamics between the mean field dynamics and the internal bifurcation structure makes the collective order possible. This Chapter concludes in Section IV.4.

IV.2 Effects of Heterogeneity on Collective Motion

First we begin with the behavior of the mean field fluctuation in our system. Fig.IV.1 shows the MSD plotted as a function of the coupling strength ϵ with the increase of the system size. Roughly speaking the MSD measures the amplitude of the mean field motion (see the discussion on the MSD in Section II.3). As the system size increases, the MSD decreases up to a certain size and then stays constant or increases to a certain constant within wide parameter region in which power spectrum has delta peaks¹. This result implies the existence of some structure and coherence in the mean field dynamics. As will see in the next, such collective behavior is rather general in our heterogeneous system and is observed more clearly than in the homogeneous GCM.

¹ Each of such a region may have some correspondence with the tongue structures shown in Section II.4.

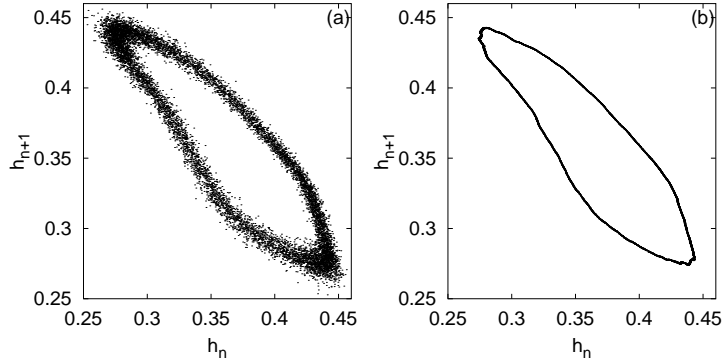


Fig. IV.2: Return map of the mean-field values h_n . $a_0 = 1.9, a_w = 0.025, \epsilon = 0.11$. The system size N is (a) 10^4 and (b) 10^7 .

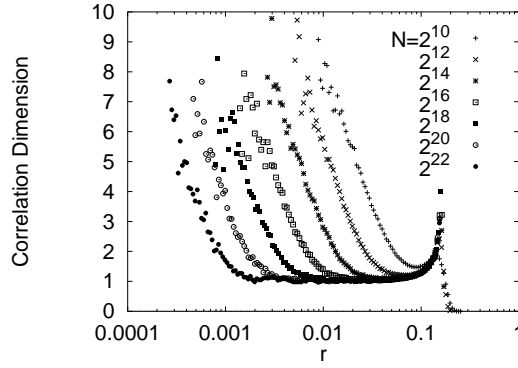


Fig. IV.3: Correlation dimension for heterogeneous GCM (Shibata & Kaneko 1997). The parameters are $a = 1.9, \epsilon = 0.11, a_w = 0.025$. Nonlinearity parameter for each element is homogeneously distributed over $a \in [1.875, 1.925]$. The mean field time series is embedded into 10 dimension.

Fig. IV.2 shows the return map of the mean field values of GCM (IV.1). The mean field dynamics indicates a clear quasiperiodic motion, though the elements never synchronize with each other and the system is in a high-dimensional chaotic state. The width around the torus-like structure seems to decrease with increasing N .

To check whether the width of scattered points around the torus motion decrease with N , we have measured the correlation dimension (Grassberger & Procaccia 1983a,b) of the mean-field time series. Within the numerical result, the width of scattered points around the torus converges to zero in the thermodynamic limit. Corresponding plots of slopes are given in Fig. IV.3, where the plateau at the value unity is expanded with N , and the *noise region* is shrunk to the scale $r \approx 0$. Accordingly, the mean field dynamics converges to dynamics on a two-dimensional torus. This is an important difference² from the homogeneous case as is shown in Fig. II.6 of Section II.3.

With the change of a_0 , a_w , or ϵ , the mean-field dynamics shows the bifurcation from torus to chaos accompanied by phase lockings. Further bifurcation proceeds to

² In the heterogeneous case, the law of large numbers is recovered around the torus motion.

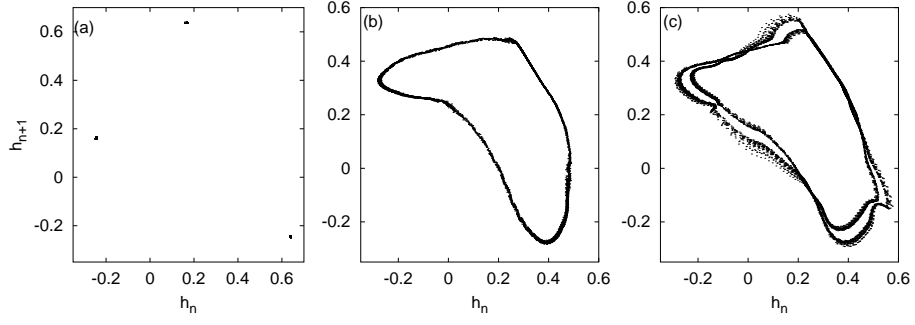


Fig. IV.4: Return map of the mean-field h_n . $a_0 = 1.9$, $a_w = 0.05$. (a) $\epsilon = 0.055$, $N = 2^{16}$, (b) $\epsilon = 0.053$, $N = 2^{18}$, (c) $\epsilon = 0.05$, $N = 2^{21}$.

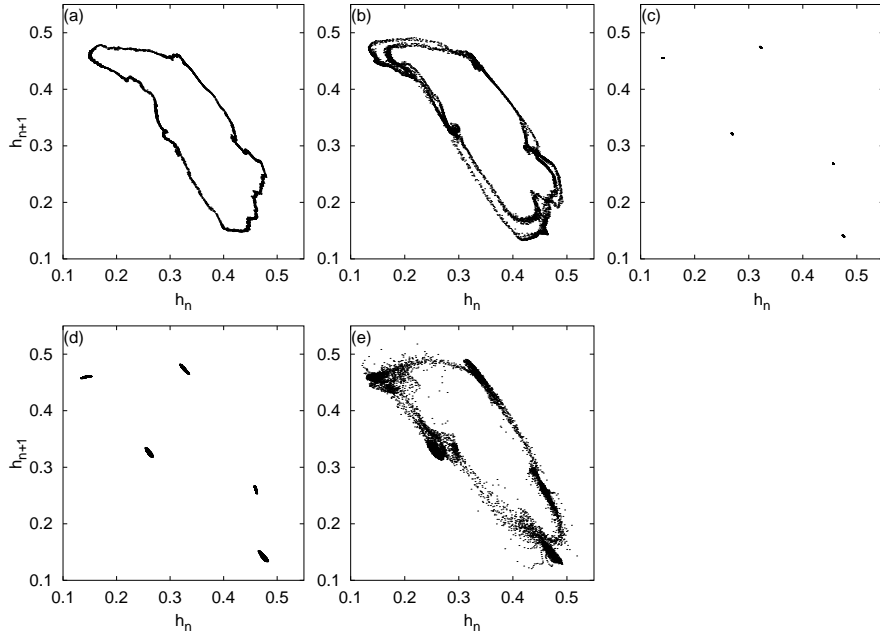


Fig. IV.5: Return map of the mean-field h_n . $a_0 = 1.9$, $a_w = 0.025$ (a) $\epsilon = 0.095$, (b) $\epsilon = 0.096$, (c) $\epsilon = 0.097$, (d) $\epsilon = 0.0975$, (e) $\epsilon = 0.098$.

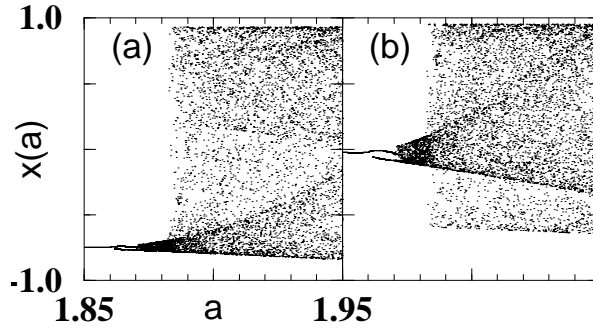


Fig. IV.6: Snapshot pattern of $x_n(i)$ plotted versus $a(i)$. Here the mean-field is locked to period-3 (to be more precise period-6). $a_0 = 1.9$, $a_w = 0.05$, $\epsilon = 0.055$. Time step 5000 (a), and 5001 (b). At the next iterate, the coherent structure of $x_n(a)$ for $a < 1.88$ moves to $x \approx 1$, while another iterate leads to the structure of (a).

higher-dimensional chaos (while some structure is still kept). Several routes to chaos are observed, including that through the doubling of torus (Figs. IV.4 and IV.5). There are two cases for the collective motion, although for both cases each element oscillates chaotically without mutual synchronization. In one case (given in Fig. IV.4) there are negative Lyapunov exponents³ (78 for (b), for $N = 500$; whose number decreases with ϵ). In the other case (given in Figs. IV.2 and IV.5), all exponents are positive. Hereafter we show how this *heterogeneity-induced order* is possible (mainly for the former case).

IV.3 Internal Bifurcation

The scenario to be presented for the *heterogeneity-induced order* consists of two parts. First, we demonstrate the formation of *internal bifurcation structure*⁴, made possible by the distribution of parameters, which leads to the self-consistent relation between each dynamics and the mean-field. Second, it is shown that the repetitive change of internal bifurcation structure makes possible to form the low-dimensional collective motion in the mean-field. The organization of the low-dimensional bifurcation in sub-systems from a high-dimensional system is a key concept for the collective dynamics.

First we study the formation of the *internal bifurcation structure*. In our system nonlinear parameters are distributed over elements. Dynamics of the i 'th element depends on the parameter $a(i)$. Hence it is relevant to draw the motion versus the parameter a . Fig. IV.6 gives snapshot patterns of $x_n(a)$ for the period-3 locking⁵ in the mean-field (Fig. IV.4(a)). It looks like an ordinary bifurcation diagram plotted against the change of external parameters, but the patterns of Fig. IV.6 are just snapshot representations of one system consisting of N elements. Still, successive plots of the pattern show that the dynamics of elements changes with $a(i)$. In Fig. IV.6 elements with $1.85 < a(i) < 1.887$ show period-3 oscillation with almost synchronization.

³ Still the extensive property in terms of the Lyapunov dimension is expected.

⁴ In Chapter III, the notion of *internal bifurcation* has been introduced, in order to specify the bifurcation in an effective map of each element, which takes place in time. In the present Chapter, as we will show below, we extend the notion of the internal bifurcation to the heterogeneous case.

⁵ The period can be 3×2^k , although this doubling is irrelevant to the following arguments. For example, the period is six for Fig. IV.4(a).

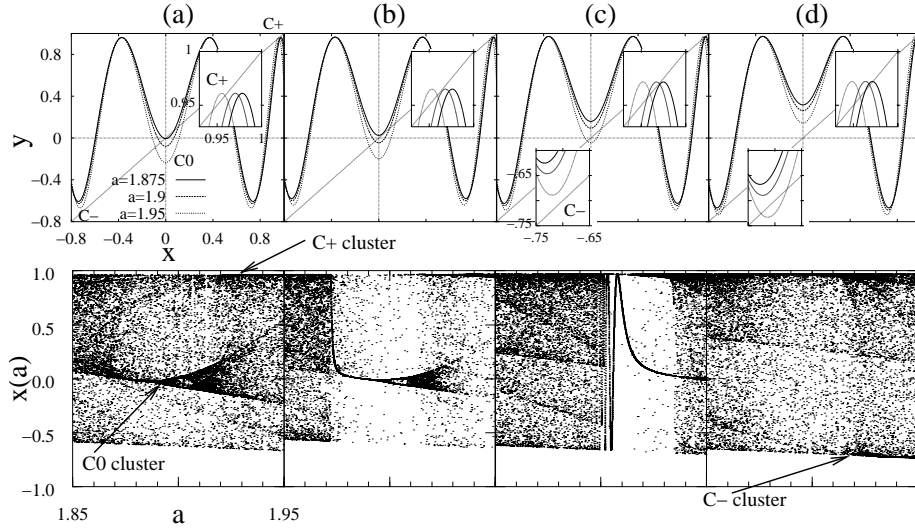


Fig. IV.7: Dynamics of the internal bifurcation structure. $a_0 = 1.9$, $a_w = 0.05$, and $\epsilon = 0.053$. In the lower column snapshot patterns are plotted at time step 1080(a), 1161(b), 1206(c), 1251(d). In the upper column, the effective maps Eq.(2) are plotted for $a = 1.875, 1.9, 1.95$ at the corresponding time steps. These steps (with unequal intervals) are chosen so that the formation and collapse of clusters are seen, in correspondence to Fig.IV.8.

With the increase of $a(i)$, tangent bifurcation occurs at one point⁶ around $a \approx 1.85$. For larger $a(i)$, period-doubling and crisis are observed in the snapshot pattern, if it is viewed as the transition of attractor with the change of control parameters. As the parameter a is larger, successive bifurcation occurs beyond which elements fall into a fully chaotic state. Hence we call the structure as internal bifurcation. We also note that the clustered motion (at small $a(i)$) and fully desynchronized motions coexist.

If the mean-field were an external parameter for each element, those bifurcations would occur in each sub-system according to their nonlinear parameters. The mean-field dynamics, in our case, is organized self-consistently from each element dynamics according to the internal bifurcation. The internal structure consisting of period-3 synchronized motion and desynchronized motion forms the period-3 oscillation of the mean-field. On the other hand the period-3 mean-field motion plays the role of external forcing which causes the period-3 clustered motion and desynchronized motion according to the each element's parameter $a(i)$.

When the coupling strength ϵ is smaller (Fig.IV.4(b)), another tangent bifurcation occurs. This bifurcation leads to the formation of the second clustered motion. As the second clustered motion is formed, the mean-field is varied, which changes the effective map for each element. Then the period-3 locking in the mean-field collapses, when we need the second scenario for the self-consistent dynamics between the internal

⁶ In the single logistic map, the third iterate of the map $y = f(f(f(x)))$ is tangential to $y = x$ at three points corresponding to the periodic points. On the other hand, for the mapping $f_{\delta_n}(x) = 1 - ax^2 + \delta_n$ with a time-dependent parameter δ_n as in the present case, the third iterate $y = f_{\delta_3}(f_{\delta_2}(f_{\delta_1}(x)))$ is tangential to $y = x$ only at one point, unless there is certain restriction to the external field δ . In other words one specific phase of the period-3 oscillation is selected in accordance with the external parameter.

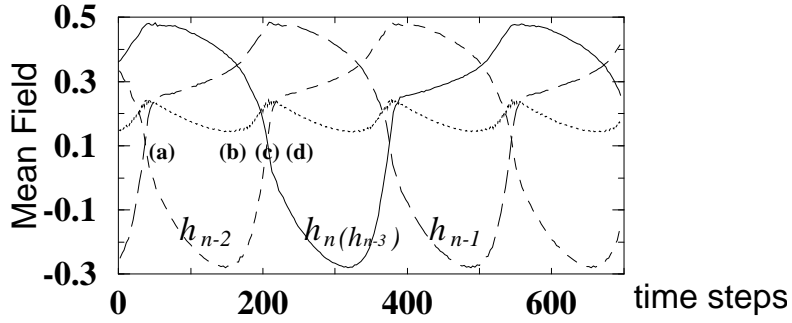


Fig. IV.8: Time series of the mean-fields $h_n(h_{n-3})$ (solid line), h_{n-1} (long dashed line), h_{n-2} (dashed line) are plotted every 3 steps($n = 3m$). The average of the 3 steps $\frac{h_n+h_{n-1}+h_{n-2}}{3}$ (dotted line) is also plotted. The steps shown as (a), (b), (c), (d) correspond to those in Fig.IV.7 respectively.

bifurcation structure and the mean-field ⁷.

As the simplest example, we discuss the case the quasiperiodic mean field motion shown in Fig.IV.4(b). Fig.IV.7 shows the snapshots of $x(a)$ corresponding to this case. We note that two clusters of coherent motions are formed for some parameter values of $a(i)$ and collapse successively, along with the quasi-periodic change of the mean-field.

To see our scenario here, we need to clarify (a) how the internal structure determines the mean-field and (b) how the mean-field modifies the stability of these internal bifurcation structure.

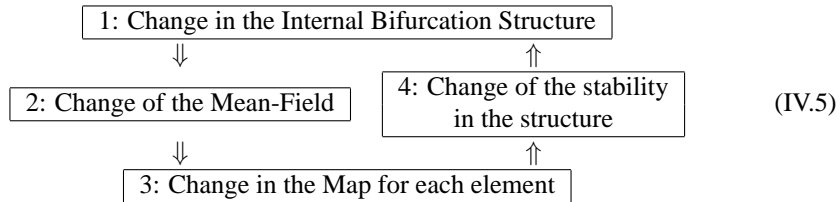
The step (a) is rather simple. The mean-field is determined by

$$h_{n-1} = \frac{1}{N} \sum_{i=1}^N f_i(x_{n-1}(i)) = \frac{1}{N} \sum_{i=1}^N x_n(i). \quad (\text{IV.3})$$

On the other hand, the stability of clustered motion is determined by the effective map for each element:

$$x_{3n} = F_{h_{3n-1}}(F_{h_{3n-2}}(F_{h_{3n-3}}(x))), \quad (\text{IV.4})$$

which is the 3rd iterate of $F_{h_n}(x) = (1 - \epsilon)(1 - ax^2) + \epsilon h_n$. Change of the mean-field modifies the shape of Eq.(IV.4), which induces the change in the stability of each clustered motion. Then the internal bifurcation structure is modified. Thus the process (b) is obtained. To sum up (a) and (b), the following feedback process exists:



(The 2nd, 3rd and 4th processes occur simultaneously which determine the dynamics in each element.)

⁷ Within a small parameter region between locking state (Fig.IV.4(a)) and quasi-periodic state (Fig.IV.4(b)), the two attractors coexist depending on the initial conditions.

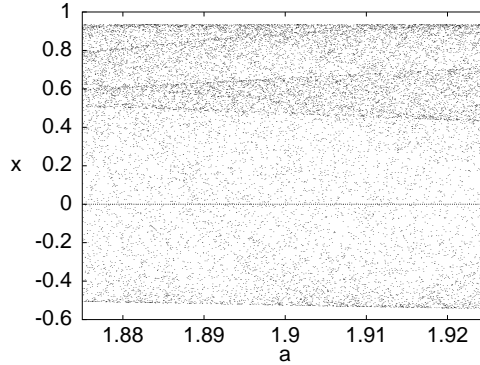


Fig. IV.9: A snapshot of $x_n(i)$ is plotted as a function of each $a(i)$ at a certain time step. The parameters are $a = 1.9, \epsilon = 0.11, a_w = 0.025$. The mean field dynamics of this parameter is shown in Fig.IV.2.

It should be noted that the time scale of the change of the structure is longer than the oscillation of each element (see Fig.IV.8). For the above case, the oscillation of each element is near period-3, while the modulation (to change the phase of period-3 oscillations) takes 170×3 steps. For the case of Fig.1a the distribution of elements has a 7-banded structure (roughly speaking), where the modulation to change the phase has a longer time scale (25×7 steps). Such slow modulation of the mean-field dynamics is formed by the above feedback diagram. This separation of time scales is necessary to have a low-dimensional collective order; otherwise high-dimensional chaotic dynamics remains.

Let us consider the above scenario in detail along Fig.IV.7, which are shown through $3n$ steps, because the clustered motion is period-3.

Two-clustered motion is formed at $x = 0$ (denoted by $c0$) and at $x = 1$ (denoted by $c+$) (Fig.IV.7(a)). The $c0$ -clustered motion breaks down at $a \approx 1.918$ by crisis and the elements with larger $a(i)$ than this value leave the cluster. The 2nd tangent bifurcation occurs near $x = 1.0$ and $a = 1.92$, and this $c+$ -clustered motion attracts elements which have left the $c0$ -cluster. This makes the mean-field h_{n-1} increase due to the Eq.(IV.3) ((a)(b) in Fig.IV.8). At the same time, h_n and h_{n-2} decrease, as is expected by successive mappings of $c0$ and $c+$ from step n . This change of the mean-field modifies the map Eq.(IV.4).

The modification of the map Eq.(IV.4) destabilizes the $c0$ -cluster and stabilizes the $c+$ -cluster (Fig.IV.7(b)(c)). The $c0$ -cluster starts to collapse from smaller values of a successively, and with this process the $c+$ -cluster grows from larger a to smaller. This makes the mean-field h_{n-1} and h_{n-2} increase, and h_n decrease ((b)(c) in Fig.IV.8). This change of the mean-field modifies the map for each element, and a new clustered motion is formed near $x = -0.7$ (denote as $c-$), besides the cluster at $x = 1$ ($c+$). The same process as above continues, by changing the roles of clusters until $c+$ -cluster collapses and $c0$ -cluster is formed (Fig.IV.7(d)). In this way the feedback (IV.5) is repeated.

IV.4 Summary and Discussion

We have shown the formation of low-dimensional collective dynamics in a coupled chaotic system with heterogeneity. The mechanism of the formation is due to the internal bifurcation structure afforded by heterogeneity, and the self-consistent feedback dynamics between the mean-field and synchronization of elements. We note that this mechanism is expected to be quite general, as long as each local dynamics allows for bifurcations with the change of some parameters, distributed by elements. Thus our scenario for the collective order can be observed in coupled systems such as Josephson junction arrays, and multi-mode laser systems, as well as in biological networks.

In Section IV.3, although we have explained the above scenario for the period-3 window case due to its simplicity, this mechanism is generally applied to our system, since each (logistic) dynamics contains a variety of windows and bifurcations.

We note that the above feedback process in Section IV.3 between the mean-field and the internal bifurcation structure is possible, since the value of a is non-identical. The role of elements is differentiated as to the synchronization and desynchronization, which temporally changes as in the case for chaotic itinerancy (Kaneko 1989a, Ikeda et al. 1989, Tsuda 1992). We also note that a slow modulation of the mean-field dynamics is formed by the feedback. This separation of time scales is necessary to have a low-dimensional collective order; otherwise high-dimensional chaotic dynamics remains in the mean-field.

In some cases the window structures in the internal bifurcation are not clearly visible. Such an examples is shown in Fig.IV.9, which corresponds to the mean field dynamics given in Fig.IV.2. In this case, it will be necessary to consider effects of the heterogeneity on the distribution function seriously. As a result, the distinction between the heterogeneous and the homogeneous cases will be clarified.

In the next Chapter, the mean field orbits of the heterogeneous GCM will be characterized, introducing *collective Lyapunov exponent*. Then, the existence of the collective chaos is clarified.

CHAPTER V

COLLECTIVE CHAOS

An algorithm to characterize collective motion is presented, with the introduction of *collective Lyapunov exponent*, as the orbital instability at a macroscopic level. By applying the algorithm to a globally coupled map, existence of low-dimensional collective chaos is confirmed, where the scale of high-dimensional microscopic chaos is separated from the macroscopic motion, and the scale approaches zero in the thermodynamic limit.

V.1 Introduction

Low-dimensional chaotic motion often arises from a system with many degrees of freedom. A classical examples is chaos in a fluid system such as Rayleigh-Bénard convection and Couette-Taylor flow, in chemical reactions such as Belousov-Zhabotinskii reaction, and in biological systems such as EEG patterns in brains and metabolic reactions in cells. In these systems, whereas some observables show low-dimensional chaotic motion, very high-dimensional chaotic motions should underlie at a microscopic scale. It is interesting to ask how macroscopic chaos coexists with such a microscopic chaotic motion (See also the discussions in Chapter I).

A canonical answer for the condition to have low-dimensional chaos at a macroscopic level is given by separation of scales distinguishable from a microscopic level. Still it is not clear how such separation is possible, since chaos can lead to the amplification of a small-scale error.

To address the question, we consider a certain dynamical system that shows some lower dimensional motion for a certain macroscopic variable (e.g., average of microscopic variables), whereas microscopic variables keep high dimensional chaos. There the number of positive Lyapunov exponents is proportional to the system size, and diverges in the *thermodynamics limit* (infinite system size limit). In this Chapter, in order to characterize such macroscopic motion, Lyapunov exponent at a macroscopic scale is introduced, which specifies the growth rate of a certain small displacement between the macroscopic orbits. By studying the dependence of the exponent on the length scale in macroscopic phase space and the system size, it is shown how the *collective chaos* is compatible with microscopic chaos, and how they are separated at the thermodynamic limit. Here chaos in the variables of the dynamical system is referred to as *microscopic chaos*.

In the next Section, the collective Lyapunov exponent is introduced by extracting some macroscopic information from a finite-size Lyapunov exponent. A

This chapter is based on Shibata & Kaneko (1998a).

method to detect the collective Lyapunov exponent is also presented. In Section V.3, heterogeneity-induced order which is studied in Chapter IV is revisited in order to demonstrate our method. Then, the existence of the *collective chaos* is clarified in the heterogeneous GCM. This chapter concludes in Section V.4.

V.2 Collective Lyapunov Exponent

First note that the conventional Lyapunov exponents for the dynamical system are not relevant to the characterization of collective motion. In order to calculate the Lyapunov exponent for the collective motion, an infinitesimal limit of disturbance to a trajectory should be taken at a ‘macroscopic’ level. Rigorously speaking, the macroscopic level appears in the thermodynamic limit (system size $N \rightarrow \infty$). Thus, it is necessary to take the thermodynamic limit first and then the limit of disturbance scale, to characterize the collective dynamics. However, in the conventional computation of the Lyapunov spectrum we first take the infinitesimal limit of disturbance applied to the orbit, and see the asymptotic behavior of the spectrum in the thermodynamic limit. Hence, the exponent cannot characterize the collective motion. This problem can be resolved by noting the order of limit to define the Lyapunov exponent.

Since we are concerned with a system of a large but finite size, the above order of limit implies that we have to keep the disturbance amplitude finite, so that the disturbance is studied at a macroscopic level (roughly speaking the disturbance at a macroscopic variable should be larger than $1/\sqrt{N}$). To study such orbital instability, the finite-size Lyapunov exponent introduced by Vulpiani et al. (Paladin et al. 1995, Aurell et al. 1996) is useful. It is given by

$$\lambda_{\delta_0}(\Delta) = \left\langle \frac{1}{\tau} \log \frac{\Delta}{\delta_0} \right\rangle, \quad (\text{V.1})$$

where τ is the maximum time such that $|x'_n - x_n| < \Delta$ for trajectories x_n and x'_n starting from x_0 and $x'_0 = x_0 + \delta_0$ respectively, while $\langle \cdot \rangle$ is an average over the trajectories starting from different initial values. The length scale Δ can be considered as the scale of observation.

Here we consider measurement of the finite-size Lyapunov exponent for macroscopic variables with a certain finite size disturbance at a macroscopic level. As long as the system size is finite, this finite-size Lyapunov exponent reflects not only the macroscopic motion but also the microscopic chaos. On the other hand, if low-dimensional macroscopic dynamics has a characteristic time scale separated from the microscopic dynamics, it will be possible to extract the growth rate of perturbation in the collective motion from the finite-size Lyapunov exponent for the macroscopic variable(s). To do so, we postulate the following assumptions that are expected to hold if the collective dynamics is low-dimensional chaos or on a torus.

First note that in the limit $\Delta \rightarrow 0$ and $\delta_0 \rightarrow 0$, the finite-size Lyapunov exponent $\lambda_{\delta_0}(\Delta)$ for macroscopic variable in finite system size is expected to converge to the maximum Lyapunov exponent λ_m , which is determined by the conventional Lyapunov exponents for the microscopic variables directly.

Considering that the collective dynamics appears by coarse-grained macroscopic variables, we postulate that in the macroscopic phase space there are length scales $\Delta \in [\Delta_m, \Delta_C]$, where the macroscopic variable is characterized by *collective Lyapunov exponent* λ_C . Below $\Delta < \Delta_m$ the microscopic chaos dominates, while the orbit is out of the attractor for $\Delta > \Delta_C$ at a macroscopic level. To have low-dimensional

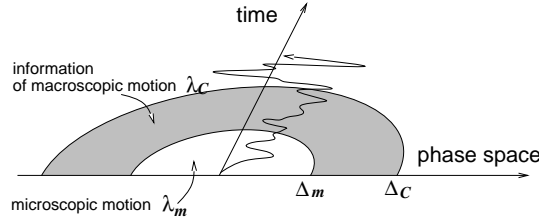


Fig. V.1: Schematic representation of the collective Lyapunov exponent.

collective dynamics, it is postulated that λ_C is independent of N (as long as it is large enough), and that Δ_m should approach zero with $N \rightarrow \infty$ while Δ_C remains finite (see Fig.V.1).

Based on the above assumptions, we can have a form of the finite-size Lyapunov exponent as a function of the scale Δ . Let δ_n denote the distance from the original trajectory at time step n . For the scale $\Delta < \Delta_m$, δ_n increases proportionally with $e^{\lambda_m n}$, i.e., $\delta_n = \delta_0 e^{\lambda_m n}$. Hence $\tau(\Delta) = \frac{1}{\lambda_m} \log \frac{\Delta}{\delta_0}$ follows, independently of the collective dynamics.

On the other hand, for the scale $\Delta_m < \Delta < \Delta_C$, δ_n grows in proportion to $e^{\lambda_C n}$ for a chaotic case with $\lambda_C > 0$, or δ_n grows in proportion to n^κ for a torus case with a certain constant κ . Considering the microscopic time scale denoted by $\tau_m = \frac{1}{\lambda_m} \log \frac{\Delta_m}{\delta_0}$, $\delta_n = \Delta_m e^{\lambda_C(n-\tau_m)}$ for a chaotic case, or $\delta_n = \Delta_m (n - \tau_m)^\kappa / C$ for a torus case with a certain constant C . The constant C may specify a property of the phase diffusion, and may reflect the macroscopic dynamics accordingly. Corresponding to each collective motion, $\tau(\Delta)$ and the finite-size Lyapunov exponent $\lambda_{\delta_0}(\Delta)$ are given by

$$\tau(\Delta) = \begin{cases} \frac{1}{\lambda_C} \log \frac{\Delta}{\Delta_m} + \frac{1}{\lambda_m} \log \frac{\Delta_m}{\delta_0} & (\text{chaos}) \\ C \left(\frac{\Delta}{\Delta_m} \right)^{\frac{1}{\kappa}} + \frac{1}{\lambda_m} \log \frac{\Delta_m}{\delta_0} & (\text{torus}) \end{cases}, \quad (\text{V.2})$$

and

$$\lambda_{\delta_0}(\Delta) = \begin{cases} \frac{\lambda_m \lambda_C \log \frac{\Delta}{\delta_0}}{\lambda_C \log \frac{\Delta_m}{\delta_0} + \lambda_m \log \frac{\Delta}{\Delta_m}} & (\text{chaos}) \\ \frac{\log \frac{\Delta}{\delta_0}}{\frac{1}{\lambda_m} \log \frac{\Delta_m}{\delta_0} + C \left(\frac{\Delta}{\Delta_m} \right)^{\frac{1}{\kappa}}} & (\text{torus}) \end{cases}, \quad (\text{V.3})$$

where Δ_m , and λ_C , or κ and C are fitted parameter to data¹, λ_m is the maximum Lyapunov exponent, and δ_0 is the value of initial disturbance. In order to obtain the values of parameters Δ_m , and λ_C , or κ and C easily, it is convenient to transform Eq.(V.3) to remove δ_0 dependence of the data. For it, we define $t(\Delta)$ as $t(\Delta) = \tau(\Delta) + \frac{1}{\lambda_m} \log \delta_0$, which characterizes the time for amplification of error from a certain scale independent of δ_0 . From Eq.(V.2), we obtain

$$t(\Delta) = \begin{cases} \frac{1}{\lambda_C} \log \Delta + \left(\frac{1}{\lambda_m} - \frac{1}{\lambda_C} \right) \log \Delta_m & (\text{chaos}) \\ C \left(\frac{\Delta}{\Delta_m} \right)^{\frac{1}{\kappa}} + \frac{1}{\lambda_m} \log \Delta_m & (\text{torus}) \end{cases}. \quad (\text{V.4})$$

From data, we can easily obtain $t - \Delta$ plot ($t - \log \Delta$ or $\log t - \log \Delta$ plot), in which

¹ Here we use C in this equation for $C^{1/\kappa}$ in the previous notation.

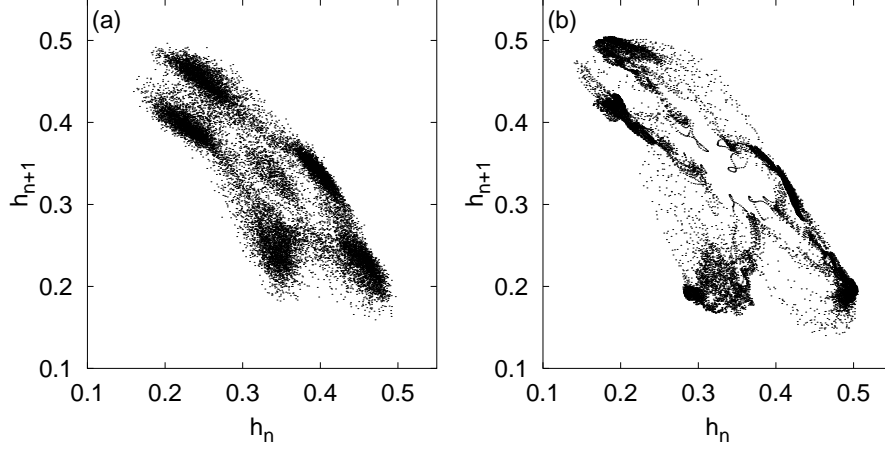


Fig. V.2: An example of return map for chaotic collective motion. The parameters are $a = 1.92 \pm 0.044$, $\epsilon = 0.1$ and (a) $N = 10^4$, and (b) $N = 10^7$. Points (h_n, h_{n+1}) are plotted over 3×10^4 steps after transient are discarded.

Δ_m appears as a shift of constant, and λ_C or κ is given by a slope in a suitable plot². In order to confirm the existence of the low-dimensional collective motion, it is necessary that Δ_m decreases with N as $1/\sqrt{N}$ for a constant λ_C .

V.3 Heterogeneity Induced Order: Revisited

To demonstrate our method and to show the existence of some lower dimensional macroscopic motion, we study a certain coupled dynamical system, which shows collective motion. Here we adopt a *heterogeneous* globally coupled map (GCM) with a distributed parameter,

$$x_{n+1}(i) = (1 - \epsilon)f_i(x_n(i)) + \frac{\epsilon}{N} \sum_{j=1}^N f_j(x_n(j)), \quad (\text{V.5})$$

where $x_n(i)$ is the variable of the i 'th element ($i = 1, 2, 3, \dots, N$) at discrete time n , and $f_i(x)$ is an internal dynamics for each element. For the internal dynamics we choose the logistic map $f_i(x) = 1 - a(i)x^2$, where the parameter $a(i)$ for the non-linearity is distributed between $[a_0 - a_w, a_0 + a_w]$ as $a(i) = a_0 + \frac{a_w(2i-N)}{N}$. (In the following, the parameters are indicated by $a = a_0 \pm a_w$). As a macroscopic variable, we adopt the mean field,

$$h_n = \frac{1}{N} \sum_{i=1}^N f_i(x_n(i)). \quad (\text{V.6})$$

in which the collective motion is contained.

As we have studied up to the present Chapter, when the coupling ϵ is small enough, oscillation of each element is mutually desynchronized, and the effective degrees of freedom increase in proportion to the number of elements N . Still, a macroscopic

² For our present purpose, C is not an important constant.

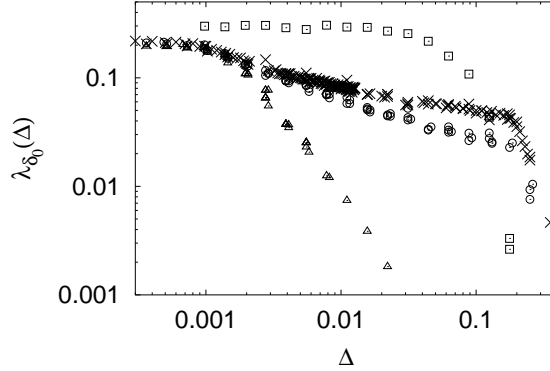


Fig. V.3: $\lambda_{\delta_0}(\Delta)$ is plotted for the model (V.5) (\odot , $a = 1.92 \pm 0.044$, $\epsilon = 0.1$; \times , $a = 1.9 \pm 0.025$, $\epsilon = 0.098$; \triangle , $a = 1.9 \pm 0.025$, $\epsilon = 0.11$; \square , $a = 1.69755 \pm 0$, $\epsilon = 0.008$). $N = 10^7$. Initial perturbation amplitude δ_0 is fixed at 1.0×10^{-7} . For computation, displacement $h'_0 = h_0 + \delta_0$ is created by perturbing the orbit as $x'_0(i) = x_0(i) + \frac{1}{N} \delta_0 \times \sigma$, where σ is a random number in $[-1, 1]$. Each point is obtained by averaging over 100 samples. Specific choice of this perturbation scheme is irrelevant to our results, as long as the collective variable is perturbed. Adopting the algorithm to be presented, the collective motion is shown to be torus (\triangle), low-dimensional chaos (\odot and \times), and high-dimensional chaos (\square).

variable is found to show some kind of ordered motion distinguishable from noise, ranging from torus to high-dimensional chaos.

For instance, Fig.V.2 gives a return map of the mean field dynamics of the GCM (V.5). With the increase of the system size N , the mean field dynamics shows some pattern that may suggest low-dimensional chaos. As is shown in the previous Chapter, the mean field dynamics shows some bifurcation from quasiperiodic motion to chaos (Figs.IV.2, IV.4, and IV.5). In these cases, microscopic motion keeps high dimensional chaos, i.e. all of the N Lyapunov exponents are positive, even if there appears quasiperiodic motion for the collective variable h_n as N goes to infinity. Here we demonstrate the existence of low-dimensional collective motion by the above collective Lyapunov exponent λ_C and by the N dependence of Δ_m .

Fig.V.3 gives the finite-size Lyapunov exponent for the mean field dynamics of the GCM (V.5). Here we perturb the orbit to give rise to a change from h_0 to $h'_0 = h_0 + \delta_0$ (see the caption of Fig.V.3 for detailed description). In Fig.V.4, t is plotted as a function of Δ . As is shown in Fig.V.4(a), the slope of the semi-log plot is independent of N . The Lyapunov exponent λ_C , characterizing the collective motion, is given by the inverse of the slope, and is estimated as 0.02, which is much smaller than the maximum Lyapunov exponent of the system (see the caption of Fig.V.5). Note also that no plateau is visible in the finite-size Lyapunov exponent in Fig.V.3 corresponding to λ_C . On the other hand, Δ_m , given by the shift of the plots, decreases with N , while Δ_C does not show significant change³ Thus the scale for the collective motion $\Delta_m < \Delta < \Delta_C$ increases with N . In Fig.V.5, N dependence of Δ_m is plotted, which gives $\Delta_m \sim \frac{1}{\sqrt{N}}$, whose form is expected from the central limit theorem. Hence the emergence of low-dimensional collective chaos at the thermodynamic limit is confirmed.

³ In this Chapter, we did not measure the scale Δ_C explicitly, because we need only the existence of such upper bound (for the perturbation), within which Eq.(V.4) can be fitted, and which does not decrease with N . Still, we can estimate Δ_C around 0.2, by extending our method to the regime $\Delta > \Delta_C$.

Summary and Discussion

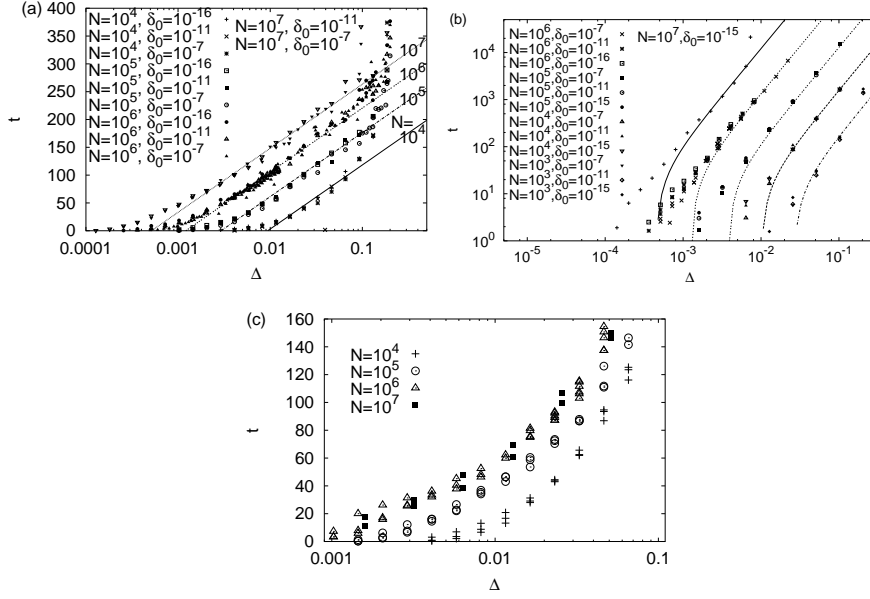


Fig. V.4: The normalized time steps $t(\Delta)$ are plotted for $N = 10^4, 10^5, 10^6$, and 10^7 , with the fitted curves Eq.(V.4). (a) *chaotic case* (with a semi-log plot), for $a = 1.9 \pm 0.025, \epsilon = 0.098$. (b) *torus case* (with a log-log plot), for $a = 1.9 \pm 0.025, \epsilon = 0.11$. The maximum Lyapunov exponent $\lambda_m = 0.41(a), 0.39(b)$ are obtained directly from the GCM (V.5). The parameters obtained by a least square fitting algorithm give (a) $\lambda_C = 0.02$, and (b) $\kappa = 0.5$. (c) *high-dimensional case*, which does not obey Eq.(V.4), (with a semi-log plot), for $a = 1.6962 \pm 0, \epsilon = 0.008$. In this case, while the return map shows some structure, t for $N = 10^6$ and 10^7 are not separated any more. For (c), the data from $\delta_0 = 10^{-7}, 10^{-11}, 10^{-16}$ are plotted by the same symbol, since the difference by δ_0 is not observed as in (a) and (b).

We have also applied the present algorithm to the case with a collective torus motion. Fig. V.4(b), ($t - \Delta$ plot), shows that κ , the inverse of the slope, is 0.5, independent of N . Indeed this exponent $1/2$ is expected from the diffusion of phase on the torus. The decrease of Δ_m with N is also plotted in Fig. V.5, which again shows the expected decrease of $\Delta_m \sim \frac{1}{\sqrt{N}}$. Hence the collective torus motion is demonstrated.

V.4 Summary and Discussion

In this Chapter, we have proposed an algorithm to characterize the collective (chaotic) motion, and applied to it to a GCM. We have introduced the collective Lyapunov exponent, to characterize the growth rate of perturbation in the collective motion. The microscopic chaotic motion exists at a small scale of the macroscopic variable, but such scale Δ_m is shown to decrease as $1/\sqrt{N}$. Hence, the macroscopic motion is separated from the microscopic motion and the emergence of low-dimensional collective motion with $N \rightarrow \infty$ is confirmed⁴.

⁴ The existence of low-dimensional torus motion is detected, as a plateau of the correlation dimension within a certain range of scale (see in Section IV.2 and Fig. IV.3). In the case of collective chaos, the plateau is not clearly visible in the plot, although the plot may suggest some signature of low-dimensionality.

Summary and Discussion

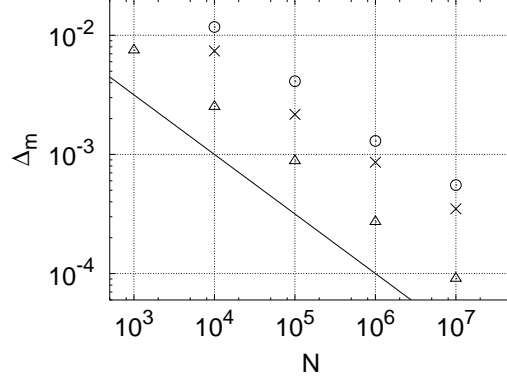


Fig. V.5: The microscopic length scales Δ_m are plotted as a function of N for several parameters. Δ_m is obtained from the fitting indicated in Fig.V.4. The parameters are \odot , $a = 1.92 \pm 0.044$, $\epsilon = 0.1$ (chaos: $\lambda_C = 0.009$, $\lambda_m = 0.42$); \times , $a = 1.9 \pm 0.025$, $\epsilon = 0.098$ (chaos: $\lambda_C = 0.02$, $\lambda_m = 0.41$); and \triangle , $a = 1.9 \pm 0.025$, $\epsilon = 0.11$ (torus: $\kappa = 0.5$, $\lambda_m = 0.392$).

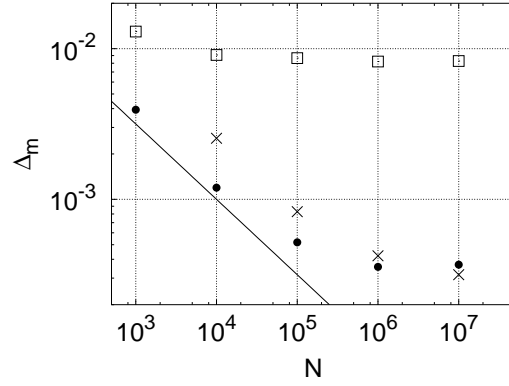


Fig. V.6: Δ_m of the quasiperiodic-like collective motion of GCM with identical parameter is plotted as a function of N . The parameters are $a = 1.86$, $\epsilon = 0.1$ (\square), $a = 1.5690$, $\epsilon = 0.01$ (\bullet), and $a = 1.6962$, $\epsilon = 0.008$ (\times).

Existence of low-dimensional collective chaos in the presence of microscopic chaos has often been suspected (Bohr et al. 1987, Grinstein 1988, Bennett et al. 1990). Indeed for a GCM with homogeneous elements (i.e., with $a = a_0 \pm 0$), such low-dimensional collective chaos has not been observed, and the collective motion there is believed to be high-dimensional as we have seen in the previous Sections. (In the next Chapter, number of the dimension of the mean field motion will be directly studied.) In Fig.V.4(c), we have also applied our algorithm to this case. The separation of scales is not clear and the data cannot be fitted with Eq.(V.4). The shift of the plot gets smaller with the increase of N . At least Δ_m does not decrease as $1/\sqrt{N}$. When the collective motion shows torus-like structure as is seen in Chapter II, it is possible to measure the scale Δ_m of each system size. In Fig.V.6, such Δ_m is plotted as a function of N . Δ_m decreases with N as $1/\sqrt{N}$ up to a certain system size. However, Δ_m stays a certain constant⁵ even with the further increase of N . Hence, the scale of the macroscopic motion in GCM with $a = a_0 \pm 0$, is not well separated from the microscopic dynamics. This gives a crucial difference between the *heterogeneous* GCM and *identical* GCM.

The $t - \Delta$ plot provides a tool to distinguish low-dimensional collective chaos from high-dimensional one. In the former case, the plot shifts as $\log(\sqrt{1/N})$ with N , while for the latter case such shift is not observed. This distinction generally holds, even if the approximation to get Eq.(V.4) may not be very good (Cencini et al. 1998).

Our present algorithm to extract macroscopic motion is applicable to any system subjected to microscopic chaos, including spatially extended systems from coupled map lattice to partial differential equations, and coupled oscillators systems (Nakagawa & Kuramoto 1994, Chabanol et al. 1997). It is also expected to be applied even if we do not know the equation of motion, since the method of (Paladin et al. 1995, Aurell et al. 1996) is based on Wolf's algorithm (Wolf et al. 1985) developed for the estimate of Lyapunov exponents from experimental data. Thus, we hope that our method developed in this letter is applicable to data obtained from experiments.

⁵ Such converged Δ_m is plotted as width of the torus-like motion in Fig.II.18, in which we discuss the asymptotic behavior of the width with the coupling strength ϵ .

CHAPTER VI

NOISELESS COLLECTIVE MOTION OUT OF NOISY CHAOS

Effect of microscopic external noise on the collective motion is studied for a globally coupled map in fully desynchronized state. Without external noise a macroscopic variable shows high-dimensional chaos distinguishable from random motions. With the increase of external noise intensity, the collective motion is successively simplified. The number of effective degrees of freedom in the collective motion is found to decrease as $-\log \sigma^2$ with the external noise variance σ^2 . It is shown how the microscopic noise can suppress the number of degrees of freedom at a macroscopic level.

VI.1 Introduction

Chaotic motion has been observed experimentally in physical, chemical and biological systems. Since the evolution of these systems is subjected by external fluctuations, the observability of deterministic chaos depends on how the external fluctuations influence on it (Oono & Takahashi 1980, Crutchfield 1983). Motivated by this point, extensive studies have been carried out about an enhancement of predictability and unpredictability of chaotic motion (Crutchfield 1983, Matsumoto & Tsuda 1983).

So far such studies are restricted to low-dimensional dynamical systems. Low-dimensional chaotic motion often arises as a macroscopic motion out of microscopic chaos with many degrees of freedom. Let us consider external fluctuations imposed on the microscopic level rather than the macroscopic level. Such a situation is probable in natural systems, such as fluid turbulence, or neural systems with a large number of neurons. Since chaos can amplify a small-scale error, it would be natural to ask a question how such a low-dimensional macroscopic chaos is possible out of high-dimensional chaotic system subjected by external fluctuations (see also the discussion in Chapter I).

In the present Chapter, in order to address this question, we focus on the effect of noise on the collective motion of the globally coupled map (GCM).

The present GCM consists of N elements iterated by a local dynamics $f(x)$ with a global coupling among elements and an external noise. Each i 'th element obeys the equation

$$x_{n+1}(i) = (1 - \epsilon)f(x_n(i)) + \frac{\epsilon}{N} \sum_{j=1}^N f(x_n(j)) + \xi_n(i), \quad (\text{VI.1})$$

This chapter is based on Shibata, Chawanya & Kaneko 1998.

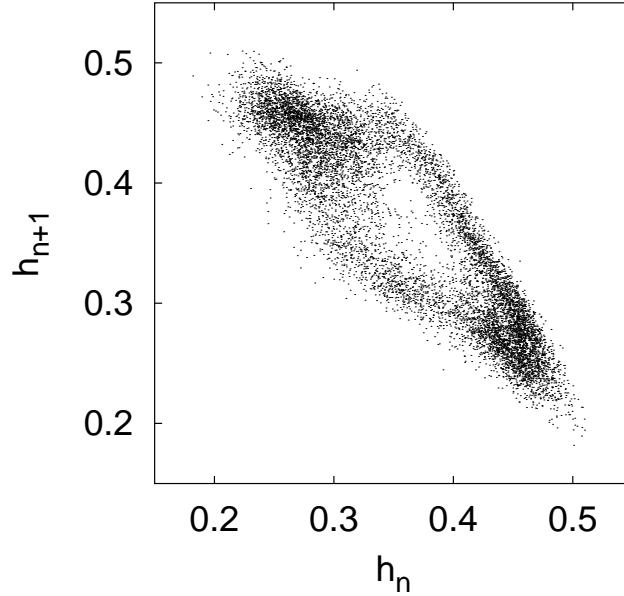


Fig. VI.1: A return map of the collective motion in GCM (VI.1) without noise. $a = 1.86$, $\epsilon = 0.1$, $\sigma = 0.0$, $N = 10^7$.

at time step n . Here, we adopt the logistic map $f(x) = 1 - ax^2$ for the local dynamics, and Gaussian random process for $\xi_n(i)$, with $\langle \xi_n(i) \rangle = 0$ and $\langle \xi_n(i) \xi_m(j) \rangle = \sigma^2 \delta_{nm} \delta_{ij}$. The variance of Gaussian distribution is denoted by σ^2 . In order to bound the system within a finite region, cut off of ξ is introduced, so that $f(f(1 + \xi) + \xi) > f(1 + \xi)$. In this Chapter, however, we study small σ regime, where the cut off effect is irrelevant for numerical calculation.

Fig. VI.1 gives an example of the collective motion in GCM (VI.1) without external noise ($\sigma = 0$). We adopt the mean field,

$$h_n = \frac{1}{N} \sum_{i=1}^N f(x_n(i)), \quad (\text{VI.2})$$

as a macroscopic observable. While the microscopic motion shows high dimensional chaos in the sense that the Lyapunov dimension is proportional to the number of element N , the macroscopic motion shows quasiperiodic-like motion as is shown in Fig. VI.1. As we have already seen in the previous Chapters, in almost all the parameter values, the mean field motion shows some coherence ranging from quasiperiodic-like motions to higher dimensional motions distinguishable from random motions. However, even if the macroscopic motion looks like quasiperiodic, scattered points around the torus-like structure depicted in Fig. VI.1 does not vanish even in the thermodynamic limit (Chapters II, and V), which indicates high dimensionality of the collective motion. So far, the mean field motion is believed to be *infinite dimensional* motion even when the torus like structure is observed (Ershov & Potapov 1997, Chawanya & Morita 1998, Shibata & Kaneko 1998*b,a*).

The addition of noise may, however, destroy such coherence among elements. It has been shown that the microscopic external noise leads the mean square deviation (MSD) of the mean field distribution decreases in proportion to $1/N^\beta$ with $\beta \leq 1$, when σ is

larger than a certain constant (Kaneko 1992). It is also reported that, the external noise sharpens the peak in the power spectrum of the collective motion (Perez et al. 1993). In this Chapter, we clarify an effect of noise on the collective motion in GCM.

In the next Section, we will provide some of the phenomenology of the collective motion in the noisy GCM. Then, the effect of noise is characterized by the Lyapunov dimension of the collective motion, which is obtained by calculating the Lyapunov exponents of the collective motion. The result suggests that the number of degrees of freedom of the collective motion decrease as $-\log \sigma$ with increasing noise intensity σ . In Section VI.3, a kinetic approach to the linear stability of the mean field dynamics is presented. Then, we obtain an argument of the logarithmic dependence of the dimension upon the noise intensity. This Chapter concludes in Section VI.4.

VI.2 Effect of Noise on Collective Motion

Consider the one-body distribution function $\rho_n(x)$ to study the behavior of the collective motion in the thermodynamic limit $N \rightarrow \infty$. Since the mean field value

$$h_n = \int f(x) \rho_n(x) dx, \quad (\text{VI.3})$$

is applied commonly for each element, and the additive noise can be represented as a deterministic diffusion process of the distribution function in the thermodynamic limit, the evolution of $\rho_n(x)$ obeys Perron-Frobenius equation written as

$$\rho_{n+1}(x) = \int dy \frac{1}{\sqrt{2\pi}\sigma} e^{-\frac{(F_n(y)-x)^2}{2\sigma^2}} \rho_n(y), \quad (\text{VI.4})$$

with $F_n(x) = (1 - \epsilon)f(x) + \epsilon h_n$.

Fig.VI.2 gives an example of return map of the mean field value obtained numerically in GCM with the external noise. The parameters a and ϵ are the same as in Fig.VI.1. Numerical calculation was carried out through integration of Eq.(VI.4) using a sufficiently large dimensional vector as an approximation of $\rho_n(x)$. As is shown in Fig.VI.2, the motion has a clearer structure than the motion without noise. By increasing σ , motions on a torus, locking states and lower dimensional chaos are observed. With further increase of σ , the collective motion collapses to a fixed point. Hence, with the increase of the noise a sort of bifurcation to lower dimensional motions is observed.

To clarify this point, it seems straightforward to measure the number of effective degrees of freedom in the collective motion. We calculate the Lyapunov dimension of the dynamics of $\rho_n(x)$. The Lyapunov exponents are given by growth rates of tangent vectors around the orbit, obtained by Eq.(VI.4). For numerical calculation, $\rho_n(x)$ in Eq.(VI.4) is approximated by a sufficiently large dimensional vector, and its linear stability around the orbit is studied.

In Fig.VI.3, the Lyapunov dimension denoted by D_C is plotted as a function of the noise variance σ^2 . For sufficiently large σ , only the stationary state is observed and D_C is zero accordingly. With the decrease of σ we have found the low dimensional collective motion ($D_C \sim O(1)$) ranging from the motion on a torus to low dimensional chaos. With the further decrease of σ , the dimension grows as

$$D_C \propto -\log \sigma^2. \quad (\text{VI.5})$$

This implies that *the number of effective degrees of freedom goes to infinity in the zero noise limit*, as is expected from the analysis of the collective motion in GCM.

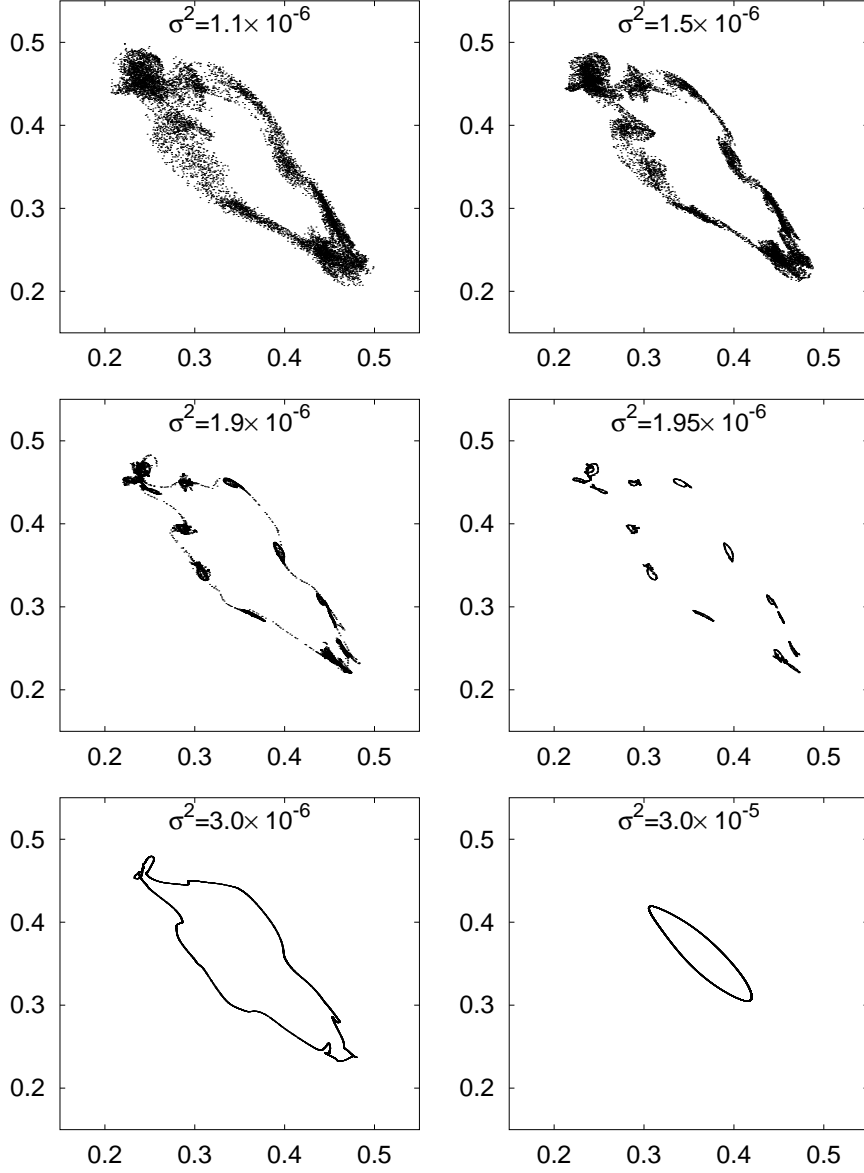


Fig. VI.2: A return maps (h_n, h_{n+1}) of the collective motion in GCM (VI.1) with noise. $a = 1.86, \epsilon = 0.1$. The noise variances are indicated in each figure. Numerical calculation was carried out with integration of Eq.(VI.4) using a sufficiently large dimensional vector as an approximation of the distribution function.

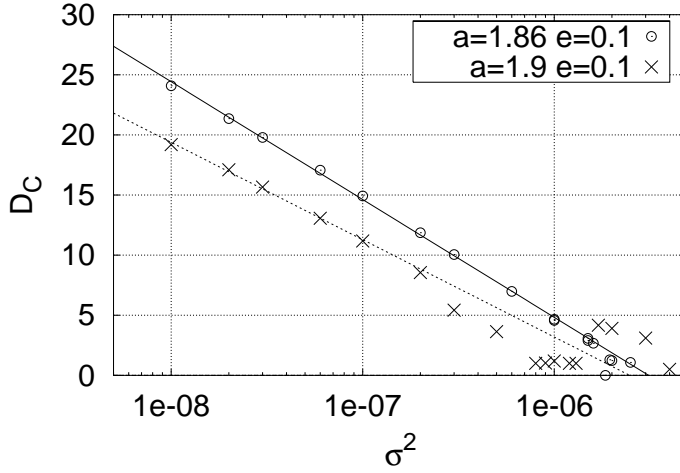


Fig. VI.3: The dimension of the collective motion is plotted as a function of noise intensity, obtained by the Lyapunov dimension. The Lyapunov exponents are calculated as growth rates of the tangent vector around the orbit, obtained by Eq.(VI.4). For numerical calculation, $\rho_n(x)$ is approximated by a sufficiently large dimensional vector, and the tangent vectors are orthonormalized at each time step.

VI.3 Strength of Noise and Complexity of Collective Motion

In the large σ regime a variety of bifurcations appears, which may strongly depend on the parameters. However, the above result suggests that the scaling relation (VI.5) will be a characteristic common to the high-dimensional collective motions in the small σ regime.

Although the evolution rule is originally given for the microscopic variables, our main interest is on the behavior of macroscopic variables which would be the only possible observable in typical cases. Thus, it is highly desirable to obtain a closed description of the behavior of the macroscopic variables, which could be written as

$$h_n = h(h_{n-1}, h_{n-2}, \dots), \quad (\text{VI.6})$$

for an idealized example. In most cases, however, it is quite difficult and may well be impossible to obtain such a description. Thus, we examine the linear response of the system against infinitesimal perturbation on the macroscopic variables, and obtain the variational equation describing the evolution of the small deviation of the macroscopic variables in a neighborhood of a trajectory¹.

In the present case, since the elements interact only through the mean field value, it is quite natural to expect that the behavior of the mean field value can be consistently described by itself. We expect that the effective number of the dimension of the collective motion gives substantial agreement with the Lyapunov dimension of the

¹ In Section III.2, we have seen the linear stability analysis around the fixed point of the mean field value. The following discussion is similar to the linear stability analysis of fixed point, though we are going to study the linear stability of the orbits.

macroscopic dynamics estimated in the above mentioned way. We concentrate on the small σ regime and give qualitative explanation for the scaling relation (VI.5).

If we consider small deviations η_n of h_n , then η_n is regarded as a function of $\{\eta_{n-1}, \eta_{n-2}, \dots\}$. The evolution of η_n from the unperturbed orbit h_n is given by,

$$\eta_n = \sum_{\tau=1}^{\infty} L_{\tau} \eta_{n-\tau} + O(\eta^2), \quad (\text{VI.7})$$

where L_{τ} is a coefficient to give the linear response of the mean field value at n step to the displacement at $n - \tau$ step. The number of the Lyapunov dimension of the mean field dynamics is estimated from the eigenvalues of this linear equation.

We should note that such estimation does not hold if the effects of perturbations at different time steps could cancel out completely, as in the case that $\rho_n(x)$ contracts into a δ -function. In the present case, however, as long as $\rho_n(x)$ has a continuous support, as is expected from the microscopic high-dimensional chaos, the effect of η_n does not disappear completely by the perturbation at the other time step.

First we estimate L_{τ} from the dynamics of the distribution function given by Eq.(VI.4). In the small noise limit ($\sigma \rightarrow 0$), from Eqs.(VI.3) and (VI.4), L_{τ} is given by

$$L_{\tau} = \epsilon \int dx \frac{dF_n^{(\tau)}(x)}{dx} \rho_{n-\tau+1}(x), \quad (\text{VI.8})$$

where $F_n^{(\tau)}(x) \equiv F_n \circ F_{n-1} \circ \dots \circ F_{n-\tau}(x)$.

For $\tau \gg 1$, $dF_n^{(\tau)}(x)/dx$ in Eq.(VI.8) changes its sign quite frequently in x . Consider the partition of x at the points such that $F_n^{(\tau)}(x) = 0$ (see Fig.III.2). Denoting the typical value of $|dF^{(\tau)}(x)/dx|$ by $d(\tau)$, the interval of partitions is estimated at $1/d(\tau)$, which decreases rapidly with τ . Since the integration in a partition becomes zero if $\rho(x)$ stays constant in that partition, the partitions where $\rho_n(x)$ changes drastically in x contribute to the estimation of L_{τ} much more than the partitions where $\rho_n(x)$ does not change so much.

In the case of small noise limit ($\sigma \rightarrow 0$), the most drastic change part of $\rho_n(x)$ comes from the inverse square-root singularities, which is the characteristic structure of distribution function for the logistic map. Hence, the integration in the partitions containing the characteristic structure in $\rho_n(x)$ is estimated at $O(\sqrt{d(\tau)})$ (see Eq.III.7). $d(\tau)$ is roughly estimated at $e^{\lambda_m \tau}$ for $\tau \gg 1$, where λ_m is the Lyapunov exponent of the local mapping². Consequently, the response L_{τ} to the perturbation grows exponentially with the rate $\frac{1}{2}\lambda_m$.

Even in the presence of finite amplitude of the noise, the above order estimation for L_{τ} is still valid for τ smaller than $\tau_c \equiv -\log \sigma / \lambda_m$, where the typical width of the partitions becomes comparable with the typical amplitude of the noise, i.e. $1/d(\tau) \sim e^{-\lambda_m \tau} = \sigma$.

For larger $\tau > \tau_c$, however, the effect of noise in smoothening the distribution $\rho(x)$ appears so that L_{τ} will start to decay with τ .

Partially integrating (VI.8), we obtain

$$\begin{aligned} L_{\tau} &= -\epsilon \int dx F_n^{(\tau)}(x) \frac{d\rho_{n-\tau+1}(x)}{dx} \\ &= -\epsilon \int dx \tilde{F}_n^{(\tau)}(x) \frac{d\rho_{n-\tau+1}(x)}{dx}, \end{aligned} \quad (\text{VI.9})$$

² Here we neglect the fluctuation of the expansion rate.

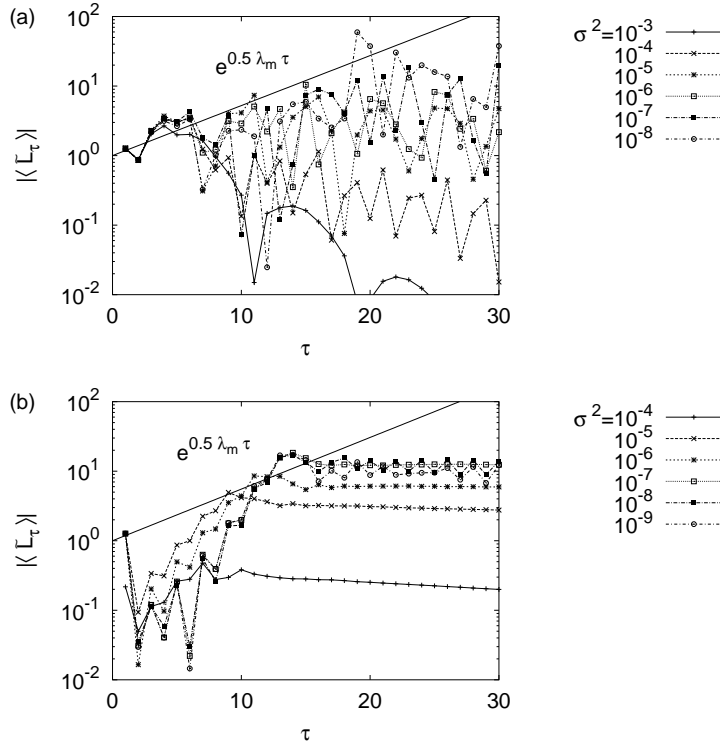


Fig. VI.4: The linear coefficient $|\langle \tilde{L}_\tau \rangle|$ is plotted as a function of τ . $\langle \cdot \rangle$ denotes time average. The parameters are (a) $a = 1.95, \epsilon = 0.1$, and (b) $a = 1.56905, \epsilon = 0.01$. The noise variance σ^2 is indicated at the right of the figure. The line indicates $e^{\frac{1}{2} \lambda_m \tau}$, in which the Lyapunov exponent λ_m of $f(x) = 1 - Ax^2$ is obtained numerically.

with $\tilde{F}_n^{(\tau)}(x) = F_n^{(\tau)}(x) - \bar{F}_n^{(\tau)}$, where $\bar{F}_n^{(\tau)}$ is the average value of $F_n^{(\tau)}(x)$ over the support of $\rho_n(x)$. With the increase of τ , $\tilde{F}_n^{(\tau)}(x)$ becomes a rapidly oscillating function about zero-mean in x , and the integration of $\tilde{F}_n^{(\tau)}(x)$ over any finite range within the support of $\rho_n(x)$ will approach to zero³. Since $|\frac{d\rho_{n-\tau+1}(x)}{dx}|$ is uniformly bounded due to the existence of the noise, L_τ converges to zero. Hence, we conclude that $L_\tau \sim e^{\frac{1}{2} \lambda_m \tau}$ for $\tau < O(\tau_c)$ whereas $L_\tau \sim 0$ for $\tau > O(\tau_c)$.

In Fig. VI.4, the time average of the coefficient $\tilde{L}_\tau = \int dx \frac{dF_n^{(\tau)}(x)}{dx} \rho_{n-\tau+1}(x)$, instead of L_τ , obtained numerically is plotted as a function of τ . Notice that the local dynamics $f(x)$ should be considered as $1 - Ax^2$, rather than $1 - ax^2$, where A is the effective nonlinear parameter shown in Chapter II. In Fig. VI.4, $|\langle \tilde{L}_\tau \rangle|$ seems to grow exponentially until its saturation after a certain time step. As the decrease of σ^2 , such a time step becomes longer. The coefficients of $|\langle \tilde{L}_\tau \rangle|$ for several noise intensity seems to constitute an envelop, whose slope is $\frac{1}{2} \lambda_m$.

Hence, as far as the linear stability is concerned, the mean field value is not sensitive to the mean field values before sufficiently long time step (before $O(\tau_c)$ steps). Thus we can consider a dynamics of h_n as a function of the mean field values of the past

³ Here we assume the map $F_n^{(\tau)}(x)$ has mixing property, which seems natural when the distribution is connected.

$O(\tau_c)$ steps at least in the neighborhood of the orbit. Since we have to consider the contribution only from the latest $O(\tau_c)$ steps, the dimension of this dynamical system is also $O(\tau_c)$. Hence, the dimension of the mean field dynamics is within the order of τ_c . Accordingly the number of effective degrees of freedom of the mean field dynamics grows as $-\log \sigma$ with the decrease of σ , and can grow arbitrary large as σ approaches zero.

VI.4 Summary and Discussion

In the present Chapter, we have shown that the noise in a microscopic level reduces the complexity of the collective motion, which is characterized by the number of degrees of freedom. It is shown numerically that the dimension of the dynamics of Perron-Frobenius equation Eq.(VI.4) satisfies the scaling relation (VI.5). On the other hand, analytic estimate of the mean field dynamics also supports Eq.(VI.5). Hence, the number of effective degrees of freedom of the collective motion in the present GCM is concluded to satisfy the scaling relation (VI.5).

Such a relation is expected to hold when the collective motion keeps high dimensional motion with microscopic chaos. Such a high dimensional collective motion is supported by the exponential growth of the linear response coefficient. When the distribution function has peaks of the height $\delta\rho(x)$ within the width δx , such an exponential growth is expected until $\tau \sim \log \delta x$ and thus a high dimensional collective motion appears. Even when the local mapping is a higher-dimensional non-hyperbolic mapping or a flow system, the present argument on the collective motion is expected to hold. Hence, the logarithmic dependence of the dimension upon the noise intensity given by the scaling relation (VI.5) will be observed in a broad range of systems.

The induced regularities by the addition of noise was also reported as Noise-Induced Order (NIO) in an one-dimensional map (Matsumoto & Tsuda 1983). The induced regularity of our system has some similarity with NIO case, in the point that the external noise destroys a dynamical structure which causes the irregular behavior. In NIO, the noise reduces the measure in the instability region where the intermittent behavior is generated. On the other hand, in the present case, the noise destroys the singularity of the distribution function, that is the source of high-dimensional instabilities of the collective motion.

In the case of NIO, however, the motion is not regular, since the noise is imposed upon the observed variable itself. On the other hand, in the present case, the noise is imposed on the microscopic variables, whereas observed is the macroscopic collective variable. Thus, the noise-induced motion is *deterministic* and low dimensional in the limit of $N \rightarrow \infty$.

We should also mention that our present result may be applicable to experimental systems, such as fluid turbulence, or neural systems consisting of a huge number of neurons with nonlinear dynamics. By controlling thermal noise or some external fluctuation, we hope that the dimensional change or noise-induced low dimensional collective motion is observed, and hence the existence of the collective chaos will be clarified.

CHAPTER VII

PERSPECTIVES AND CONCLUDING REMARKS

In this Thesis, we have studied the collective motion in globally coupled map (GCM) from various of angles. The collective motion in GCM with identical elements has been studied precisely in Chapters II and III. The collective motion in the heterogeneous systems or in the noisy systems has been also investigated in Chapters IV and VI. As we have seen in Chapter V, the existence of the collective chaos has been suggested in the heterogeneous systems, and as in Chapter VI, the noisy systems also show low-dimensional chaos in the macroscopic variables. In this final Chapter, connections among these studies are discussed, and future problems on the collective motion of and beyond GCM are presented.

VII.1 Concluding Remarks

This thesis has been constructed from two viewpoints. One is the viewpoint of *collective chaos*, and the other is the viewpoint of *a network of chaotic elements*. From the former point of view, we ask how (low or finite dimensional) chaotic motion in a macroscopic variable is possible out of essentially very high-dimensional dynamical systems such as fluid systems. On the other hand, from the latter point of view, we ask what is universal phenomena observed in network systems consisting of a huge number of dynamical elements.

When the coupling strength among elements constituting a huge network, the tendency to synchronize with each other is quite weak. The system is high dimensional state in the sense that the Kolmogorov-Sinai entropy is proportional to the system size. However, macroscopic variables do not obey the law of large number, and accordingly the motion of the variables does not vanish in the thermodynamic limit. This implies a collective behavior of the system. In Chapter II, the collective behavior was studied in GCM. Several coherent motions exist, even in fully desynchronized state. The macroscopic variable was found to show some kind of ordered motion distinguishable from noise, ranging from torus to high-dimensional chaos. To characterize the collective behavior, we introduced scaling transformation of parameters, and detected in parameter space a *tongue-like bifurcation structure* in which collective motions is possible.

From the dynamical system point of view, the collective motion suggests that a stationary state of the distribution function of the elements is unstable. Stability of the

stationary state was studied in Chapter III. It was shown that the fixed point solution of the mean field dynamics is unstable. Based on this analysis, the scaling relation of the amplitude was studied. Next, we demonstrated the origin of the slow motion of the collective motion. The mechanism of the bifurcation of the collective motion was also investigated.

In Chapter IV, the collective behavior is studied in GCM with *distributed nonlinearity*. It is shown that the heterogeneity enhances regularity in the collective dynamics. Low-dimensional quasiperiodic motion is often found for the mean-field, even if each element shows chaotic dynamics. The mechanism of this order is due to the formation of an internal bifurcation structure, and the self-consistent dynamics between the structures and the mean-field.

The *collective chaos* is a low (or finite) dimensional chaotic motion in a macroscopic variable of the high-dimensional chaotic systems. In Chapter V, an algorithm to characterize a collective motion is presented, with the introduction of *collective Lyapunov exponent*, as the orbital instability at a macroscopic level. By applying the algorithm to a GCM, existence of low-dimensional collective chaos is confirmed, where the scale of high-dimensional microscopic chaos is separated from the macroscopic motion, and the scale approaches zero in the thermodynamic limit.

The *collective chaos* is also found in noisy systems. In Chapter VI, effect of microscopic external noise on the collective motion is studied for a GCM in fully desynchronized state. Without external noise a macroscopic variable shows high-dimensional chaos distinguishable from random motions. With the increase of external noise intensity, the collective motion is successively simplified. The number of effective degrees of freedom in the collective motion is found to decrease as $-\log \sigma^2$ with the external noise variance σ^2 . It is shown how the microscopic noise can suppress the number of degrees of freedom at a macroscopic level.

The result in the noisy system implies that the number of degrees of freedom in the homogeneous GCM is infinity. The *collective chaos* appears under the presence of *heterogeneity* or *noise*.

VII.2 Future Problems on Globally Coupled Map

Strange Coherence The present result indicates that the heterogeneity or noise in the system makes the collective chaos possible. In the homogeneous GCM, however, the number of degrees of freedom is suggested to be infinity. It is not clear whether the macroscopic motion of the homogeneous system should be considered as a chaos. While the macroscopic motion does not disappear in the thermodynamic limit, it might be doubted that the macroscopic and microscopic scale is separated. Here we phrase this macroscopic motion “*strange coherence*”.

Finite and Infinite System Even when the system indicates the strange coherence, the macroscopic variable shows some lower-dimensional-like motion. In Fig.II.2, we have seen that the quasiperiodic-like motion appears as increasing the system size from 10^5 to 10^7 . What happens when the size is increased from $N = 10^5$ to $N = 10^7$?

A canonical answer for this might be given by considering the finite size effect and the motion of the infinite size system. In the motion of the system with infinite number of elements, infinitely many unstable modes of the macroscopic motion probably exist, as we have seen in the preceding Chapters (e.g. Chapters III and VI). At least quite many unstable modes exist. In a finite system, we observe shadow of the motion of the

infinite size system, and the amplitude of the finite size fluctuation becomes smaller than the characteristic amplitude for a unstable mode as the system size is increased from 10^5 to 10^7 . We observed one of the unstable modes with the increase of the system size from 10^5 to 10^7 .

If it is true, with the increase of the system size, the characteristic amplitude of each unstable mode and the fluctuation of the finite size effect successively cross over each other, and unstable modes should appear one after another. However, it has not been confirmed within our numerical analysis. How can we confirm the above statement?

If the above scenario is probable, what is the sequence of the unstable modes appeared as the increase of the system size? Most probably, the sequence may be determined by the magnitude of the characteristic amplitude of each mode.

In Chapter VI, we have seen that the number of effective degrees of freedom increases as decreasing noise. This can be regarded as successive appearance of the unstable modes with the decrease of noise. Does the sequence of the unstable modes appeared in the noisy system correspond to the sequence of the noiseless system? These questions may be relevant to the selection rule of the macroscopic motion.

Singularity and Regularity We have seen that the singularity of the distribution function is an important part for the instability of the macroscopic motion (Chapter III). The singular point evolves according to the local mapping $f(x)$ until the concentration of the singular distribution essentially decays. In this sense, we can consider that the microscopic and macroscopic motion are not separated completely in the homogeneous GCM.

When the *heterogeneity* or the *external noise* exists in the system, however, the effect of the singularity on the macroscopic motion is expected to be reduced. We have seen precisely how the existence of noise weakens the effect of the singularity in Chapter VI.

We should mention that *random connection networks* of chaotic elements are almost the same with the noisy systems. Here the random connection networks means that arbitrary two elements are randomly chosen to be connected or not connected with certain coupling strength. The coupling strength is the same over the connections. Then, the value of coupling term in the evolution summed over connections is distributed. The variance of the distribution is given according to the ratio of the connections. Thus we expect that the random connection network of the chaotic elements is essentially the same with the noisy network systems.

On the other hand, it may not be simple how the heterogeneity reduces the effect of singularity. The distribution of the nonlinear parameter a can be regarded as a kind of *static fluctuations*. However, within the parameter distribution, there exist many parameters corresponding to the *window*. This implies that the distribution of the nonlinear parameter a is not regarded just as noise. We need further studies of what kind of effect is brought about by the heterogeneity as a whole on the macroscopic motion.

In these cases, one of the effect of the noise or heterogeneity is certainly to reduce the influence of the singularity on the macroscopic motion. Accordingly the number of degrees of freedom of the macroscopic motion decreases.

On the other hand, lower dimensional motions observed in these systems are relevant to *regular part* of the distribution function. Here, the regular part denotes the longer range structure of the distribution function in x , for instance, the distribution of the singular points. Instability of the macroscopic motion brought about by the regular part is an important future problem (Chapter III).

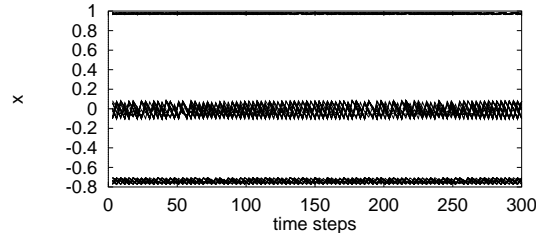


Fig. VII.1: One of coexisting attractors is shown as a time series of elements. In this case, elements are accumulated to three bands. Time series of 100 elements out of 10^5 are plotted every third time steps. A lot of attractors exist depending on the population ratio to each band, while elements are desynchronized from each other. The parameters are $a = 1.85$, $\epsilon = 0.018$, $N = 10^5$.

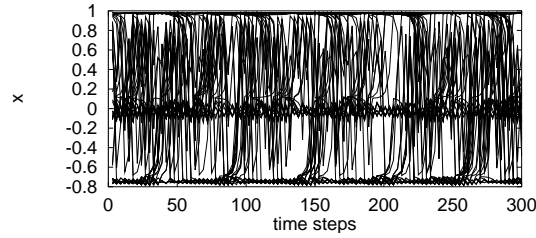


Fig. VII.2: Time series of elements for the same parameter in Fig.VII.1 starting from different initial condition. In contrast with Fig.VII.1, elements spread over x . The mean field dynamics for this time series shows quasi-periodic-like motion. Time series are plotted for 100 elements at every three steps. The parameters are $a = 1.85$, $\epsilon = 0.018$, and $N = 10^5$.

Multiple Attractors, and Coexistence of Different Types of Motion Here we study the coexistence of several attractors of the macroscopic variables that can appear in the GCM. In Section II.4, we have seen one of the examples of multiple attractors of the collective motion in connection with the hysteresis phenomenon. The existence of multiple attractors of the collective motion brings some mathematical question on the one hand. On the other hand, some possibilities of application of such multiple attractors can be considered.

The most straightforward examples are *band splitting* mechanism of multiple attractors. Here, in the *p-band splitting*, the distribution of $x_n(i)$ splits into p disconnected regions. There is no mixing of elements among disconnected regions. An example, for $p = 3$ is shown in Fig.VII.1. Since the number of elements at each region does not change in time, the population ratio of elements at each region gives a time invariant index for an attractor. Depending on the population ratio, there are a lot of attractors. (See e.g. (Kaneko 1995) for the case with a tent map).

The next example of multiple attractors is the coexistence of two types of attractors, one with a band splitting structure (Fig.VII.1) and the other without a band splitting structure (Fig.VII.2). In an attractor with a band splitting structure, elements are accumulated in a few regions. However in an attractor without such structure, elements spread over the whole range of x . Moreover for the former type, there exists a lot of attractors with a different population ratio in each region, as is explained in the first example.

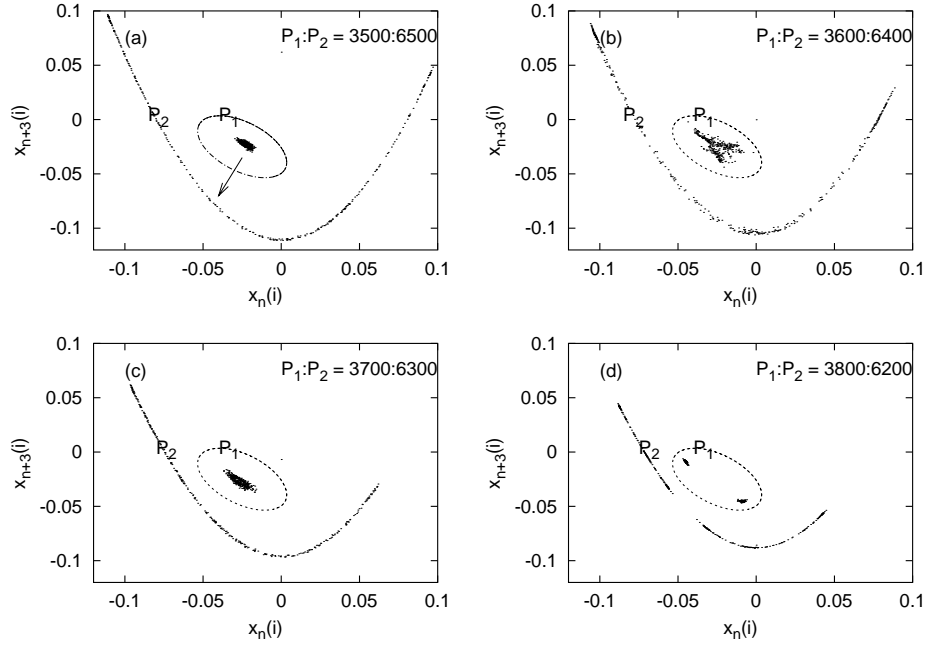


Fig. VII.3: Return maps of element motions to show the coexistence of different kinds of motions. P_1 (circled) and P_2 represent the element motion belonging to a different band in the dynamics, respectively. Two kinds of motions (P_1 , and P_2) co-exist. $P_1 : P_2$ in each figure indicates the number of population in each group. With the change of ratio, two kinds of motions are varied. The parameters are $a = 1.88$, $\epsilon = 0.04$, $N = 10^4$.

Another important topic related to the multiple attractor is the coexistence of different kinds of element motions. When the elements are accumulated into few bands, depending on the ratio of population in bands, the motion of elements in each band is different. In Fig. VII.3, two kinds of element motions are plotted for attractors with a different ratio of population splitting into bands. At this parameter, there is a three-band structure, and elements are accumulated into two groups of these three bands. Note that while these groups are similar to clusters (cf. Kaneko (1990a)), elements $x_n(i)$ in each group take different values each other. Depending on the ratio of population in the two groups, two kinds of element motion coexist.

The *clustering* also provides a mechanism to form a group, and the motion of elements depend on its group. However, we should notice that above phenomena is different from the clustering, because the elements do not synchronized each other. As a grouping mechanism, we may need to extend the concept of clustering. It should be studied what kind of grouping is possible with globally coupled dynamical systems. Relevance of such grouping to the problem of cell differentiation is discussed in Kaneko & Yomo (1994) and Furusawa & Kaneko (1998).

VII.3 Future Problems beyond Globally Coupled Map

Collective Motion and Slaving Principle As we have mentioned in this Thesis, the present collective motion cannot be observed in the microscopic variables. Indeed, no Lyapunov exponent for the microscopic variables exists corresponding to the collective motion. Thus, we need to observe a certain *macroscopic variable* to detect lower dimensional-like motions such as quasiperiodic motion or low-dimensional chaos.

We can also consider a phenomenological description for such a macroscopic variable. In this case, one may describe the macroscopic motion with a lower dimensional motion and a stochastic process around the motion. In order to understand the phenomena, we may mainly discuss the bifurcation structure of this phenomenological model, which is expected to be used only with the macroscopic variable. Here, the *slaving picture* may hold in some sense, and the microscopic variables disappear (Haken 1978). From the view point of the collective motion, we deal with the hierarchical structure of a phenomenon, while from the view point of the slaving, we do not consider such hierarchical structure.

Imagine an oscillatory phenomenon, whose model we are going to construct. First we choose a certain description level, for instance, the model that describes the position of elements constituting the system, or something. Then, if one constructs a good model, it shows some oscillatory trajectory. We can study the model to clarify whether the oscillatory trajectory is the collective motion of these elements with effectively high degrees of freedom or the most of the variables are eliminated with the slaving picture. It might be an interesting problem to examine whether the phenomena is the collective motion or is viewed from the slaving principle without constructing a detailed model.

Beyond Globally Coupling In this Thesis, we have only studied the globally coupled systems. We should also study the collective motion in systems with another kind of coupling.

In coupled map lattice, the existence of the collective chaos has been suspected (Bohr et al. 1987, Grinstein 1988, Bennett et al. 1990). They have discussed the correlation length scale in spatiotemporal chaotic systems. One can easily imagine that the correlation length scale is finite. Hence, they conclude that the coherent motion does not exist in the zeroth wave number mode.

However, the present result indicates that the stability of the distribution function should be discussed rather than the correlation length scale. It is also a future problem of what condition is necessary to have some coherent motion in *much longer* length scale than the correlation length scale, (though such length scale might be much shorter than infinity).

While the connection relations among elements does not change in time in coupled map lattice and globally coupled map, a model where the connection relations change dynamically in time is also presented (Shibata & Kaneko 1999). It should also be studied the collective motion in such systems.

Hamiltonian Systems The element in GCM is at a macroscopic level, and each element shows macroscopic chaos, i.e. the logistic map is adopted for the dynamics of each element. Then, if one studies a correspondence of the results of GCM to physical phenomena strictly, the motion of the macroscopic variable of GCM may be considered as much larger scale phenomenon than the macroscopic chaos with a certain scale that we usually suppose.

In many dissipative systems showing the macroscopic chaos, such as fluid systems, it is supposed that some Hamiltonian dynamics with large degrees of freedom should underlie. We also ask the problem of collective chaos from the viewpoint of Hamiltonian dynamics at a microscopic level, though the introduction of dissipation is difficult. This question will be relevant to many important problems in nonequilibrium physics. Here, we consider one of these problems.

When a lower dimensional collective motion appears at a macroscopic level from a high-dimensional Hamiltonian system (with dissipation), it may be possible to harness such a motion. The energy of the system with such a motion might be transduced into mechanical work easier than the energy of the system without such a motion. Thus, the appearance of such collective motion might bring some substantial change to the system. In order to clarify this point, we need to consider appropriate *thermodynamic entropy* and effect of the collective motion on the thermodynamic entropy.

VII.4 Coherent Irregularity

Kazuhisa Tomita has left profound speculation on the significance of the concept *chaos* (Tomita 1984a,b), in which he reconsidered the concept of ‘*coarse graining*’ comparing *macroscopic chaos* with *molecular chaos*.

The macroscopic description of thermodynamics is possible on the basis of molecular chaos. In order to obtain the macroscopic description on contracting the microscopic information, *coarse graining* is necessary. He pointed out that in addition to the property of ergodicity, a huge number of degrees of freedom and a loss of the dynamical coherence among them (*incoherence*) are usually indispensable.

On the other hand, in the case of macroscopic chaos, irregularity is not a consequence of the projection of a huge number of components onto a few degrees of freedom, but the consequence of dynamical feedback with the expansion and folding of phase space due to the nonlinearity. This does not change even if we improve the accuracy of measurement. He called this ‘*intrinsic coarsening*’. For this macroscopic chaos, an incoherent stochastic picture does not hold as in the case of statistical mechanics. Chaotic dynamics has coherence of its own, however, irregular it is. He termed such property ‘*coherent irregularity*’.

The collective motion of network of such macroscopic chaos is considered to substantially reflect these characteristics. Though he pointed out the coherent irregularity of macroscopic chaos itself, we may say that in the network of chaotic elements, such property appears as coherence between elements even for arbitrary small coupling strength. Kaneko called this property ‘*hidden coherence*’ (Kaneko 1992).

In the present collective motion, we might say that the coherent irregularity appears as the recovery of predictable property of the macroscopic motion. In fact, as is seen in Chapter V, the collective Lyapunov exponent is much smaller than the Lyapunov exponent of the microscopic motion. This might imply that we must rethink so-called the ‘*butterfly effect*’ in high-dimensional dynamical systems such as the atmospheric system around the earth. High-dimensional dynamical systems are not so simple as are expected by the butterfly effect.

Kazuhisa Tomita also discussed the possibility of ‘soft phenomenology’ based on the *macroscopic chaos* (Tomita 1984b), considering the analogy with the *molecular chaos*.

He asked the reason why we have *two* fundamental laws in thermodynamics. In the process of the energy transfer associated with a change in state, the amount of

transferred energy and the associated degrees of freedom should be considered on the basis of the molecular chaos. For these two aspects, on the one hand, requiring the energy conservation in the process, the associated degrees of freedom can not be restricted within the macroscopy (the first law). On the other hand, supposing that only the macroscopic degrees of freedom are controllable, the energy conservation within this degrees of freedom can not be expected (the second law).

On the basis of macroscopic chaos, what kind of phenomenology may we expect? He developed a similar discussion between the amount of transferred information instead of energy and the associated degrees of freedom as ‘information dynamics’ for the complex systems of nested hierarchical structure, where small subsystems are embedded in a larger system such as a biological system.

In such complex systems, it is almost inevitable to understand the nature of high-dimensional dynamical systems. The study of the collective motion in this Thesis might reveal one aspect of such hierarchical systems. However, it is still unknown what quantity is important for developing the phenomenology on the basis of macroscopic chaos. While we expect that the concepts developed in the model is relevant to a variety of natural systems, in order to discuss the expected phenomenology, we have to consider the relevance more concretely. It might reveal out the significance of the collective motion. He claimed that ‘the second law’ of phenomenology on the basis of macroscopic chaos is much more abundant than that of the thermodynamics.

REFERENCES

- Aertsen, A. & M. Erb, G. P. (1994), ‘Dynamics of functional coupling in the cerebral cortex: an attempt at a model-based interpretation’, *Physica* **75D**, 103–128. and references cited therein. 15
- Arecchi, F. T. (1991), ‘Rate processes in nonlinear optical dynamics with many attractors’, *Chaos* **1**, 357. 15
- Aurell, E., Boffetta, G., Crisanti, A., Paladin, G. & Vulpiani, A. (1996), ‘Growth of noninfinitesimal perturbations in turbulence’, *Physical Review Letters* **77**, 1262. 67, 73
- Bennett, C. H., Grinstein, G., He, Y., Jayaprakash, C. & Mukamel, D. (1990), ‘Stability of temporally periodic states of classical many-body systems’, *Physical Review* **A41**, 1932. 12, 73, 87
- Bergé, P., Pomeau, Y. & Vidal, C. (1984), *L’ordre dans le Chaos*, Hermann, Paris. 9
- Bohr, T., Grinstein, G., He, Y. & Jayaprakash, C. (1987), ‘Coherence, chaos, and broken symmetry in classical, many-body dynamical systems’, *Physical Review Letters* **85**, 2155. 12, 73, 87
- Bracikowski, C. & Roy, R. (1991), ‘Chaos in a multimode solid-state laser system’, *Chaos* **1**, 49. 15
- Brandstätter, A., Swift, J., Swinney, H. L., Wolf, A., Farmer, J. D., Jen, E. & Crutchfield, P. J. (1983), ‘Low-dimensional chaos in a hydrodynamic system’, *Physical Review Letters* **51**, 1442–1445. 9
- Buchman, T. G. (1996), ‘Physiological stability and physiologic state’, *J. Trauma* **41**, 599–605. 13, 15
- Cencini, M., Falcioni, M., Vergni, D. & Vulpiani, A. (1998), ‘Macroscopic chaos in globally coupled maps’, *preprint*. xxx.lanl.gov:chao-dyn/9804045. 73
- Chabanol, M., Hakim, V. & Rappel, W. (1997), ‘Collective chaos and noise in the globally coupled complex Ginzburg-Landau equation’, *Physica* **D103**, 273–293. 73
- Chaté, H., Lemaitre, A., Marcq, P. & Manneville, P. (1996), ‘Non-trivial collective behavior in extensively-chaotic dynamical systems: an update’, *Physica* **A 224**, 447–457. 16
- Chaté, H. & Manneville, P. (1992), ‘Collective behaviors in spatially extended systems with local interactions and synchronous updating’, *Progress of Theoretical Physics* **87**, 1. 12, 16

REFERENCES

- Chawanya, T. & Morita, S. (1998), 'On the bifurcation structure of the mean-field fluctuation in the globally coupled tent map systems', *Physica* **D116**, 44. 16, 17, 39, 75
- Chialvo, D. R., Gilmour, R. F. & Jalife, J. (1990), 'Low dimensional chaos in cardiac tissue', *Nature* **343**, 653. 9
- Cole, B. J. (1991), 'Is animal behaviour chaotic? evidence from the activity of ants', *Proc. R. Soc. Lond.* **224B**, 253–259. 9, 13
- Collet, P. & Eckmann, J. P. (1980), *Iterated Maps of the Interval as Dynamical Systems*, Berkhauser, Boston. 11, 16, 35
- Crutchfield, J. P. (1983), Noisy chaos, PhD thesis, University of California, Santa Cruz. and references cited therein. 74
- Crutchfield, J. P., Farmer, J. D. & Huberman, B. A. (1982), 'Fluctuations and simple chaotic dynamics', *Physics Reports* **92(2)**, 45–82. 11
- Eckmann, J. P. & Ruelle, D. (1985), 'Ergodic theory of chaos and strange attractors', *Reviews of Modern Physics* **57**, 617. 9
- Ershov, S. V. & Potapov, A. B. (1995), 'On mean field fluctuations in globally coupled maps', *Physica* **D86**, 532–558. 16, 17, 39
- Ershov, S. V. & Potapov, A. B. (1997), 'On mean field fluctuations in globally coupled logistic-type maps', *Physica* **D106**, 9–38. 16, 17, 32, 34, 35, 38, 42, 75
- Feigenbaum, M. J. (1978), 'Quantitative universality for a class of nonlinear transformations', *Journal of Statistical Physics* **19(1)**, 23–52. 11
- Fox, R. F. & Keizer, J. (1991), 'Amplification of intrinsic fluctuations by chaotic dynamics in physical systems', *Physical Review* **43A**, 1709. and references cited therein. 12
- Furusawa, C. & Kaneko, K. (1998), 'Emergence of rules in cell society: Differentiation, hierarchy, and stability', *Bull. Math. Biol.* **60**, 659–687. 86
- Gaspard, P., Briggs, M. E., Francis, M. K., Sengers, J. V., Gammon, R. W., Dorfman, J. R. & Calabrese, R. V. (1998), 'Experimental evidence for microscopic chaos', *Nature* **394(27)**, 865–868. 12
- Gaspard, P. & Wang, X.-J. (1993), 'Noise, chaos, and (ϵ, τ) -entropy per unit time', *Physics Reports* **235(6)**, 291–343. 12
- Gibbs, H. M., Hopf, F. A., Kaplan, D. L. & Shoemaker, R. L. (1981), 'Observation of chaos in optical bistability', *Physical Review Letters* **46(7)**, 474. 9
- Glansdorff, P. & Prigogine, I. (1971), *Thermodynamic Theory of STRUCTURE, STABILITY AND FLUCTUATIONS*, Jon Wiley & Sons Ltd., New York. 13
- Godin, P. J. & Buchman, T. G. (1996), 'Uncoupling of biological oscillators: A complementary hypothesis concerning the pathogenesis of multiple organ dysfunction syndrome', *Crit. Care. Med.* **24**, 1107–1116. 13, 15

REFERENCES

- Grassberger, P. & Procaccia, I. (1983*a*), ‘Characterization of strange attractors’, *Physical Review Letters* **50**, 346. 20, 59
- Grassberger, P. & Procaccia, I. (1983*b*), ‘Measuring the strangeness of strange attractors’, *Physica* **D9**, 189. 20, 59
- Grinstein, G. (1988), ‘Stability of nonstationary states of classical, many-body dynamical systems’, *J. Stat. Phys.* **51**, 803. 12, 73, 87
- Haken, H. (1978), *Synergetics*, second edn, Springer, Berlin. 36, 87
- Ikeda, K., Matsumoto, K. & Otsuka, K. (1989), ‘Maxwell-bloch turbulence’, *Progress Theoretical Physics Supplement* **99**, 295. 17, 65
- Just, W. (1995), ‘Bifurcations in globally coupled maps lattices’, *Journal of Statistical Physics* **79**, 429–449. 16, 39
- Kaneko, K. (1984), ‘Period-doubling of kink-antikink patterns, quasi-periodicity in antiferro-like structures and spatial intermittency in coupled logistic lattice –toward a prelude to a “field theory of chaos”—’, *Progress of Theoretical Physics* **72**, 480. 13, 17
- Kaneko, K. (1989*a*), ‘Chaotic but regular posi-nega switch among coded attractors by cluster size variation’, *Physical Review Letters* **63**, 219. 65
- Kaneko, K. (1989*b*), ‘Pattern dynamics in spatiotemporal chaos’, *Physica* **D34**, 1. 17
- Kaneko, K. (1990*a*), ‘Clustering, coding, switching, hierarchical ordering, and control in a network of chaotic elements’, *Physica* **D41**, 137–172. 15, 17, 86
- Kaneko, K. (1990*b*), ‘Globally coupled chaos violates the law of large numbers’, *Physical Review Letters* **65**, 1391. 16, 17, 35
- Kaneko, K. (1990*c*), Simulating physics with coupled map lattice, in K. Kawasaki, A. Onuki & M. Suzuki, eds, ‘Formation, Dynamics and Statistics of Patterns.’, World Scientific, Singapore. 17
- Kaneko, K. (1992), ‘Mean field fluctuation of a networks of chaotic elements’, *Physica* **D65**, 368–384. 16, 17, 32, 34, 35, 38, 76, 88
- Kaneko, K. (1995), ‘Remarks on the mean field dynamics of networks of chaotic elements’, *Physica* **D86**, 158–170. 16, 17, 38, 85
- Kaneko, K. (1997), ‘Dominance of milnor attractors and noise-induced selection in a multi-attractor system’, *Physical Review Letters* **78**, 2736–2739. 17
- Kaneko, K. (1998), ‘On the strength of attractors in a high-dimensional system: Milnor attractor network, robust global attraction, and noise-induced selection’, *Physica* **124D**. 17
- Kaneko, K., ed. (1993), *Theory and Applications of Coupled Map Lattices*, Jon Wiley & Sons, New York. 13
- Kaneko, K. & Yomo, T. (1994), ‘Cell division, differentiation and dynamic clustering’, *Physica* **75D**, 89–102. 15, 86

REFERENCES

- Keizer, J. & Fox, R. F. (1992), 'Reply to "Comments on the amplification of intrinsic fluctuations by chaotic dynamics"', *Physical Review* **46**, 3572. preceding Comment : (Nicolis & Balakrishnan 1992). 12, 93
- Ko, E. P., Yomo, T. & Urabe, I. (1994), 'Dynamics clustering of bacterial population', *Physica* **75D**, 81–88. 15
- Kuramoto, Y. (1975), Self-entrainment of a population of coupled non-linear oscillators, in 'Lecture Notes in Physics', Vol. 63, Springer, New York, p. 420. 57
- Libchaber, A. & Maurer, J. (n.d.), 'Une expérience de payleigh-bénard de géométrie réduite; multiplication, accrochage, et démultiplication de fréquences', *J. Phys. (Paris) Colloq.* **41**, C3–51. 9
- Lorenz, E. N. (1963), 'Deterministic nonperiodic flow', *J. Atmos. Sci.* **20**, 130. 7, 8, 9
- Markus, M., Müller, S. C. & Hess, B. (1985), 'Observation of entrainment, quasiperiodicity and chaos in glycolyzing yeast extracts under periodic glucose input', *Ber. Bunsenges, Ohys, Chem.* **89**, 651–654. 9
- Matsumoto, K. & Tsuda, I. (1983), 'Noise-induced order', *Journal of Statistical Physics* **31**, 87–106. 74, 81
- Miramontes, O., Sole, R. V. & Goodwin, B. C. (1993), 'Collective behavior of random-activated mobile cellular automata', *Physica* **63D**, 145–160. 13
- Morita, S. (1996), 'Bifurcation in globally coupled chaotic maps', *Phys. Lett. A* **211**, 258–264. 16, 17, 39
- Nakagawa, N. & Komatsu, T. (1998), 'Collective motion occurs inevitably in a class of populations of globally coupled chaotic elements', *Physical Review E* **57**, 1570. 16, 17, 29
- Nakagawa, N. & Kuramoto, Y. (1993), 'Collective chaos in a population of globally coupled oscillators', *Progress of Theoretical Physics* **89**, 313–323. 17
- Nakagawa, N. & Kuramoto, Y. (1994), 'From collective oscillations to collective chaos in a globally coupled oscillator system', *Physica* **D75**, 74–80. 73
- Nicolis, G. & Balakrishnan, V. (1992), 'Comments on the amplification of intrinsic fluctuations by chaotic dynamics', *Physical Review Letters* **46**, 3569. Reply to this comments : (Keizer & Fox 1992). 12, 93
- Nicolis, G. & Prigogine, I. (1977), *Self-Organization in Nonequilibrium Systems, From Dissipative Structures to Order through Fluctuations*, Jon Wiley & Sons Inc., New York. 13, 36
- Okuda, K. (1993), 'Variety and generality of clustering in globally coupled oscillators', *Physica* **D63**, 424–436. 17
- Olsen, L. F. & Degn, H. (1977), 'Chaos in an enzyme reaction', *Nature* **267**, 177. 9
- Oono, Y. & Takahashi, Y. (1980), 'Chaos, external noise and fredholm theory', *Progress of Theoretical Physics* **63**, 1804–1807. 74

REFERENCES

- Ott, E. (1993), *Chaos in Dynamical Systems*, Cambridge University press, Cambridge. 9, 16
- Paladin, G., Serva, M. & Vulpiani, A. (1995), 'Complexity in dynamical-systems with noise', *Physical Review Letters* **74**, 66. 67, 73
- Perez, G. & Cerdeira, H. A. (1992), 'Instabilities and nonstatistical behavior in globally coupled systems', *Physical Review A* **46**, 7492–7497. 16, 38
- Perez, G., Sinha, S. & Cerdeira, H. A. (1993), 'Order in the turbulent phase of globally coupled maps', *Physica* **D63**, 341–349. 16, 17, 76
- Pikovsky, A. S. & Kurths, J. (1994a), 'Collective behavior in ensembles of globally coupled maps', *Physica* **D76**, 411–419. 16, 17
- Pikovsky, A. S. & Kurths, J. (1994b), 'Do globally coupled maps really violate the law of large numbers?', *Physical Review Letters* **72**, 1644. 16, 17, 38
- Rössler, O. E. (1976), 'Chaotic behavior in simple reaction systems', *Z. Naturforsch* **31a**, 256–264. 10
- Roux, J. C., Simoyi, R. H. & Swinney, H. L. (1983), 'Observation of a strange attractor', *Physica* **8D**, 257. 9
- Shaw, R. (1981), 'Strange attractors, chaotic behavior, and information flow', *Z. Naturforsch* **36a**, 80–112. 11
- Shaw, R. (1984), *The Dripping Faucet as a Model Chaotic System*, Aerial Press, Inc., Santa Cruz. 11
- Shibata, T. (1996), Co-operative behavior in coupled chaotic systems (in japanese), Master's thesis, University of Tokyo, Komaba. published in *Bussei Kenkyu (Kyoto)* **66**, (1996), 1064–1136. 57
- Shibata, T., Chawanya, T. & Kaneko, K. (1998), 'Noiseless collective motions out of noisy chaos', *Physical Review Letters* . submitted. 17, 74
- Shibata, T. & Kaneko, K. (1997), 'Heterogeneity induced order in globally coupled chaotic systems', *Europhysics Letters* **38(6)**, 417–422. 16, 17, 57, 59
- Shibata, T. & Kaneko, K. (1998a), 'Collective chaos', *Physical Review Letters* **81**, 4116. 16, 17, 66, 75
- Shibata, T. & Kaneko, K. (1998b), 'Tongue-like bifurcation structures of the mean-field dynamics in a network of chaotic elements', *Physica* **124D**, 163–186. 15, 16, 17, 37, 75
- Shibata, T. & Kaneko, K. (1999), 'Coupled map gas: Dynamical creation and collapse of clusters in a elastic network of mobile chaotic elements'. in preparation. 87
- Simon, H. A. (1981), *The Sciences of the Artificial*, second edn, The MIT Press, Cambridge. 13
- Simoyi, R. H., Wolf, A. & Swinney, H. L. (1982), 'One dimensional dynamics in a multi-component chemical reaction', *Physical Review Letters* **49**, 245. 9

REFERENCES

- Testa, J., Pérez, J. & Jeffries, C. (1982), 'Evidence for universal chaotic behavior of a driven nonlinear oscillator', *Physical Review Letters* **48(11)**, 714. 9
- Tomita, K. (1984a), Coarse graining revisited — the case of macroscopic chaos, in Y. Kuramoto, ed., 'Chaos and Statistical Methods', Springer, pp. 2–13. 88
- Tomita, K. (1984b), 'The significance of the concept 'chaos'', *Progress of Theoretical Physics, Supplement* **79**, 1–25. 88
- Tsuda, I. (1992), 'Chaotic itinerancy as a dynamical basis of hermeneutics in brain and mind', *World Futures* **32**, 313. 17, 65
- Watanabe, S. & Strogatz, S. H. (1994), 'Constants of motion for superconducting josephson arrays', *Physica* **74D**, 197–253. and references cited therein. 15
- Wolf, A., Swift, J. B., Swinney, H. L. & Vastano, J. A. (1985), 'Determining Lyapunov exponents from a time-series', *Physica* **16D**, 285. 73